

https://doi.org/10.1038/s42003-024-06690-9

Cell-free expression with a quartz crystal microbalance enables rapid, dynamic, and label-free characterization of membrane-interacting proteins

Check for updates

1

Aset Khakimzhan¹, Ziane Izri¹, Seth Thompson¹, Oleg Dmytrenko **®**², Patrick Fischer², Chase Beisel **®**^{2,3} & Vincent Noireaux **®**¹ ⊠

Integral and interacting membrane proteins (IIMPs) constitute a vast family of biomolecules that perform essential functions in all forms of life. However, characterizing their interactions with lipid bilayers remains limited due to challenges in purifying and reconstituting IIMPs in vitro or labeling IIMPs without disrupting their function in vivo. Here, we report cell-free transcription-translation in a quartz crystal microbalance with dissipation (TXTL-QCMD) to dynamically characterize interactions between diverse IIMPs and membranes without protein purification or labeling. As part of TXTL-QCMD, IIMPs are synthesized using cell-free transcription-translation (TXTL), and their interactions with supported lipid bilayers are measured using a quartz crystal microbalance with dissipation (QCMD). TXTL-QCMD reconstitutes known IIMP-membrane dependencies, including specific association with prokaryotic or eukaryotic membranes, and the multiple-IIMP dynamical pattern-forming association of the *E. coli* division-coordinating proteins MinCDE. Applying TXTL-QCMD to the recently discovered Zorya antiphage system that is unamenable to labeling, we discovered that ZorA and ZorB integrate within the lipids found at the poles of bacteria while ZorE diffuses freely on the non-pole membrane. These efforts establish the potential of TXTL-QCMD to broadly characterize the large diversity of IIMPs.

Lipid bilayers form the physical boundaries between the inner compartment of a living cell and the environment. To sense and interact with their surroundings, cells synthesize integral and interacting membrane proteins (IIMPs) that localize either into or at the surface of phospholipid membranes. IIMPs constitute a large family of biomolecules achieving broad cellular functions that interface cells with their milieu^{1,2}. Lipid bilayers also serve as physical templates for IIMPs to organize cellular functions, comprising, for instance, the formation of dynamical patterns³ and anchoring cytoskeletons^{4,5}. Characterizing IIMPs non-disruptively, such as the biochemistry and biophysics of their interactions with membranes, is often challenging to achieve in vivo as they usually require labeling with fluorescent reporters or affinity tags⁶. Conversely, the reconstitution of IIMPs in vitro provides easier access to their biochemical and biophysical characterization⁷. Yet, this approach necessitates difficult recombinant purification and reconstitution procedures that prevent rapid exploration of their properties⁸.

Cell-free transcription-translation (TXTL) simplifies and outpaces traditional recombinant approaches by enabling the scalable synthesis of proteins outside living cells, including IIMPs, in a matter of hours from plasmids or linear DNA⁹⁻¹¹. Many TXTL reactions can be prepared concurrently, thus facilitating the rapid and parallel characterization of reaction products. To fold properly and not precipitate, IIMPs synthesized in TXTL require either the presence of non-natural substrates like surfactants or natural membranes made of phospholipids¹²⁻¹⁵, which is typically achieved by adding liposomes or nanodiscs to the TXTL reaction. Liposomes added to TXTL reactions are known to precipitate¹⁶. Consequently, the liposome approach to TXTL of IIMPs is limited and has been scarcely used. While nanodiscs offer a simple method to synthesize IIMPs in TXTL ¹⁶⁻¹⁸, they are limited in lipid compositions¹⁹, reducing the scope of IIMP-lipids interactions that can be studied. IIMPs can also be synthesized in TXTL reactions encapsulated into liposomes, a system known as synthetic cells²⁰. In these

¹School of Physics and Astronomy, University of Minnesota, Minneapolis, MN, 55455, USA. ²Helmholtz Institute for RNA-based Infection Research (HIRI), Helmholtz-Centre for Infection Research (HZI), 97080 Würzburg, Germany. ³Medical Faculty, University of Würzburg, 97080 Würzburg, Germany. ☑ e-mail: noireaux@umn.edu settings, too, disruptive fluorescent labelling is required to visualize the interaction with the membrane and the lipid composition of such liposomes is limited. Preparing TXTL-based synthetic cells with complex membrane compositions, such as *E. coli* phospholipids, is limited, as the efficacy of liposome production rapidly decreases with the complexity of the lipid composition. Thus, there is a lack of an approach that enables the sensitive and label-free characterization of IIMPs' interactions with lipid membranes of arbitrarily complex membrane composition.

In this work we achieved rapid, sensitive, and label-free characterization of IIMPs' interactions with supported lipid bilayers (SLBs) by combining the versatility of TXTL with the sensitivity of a quartz crystal microbalance with dissipation (QCMD)²¹ (Fig. 1). A QCMD is a tool to sensitively measure the added mass and the rates of molecular adsorption. This measurement is performed by continuously tracking the changes in the sensor's resonant frequency, which, to a first approximation, is proportional to the mass deposited on the sensor²². We used the change in the resonant frequency of the QCMD to measure the interaction between IIMPs and a given phospholipid composition of the bilayer. The proof of concept of such an approach has been established for single IIMPs^{23,24}, but the method has never been generalized to multiple and interacting IIMPs, membranedependent dynamical patterns, and complex phospholipid membrane compositions. This approach provides a high signal-to-noise ratio due to minimal nonspecific adsorption of the TXTL components onto SLBs. IIMPs, without any modifications such as the addition of fluorescent reporters, are dynamically synthesized on the SLBs inside the QCMD while monitoring the signal, which eliminates recombinant expression, purification, and reconstitution procedures. SLBs made of complex phospholipid compositions that are analogous to the ones found in living cells can be prepared onto QCMD sensors, circumventing the limitations of the other methods.

Results

TXTL reactions have minimal nonspecific adsorption on SLBs

The TXTL system uses the endogenous *E. coli* core RNA polymerase and sigma factor 70 present in the lysate as the sole primary transcription mechanism. This system does not contain any remaining live *E. coli* cells (Fig. S1). Genes are expressed either from plasmids or linear dsDNA, from *E. coli* promoters (e.g., P70a), or from the T7 promoter via a transcriptional activation cascade (Fig. S2), as previously described^{25–27}.

The interaction with and integration of IIMPs into membranes depend on the membrane's phospholipid composition²⁸. Consequently, the diversity of SLBs that can be fabricated on the QCMD sensor determines the breadth of IIMPs that can be characterized, in particular IIMPs specific to the membranes of either bacteria or higher organisms. To make SLBs on the QCMD sensor, we used the solvent-assisted lipid bilayer formation method

(SALB)²⁹⁻³¹, as it is fast and consistent (Fig. 2a). Our model eukaryotic membrane is made of EggPC, a mixture of PC phospholipids extracted from chicken eggs, with various aliphatic chain lengths. Our model prokaryotic cell membrane is made of *E. coli* lipids (ECL) from *E. coli* cells. ECL is composed of mainly PE (phosphatidylethanolamine, ~75% mol), PG (phosphatidylglycerol, ~20% mol), and CL (cardiolipin, ~5% mol)³². We also studied the interactions of IIMPs with other SLBs made from mixtures of pure phospholipids. In these cases, the SLBs were made using the most abundant phospholipid found in EggPC (DOPC) or ECL (DOPE). A TXTL reaction contains a broad variety of biological molecules in large concentrations; it is thus important to make sure that they do not produce large nonspecific adsorption on the sensor-SLB system in the absence of IIMP synthesis. We devised a procedure so that SLBs cover the whole sensor and have minimal nonspecific TXTL adsorption.

The SLBs were made in four steps (Fig. 2a). In step I, the QCMD sensor is washed with a Tris NaCl buffer, which is replaced in step II by an isopropyl alcohol (IPA) solution. In step III, phospholipids dissolved in IPA are introduced onto the sensor. The spontaneous SLB formation occurs in step IV, as the IPA with the dissolved phospholipids is gradually replaced with a Tris NaCl buffer³¹. The difference between the stabilized resonance frequency ($\Delta f = 0$) from steps I to IV is proportional to the mass of the SLB on the sensor^{33,34}. When no phospholipids are added to the IPA during step III, the difference is zero (Fig. S3). In all the subsequent data presented, the resonance frequency at the end of step IV, before adding the TXTL reaction onto the QCMD sensor, was taken as the reference and set to zero. A shortlived dip in frequency is systematically produced at the beginning of each step. This is due to the introduction of a different solution into the QCMD modules (Fig. 2a). This short-lived dip in frequency, also present when a TXTL reaction is introduced into the QCMD chambers, is irrelevant to the measurement of the interaction between the IIMPs and the SLBs.

To determine whether an SLB fully covers the sensor, is stable, and does not allow nonspecific TXTL adsorption, a blank TXTL reaction (with only the plasmid P70a-T7rnap, 0.15 nM) was incubated into the QCMD module in contact with the SLB-sensor system. SLBs were made with different concentrations of phospholipids to determine at which phospholipid concentration nonspecific TXTL adsorption is not observed. This assay was carried out for each SLB tested in this work. In the case of an EggPC membrane, the full coverage of the QCMD sensor is achieved at a phospholipid concentration at or above 0.65 mM (0.5 mg/mL) in IPA, as observed by the flat frequency shifts (Fig. 2b). Below a concentration of 0.65 mM, an EggPC membrane shows nonspecific TXTL adsorption as observed by the decrease in Δf for lower phospholipid concentration (Fig. 2c). The minimal phospholipid concentration to get SLBs that fully cover the QCMD sensor was first determined for our four base SLBs, namely EggPC, DOPC, DOPE, and ECL SLBs (Fig. 2c-f, Fig. S4, Table S1).

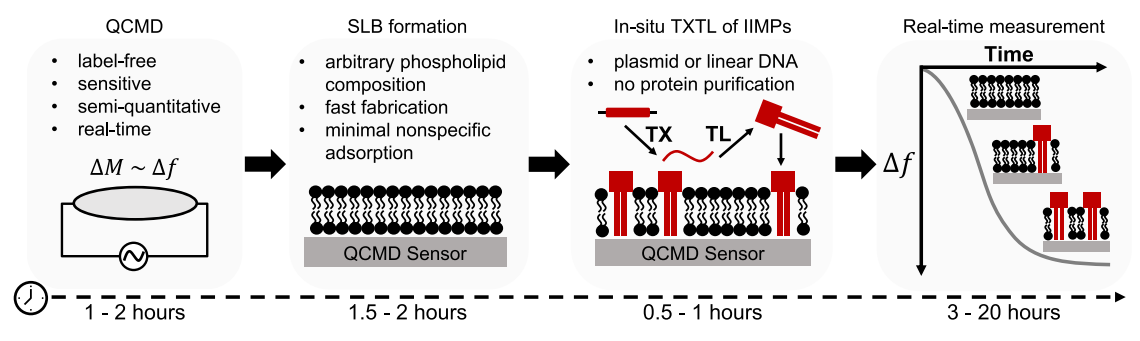


Fig. 1 | Workflow of the TXTL-QCMD experimental procedure. The TXTL-QCMD procedure allows non-disruptive semi-quantitative measurement of the interactions between in situ synthesized proteins and lipid bilayers. The first step of the procedure is the QCMD module setup, which takes ~2 hours. The second step of the experiment is the fabrication of the supported lipid bilayer (SLB). Using the solvent-assisted lipid bilayer formation method (SALB), SLBs of arbitrary phospholipid compositions are made in 2 hours. The third step is the preparation of the

TXTL reaction, which involves mixing the TXTL components with a plasmid or a linear construct of interest. TXTL enables characterizing IIMPs that require cotranslational integration. The last step is the incubation of the prepared TXTL reactions in contact with the SLB-sensor system. Typically, the reactions are incubated overnight; however, in some cases, as few as 3 hours are sufficient to obtain experimentally relevant data.

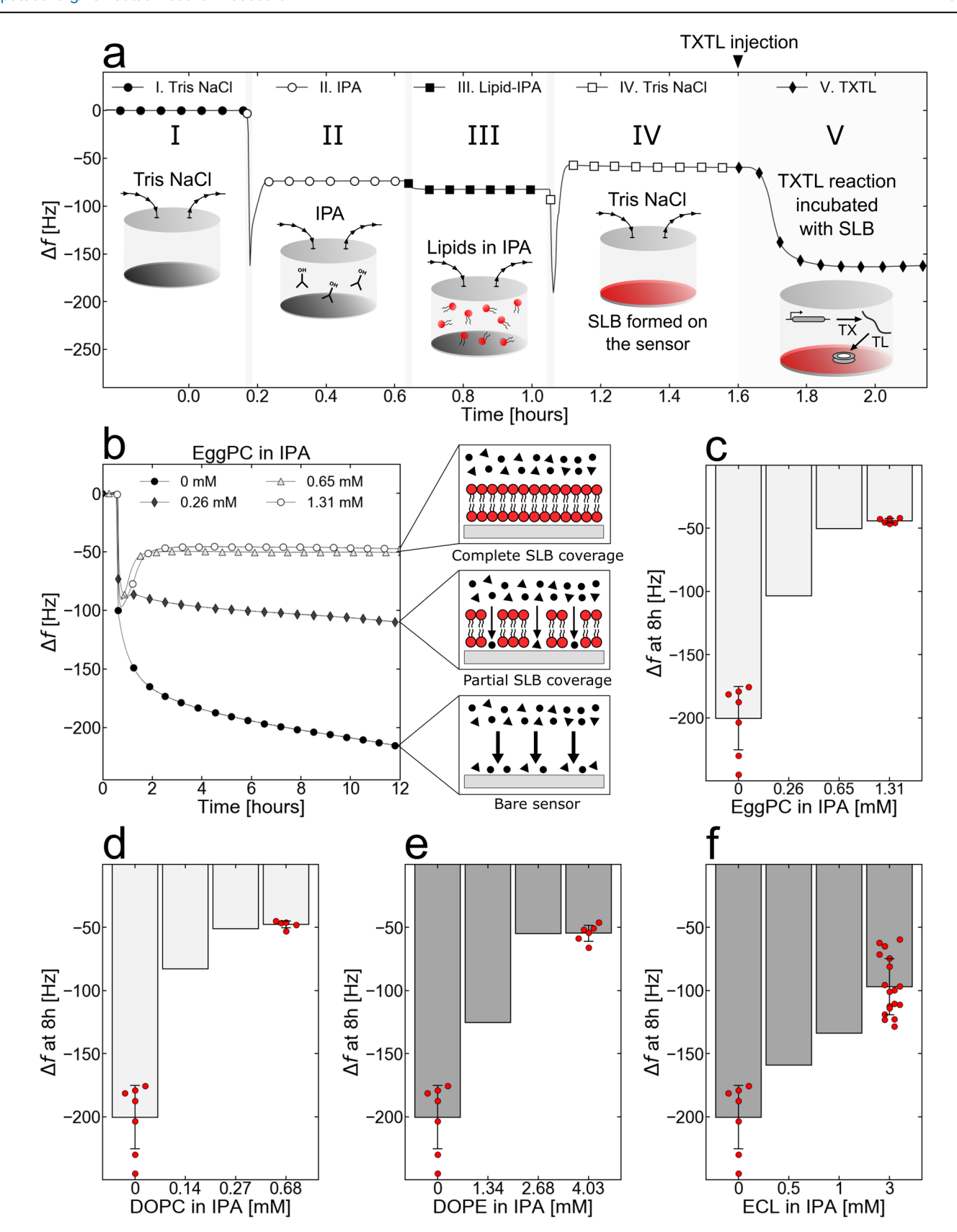


Fig. 2 \mid An optimal lipid-isopropanol concentration during SALB is critical for complete SLB coverage and minimal TXTL nonspecific adsorption.

a Experimental steps of SALB formation (steps I–IV) followed by the nonspecific adsorption characterization with a TXTL reaction that only synthesizes the T7 RNA polymerase (step IV, plasmid P70a-*T7rnap* 0.15 nM). **b** The adsorption kinetics of a blank TXTL reaction (plasmid P70a-*T7rnap*, 0.15 nM) depend on the EggPC phospholipids concentration in IPA during step II. The cartoon frames on the right

explain the different levels of nonspecific adsorption to the SLB-sensor system. **c** Changes in frequency after 8 hours of incubation (blank TXTL reaction with only P70a-T7rnap, 0.15 nM) as a function of phospholipids concentration in IPA step II for EggPC. **d**-f Same as **c**. for DOPC, DOPE, and *E. coli* lipids (ECL) total respectively. The bar level and error bars are the mean and standard deviation of at least n=5 independent experiments.

Interestingly, the concentrations needed for full coverage varied depending on the type of lipids, presumably due to the charge of the lipid head. Lipids with PC headgroups formed SLBs at smaller concentrations compared to the lipids with the more polar PE headgroups. ECL requires an even larger concentration and is composed of PE lipids along with more polar and charged lipids with PG and CL headgroups.

We found that the four major phospholipid compositions used in this work can be used reproducibly for QCMD-TXTL experiments without nonspecific adsorption from the TXTL components (Table S1). Achieving full coverage of the QCMD sensor with lipid bilayers is a striking result that shows the natural resistance of phospholipid membranes to nonspecific adsorption of a complex physiological solution like a TXTL reaction composed of 10 mg/mL of proteins, tRNAs, and rRNAs, ~250–300 mM salts and many other chemicals^{27,35}. The affinity of TXTL to the different SLBs can be estimated by comparing the frequency shifts between the pre-TXTL (step IV) and post-TXTL Tris NaCl flushes (Fig. S5a). One reason for the affinity of TXTL to the DOPE and ECL SLB-sensor systems is larger than to DOPC and EggPC SLBs is because the proteins in the lysate bind to bilayers composed of their naturally occurring lipids (PE, PG, CL) (Fig. S5b).

Cell-free synthesized IIMPs interact specifically with their natural membranes

To test the QCMD-TXTL approach to membrane protein-lipid interaction specificities, we chose two proteins known to preferentially reside in different natural membranes. We performed a set of TXTL reactions that synthesize either the pore-forming protein Alpha-Hemolysin (AH) from S. aureus, known to target mammalian cells rich in PC36, and the largeconductance mechanosensitive channel MscL from E. coli in membranes (ECL) mostly composed of PE, PG, and CL. To quantify the amount of protein produced in the QCMD chamber, we used a fusion AH-eGFP proven to be functional in TXTL because it is produced as a soluble protein and thus easy to quantify³⁷. Both genes were cloned under the T7p14 promoter and expressed via the T7 transcriptional activation cascade (T7p14ah-egfp, T7p14-mscL) (Fig. 3a). AH assembles into a heptameric pore³⁸, while MscL assembles into a pentamer channel³⁹. We observed a net frequency drop relative to the blank only when MscL was synthesized onto the ECL SLB. Conversely, we observed a net frequency drop only when AHeGFP was synthesized onto the EggPC SLB (Fig. 3b, c). Replicates of these experiments confirmed these results (Figs. S6, S7). The same protein-lipid specificities were observed with DOPE (interaction with AH-eGFP, no interaction with MscL) and DOPC (no interaction with AH-eGFP, interaction with MscL) SLBs (Fig. S8). A delay in frequency shift was observed for AH, presumably because it must reach a critical concentration before interacting with the membrane⁴⁰. MscL pre-synthesized in TXTL reactions without membranes did not produce a frequency change (Fig. S9), which is expected because its integration is coupled to its translation. Cotranslational integration also indicates that MscL most likely first integrates into bilayers as a monomer and afterwards assembles in the bilayer into the pentameric MscL. Unlike MscL, AH is a soluble pore-forming toxin that can be pre-synthesized 24 hours before being added onto the QCMD chip and still integrates into the PC SLB (Fig. S10), without a delay as it is introduced into the QCMD module at a large concentration. The concentration of IIMP produced in the QCMD chamber of volume 40 µL was estimated with AH-eGFP to be 1-2 µM (Fig. S11). We found this concentration range relevant as it corresponds to the average protein concentration in E. coli⁴¹. Using MscL, we estimated the resolution of the mass added to the SLB to be on the order of 1 ng, which is a hundred times more sensitive than a standard protein gel (Fig. S12). This estimation also shows that about twenty times more proteins are synthesized in the 40 µL-QCMD chambers with respect to the membrane's maximum binding capacity.

When proteins are inserted into an SLB fully covering the QCMD sensor, the possibilities are that lipids are expelled from the SLB, the surface area per lipid decreases, or lipid protrusions form. Previous studies done by AFM have not shown the formation of lipid protrusions²³. To determine if some lipids are expelled from the SLB during the incubation of either a blank

TXTL reaction or an IIMP-synthesizing reaction, in this case, an MscLsynthesizing TXTL reaction, we added a fluorescent lipid (Rhodamine-PE, Rhod-PE). After 12 h of incubation, we dissolved the SLBs in IPA and measured the fluorescence. First, adding 3% of Rhod-PE to the SLB did not affect the integration of MscL into the DOPE SLBs (Fig. S13a). With that confirmed, we fabricated a DOPE + Rhod-PE SLB on the sensor and incubated it with four different conditions: a TXTL feeding solution (TXTL reaction without the lysate), a blank TXTL reaction (0.15 nM P70a-T7rnap), an MscL TXTL reaction (0.15 nM P70a-T7rnap, 5 nM T7p14-mscL), and 1% SDS (Fig. S13b). After 12 h of incubation, we dissolved the SLBs of each condition with IPA and measured the fluorescence intensity. It appears that neither the blank TXTL reaction nor the MscL TXTL reaction demonstrate an effect of lipid expulsion larger than the 8% uncertainty of the measurements (Fig. S13c). This either indicates that MscL occupies a relatively small percentage of the SLB, such that the expulsion of lipids would be unnoticeable or that the SLB can compact to accommodate the MscL channels without being expelled. The compaction is indeed possible as demonstrated in experiments with model lipid bilayers⁴², with the area per lipid contracting by almost 30% in some cases.

To determine whether IIMPs specific to different lipid kingdoms can coexist in hybrid membranes, such as the one that could be developed in engineered biochemical systems⁴³, we devised hybrid SLBs made of EggPC and ECL. We measured the shift in frequency Δf of blank TXTL reactions (plasmid P70a-T7rnap only) and of TXTL reactions expressing ah-egfp and mscL (Fig. 3d, Fig. S14). The shift in frequency Δf was measured after eight hours of incubation, taken as an amount of time sufficient for the TXTL reaction and interaction with the SLB to reach equilibrium. We first established that at any ratio of phospholipids, the hybrid membrane formed remains devoid of nonspecific adsorption. In contact with the blank TXTL reaction, at any EggPC ratio, the frequency shift stabilized within 2 hours of incubation (Fig. S14a). We also observed a slight linear increase in the Δf with the increase of the EggPC ratio, which accounts for slight nonspecific interactions of the TXTL reaction with E. coli SLBs. For AH-eGFP, we observed a sigmoidal decrease of Δf as the EggPC ratio increased, whereas for MscL Δf increased linearly with the increase of the EggPC ratio, consistent with the respective specificity of AH-eGFP and MscL integration into EggPC and ECL. Considering the cooperativity of the assembly of multimeric complexes in the plasma membrane of bacteria⁴⁴, the sigmoidal dependence for AH-eGFP is expected⁴⁵, while the linear dependence observed for MscL is surprising. When the MscL TXTL reaction was incubated onto DOPE-DOPC hybrid SLBs, MscL exhibited a sigmoidal increase with the increase of the DOPC ratio (Fig. S15). These experiments underline the existence of different self-assembly and integration mechanisms, depending on the presence of lipids, such as DOPG or CL, present in ECL but absent in DOPE⁴⁶⁻⁴⁸.

SLBs' lipid compositions can be broadly tuned

Although PC (eukaryotes) and PE (bacteria) are usually the predominant phospholipids in natural cell membranes^{49–51}, other headgroups are similarly essential for the function of IIMPs²⁸. For example, some IIMPs only anchor to specific phospholipid heads other than PE or PC²⁸, while other IIMPs require the presence of anionic phospholipids to bind⁵². While making SLBs from a mixture of different phospholipids is technically feasible with the SALB method (Fig. 4a), one must determine the degree of nonspecific adsorption of TXTL on the SLBs. We measured the concentrations of DOPG, CL, and DPPS (1,2-dipalmitoylphospho-L-serine) into three of our base SLBs (DOPC, EggPC, and DOPE) for which nonspecific TXTL adsorption is absent (Fig. 4a). We used the PS sensing protein LactC2 to show that one can adjust quantitatively the amount of an added lipid to an SLB.

The added lipid percentage of the lipid-IPA mixture is defined as the ratio of the molarity of the added lipid over that of the base lipid. Using a blank TXTL reaction (plasmid P70a-T7rnap, 0.15 nM), we found that adding DOPG up to 30% to either DOPC or DOPE SLBs did not produce nonspecific TXTL adsorption (frequency drifts of <1 Hz/hour) (Fig. 4b and

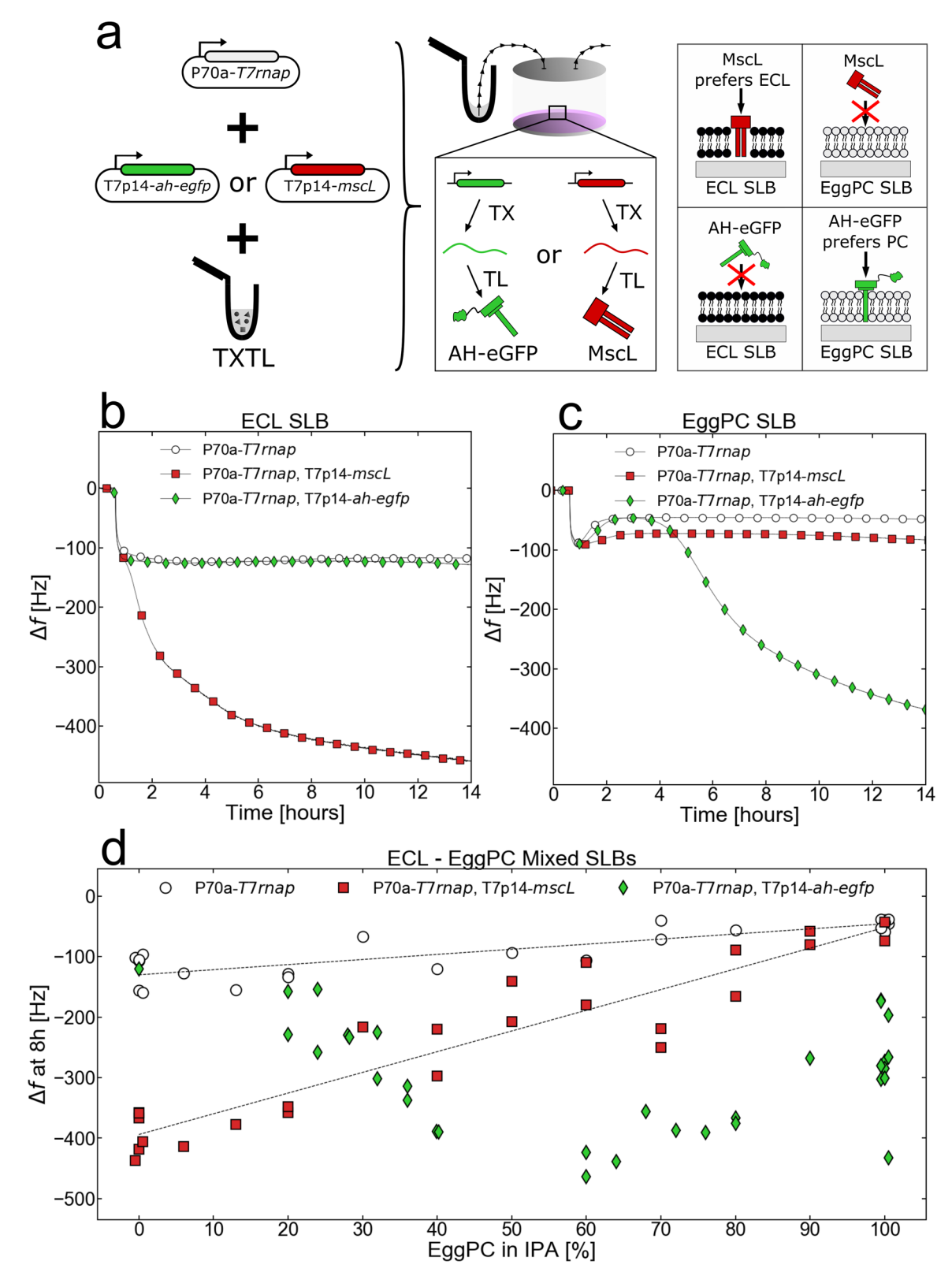


Fig. 3 | In situ cell-free synthesized MscL and AH-eGFP exhibit their natural phospholipid affinities in 'pure' and 'mixed' SLBs. a MscL or AH-eGFP is synthesized into the QCMD module on top of either a PC-rich EggPC SLB or a PE-rich E. coli lipids (ECL) SLB. The rightmost cartoon demonstrates the expected protein-lipid preferences of both proteins. b, c Adsorption kinetics of blank (P70a-T7rnap, 0.15 nM), AH-eGFP (P70a-T7rnap, 0.15 nM, T7p14-ah-egfp, 5 nM), and MscL (P70a-T7rnap, 0.15 nM, T7p14-mscL, 5 nM) synthesizing TXTL reactions in contact with an ECL SLB and an EggPC SLB respectively. d The frequency changes after

8~hours~of~incubating~either~blank~(P70a-T7rnap,~0.15~nM),~AH-eGFP~(P70a-T7rnap,~0.15~nM,~T7p14-ah-egfp,~5~nM),~or~MscL~(P70a-T7rnap,~0.15~nM,~T7p14-mscL,~5~nM)~TXTL~reactions~in~ECL–EggPC~Mixed~SLBs.~The~x-axis percentage indicates the concentration of EggPC~(and~ECL)~relative to the working concentration from Table S1. For example, 40% EggPC means that the Lipid-IPA mix contains 0.52 mM of EggPC phospholipids (40% of 1.3 mM) and 1.8 mM of ECL phospholipids (60% of 3 mM). All of the performed replicates are shown in the figure as individual data points.

Fig. S16). We also found that up to 10% of CL added to DOPE SLBs (Fig. S17) and in DOPC SLBs (Fig. S18a) did not produce nonspecific adsorption. The conditions for which nonspecific TXTL adsorption is not observed when both DOPG and CL are added to a DOPC SLB were also determined (Fig. 4c, Fig. S18b, c). As the concentration of CL in the lipid-IPA mix is increased, the amount of DOPG must be decreased to prevent nonspecific TXTL adsorption. The limit concentration of each of the tested added lipids was determined by following the same procedure (Table S1).

LactC2 is a mammalian signaling protein that binds specifically to PS phospholipids $^{53-55}$. When eGFP-LactC2 was synthesized (plasmid P70a-egfp-lactc2, 5 nM) on DPPS-EggPC SLBs, the shift in frequency Δf was linearly proportional to the amount of DPPS added to the IPA-EggPC-DPPS solution used to form the SLB (Fig. 4d, e, Fig. S19). Because more eGFP-LactC2 proteins were synthesized than DPPS sites in the SLB available for binding (Fig. S19c), this experiment shows that the amount of DPPS in an EggPC base SLB corresponds to the proportion of DPPS used to make the SLB.

The E. coli Min system produces oscillations on SLBs

To determine whether the TXTL-QCMD approach enables the sensing of membrane-based dynamical patterns on and greater than mesoscopic scales, we assayed the *E. coli* Min system that uses the inner membrane to position the division machinery via pole-to-pole dynamical oscillations⁵⁶. In vitro, the three Min proteins MinD, MinE, and MinC create a myriad of oscillatory patterns in vesicles⁵⁷⁻⁶⁰ and on SLBs⁶¹⁻⁶⁴. These patterns are the result of the reaction-diffusion dynamics of MinD and MinE. Upon ATP binding, MinD forms a dimer that binds to the inner bacterial membrane, which accelerates MinD recruitment at the membrane. MinE, which forms a dimer in the cytoplasm, binds to the MinD dimer at the membrane and catalyzes the hydrolysis of the ATP bound to MinD, effectively releasing MinD from the membrane⁶⁵⁻⁶⁸. While not essential for oscillations⁵⁷, MinC is known to bind to MinD and 'ride' the MinD waves⁶⁹. Visualizing MinCDE dynamical patterns requires fluorescent tagging of the proteins, which can interfere with the function of proteins⁷⁰.

First, we performed a set of experiments in which we only synthesized MinD onto the SLBs (10 nM linear P70a-minD). Previous studies have shown that anionic phospholipids, such as PG and CL, facilitate MinD interaction with the membrane⁷¹. We added either DOPG or CL to a DOPC SLB (Fig. 5a). No oscillations were observed on pure DOPC SLBs, while on the DOPG-DOPC and CL-DOPC SLBs the synthesized MinD-induced oscillations with 5.5 min and 6.7 min mean periods respectively in the first two hours (Fig. 5b). While MinC is not necessary for the Min oscillations⁵⁷, it has been reported that both MinD and MinE are required to form spatiotemporal patterns³. Proteomics of our TXTL system showed trace amounts of MinD, whereas MinE and MinC were not detected³⁵. Blank TXTL reactions never produced spontaneous oscillations on SLBs. The synthesized MinD oscillations exhibited two different modes: an unstable and large-amplitude mode in the first 2 hours of incubation and a stable smallamplitude mode for the rest of the reaction (Fig. S20a-c). In both modes, the period was around 10 minutes, longer than the 1 minute periods observed in confined systems such as E. coli bacteria⁵⁶ or micron-sized microwells⁷². The oscillations stopped with an increase in Δf of 2-10 Hz depending on the replicate, which we interpret as the final unbinding of MinD from the SLB after the ATP that fueled the oscillations has been depleted (Fig. S20d). Next, we determined the ranges of concentrations of DOPG and CL that can be added to either a pure DOPC (not found in E. coli membranes) or pure DOPE (major phospholipid in E. coli membranes) SLB for which the Min oscillations were observed when MinD (10 nM linear P70a-minD) only was synthesized in the TXTL reaction. To track the effect of DOPG concentrations, we counted the number of oscillations during the first mode (larger oscillations), and the duration of the oscillations during the second mode (smaller oscillations). In this series of experiments, the behavior of the initial mode was strongly dependent on the charge of the SLB, with both the DOPE and DOPC base SLBs exhibiting optimal DOPG molar ratios of 5-10% and 20-25%, respectively (Fig. 5c, Figs. S21, S22). The difference in the optimal DOPG percentage can be partially attributed to the difference in the availability of the positive charge in the zwitterionic headgroups of DOPE and DOPC. When the reaction duration was measured, we noticed that the DOPE SLBs were significantly more robust to variations in the DOPG concentration compared to the DOPC SLB (Fig. 5d, Figs. S23, S24). Similarly, as we increased the concentration of CL in the SLB, we observed an increase in the number of oscillations in the first 2 hours alongside the increase of oscillation lifetime for the DOPC SLB cases (Fig. 5e, f). Changes in the CL concentration in DOPE base SLB did not significantly affect the behavior of the pattern-forming reactions. Overall, the DOPE base SLB provided more robustness to lipid composition changes compared to the DOPC base SLBs for observing oscillations. When DOTAP, an artificial cationic lipid, was added to DOPC, DOPG-DOPC, DOPE, and DOPG-DOPE SLBs, the oscillations became weaker as the concentration of DOTAP increased (Figs. S25-S27). This shows that Min patterns are sensitive to the charges present in the SLB, with negative charges helping their formation, while positive charges inhibit oscillations. This result can be considered together with the fact that the E. coli inner membrane has a highly nonuniform density of PG and CL, with larger densities localized at the poles, especially for CL73-75. Min patterns in E. coli must be able to maintain oscillatory order in these locally different phospholipid compositions simultaneously, thus requiring the patterns to be robust to anionic phospholipid variation.

We co-synthesized either MinC or MinE with MinD in the presence of a DOPE-based SLB with 10% DOPG (Fig. 5g) to determine the effect of each on the MinD oscillations. In the presence of MinC (2 nM linear P70aminC), the period of the oscillations remained unchanged while their amplitude increased. Adding MinE in some of the reactions produced a doubling of the mass oscillation period (Fig. 5h), which is likely an oscillatory regime in which MinE is recruited by MinD on some regular distance as observed in previous MinDE SLB experiments⁶². This regime did not occur in all the MinDE experiments that we tested but revealed patterns that can exist on the sensor when both minD and minE were expressed at optimal concentrations. To determine the concentrations of P70a-minE for which the pattern-forming reaction is the longest, we performed a series of experiments in which the minD expressing DNA concentration was fixed (10 nM linear P70a-minD), while the concentration of the minE-expressing DNA was varied (linear P70a-minE). These minE DNA ranges were performed for the optimal DOPG concentrations of both the DOPE (10% DOPG) (Fig. S28) and DOPC (20% DOPG) (Fig. S29) base SLBs and for the pure ECL SLB (Fig. S30). The DOPG/DOPC SLB demonstrated a decay in the reaction time as the MinE-expressing DNA was increased in concentration. DOPG/DOPE and ECL SLBs demonstrated robustness to the MinE variation up to 0.1 nM of added P70a-minE and no prolonged oscillations with P70a-minE concentrations greater than 0.1 nM (Fig. 5i). These results support that PE phospholipids play an integral role in the robustness of Min patterns, and that PG is not the only critical headgroup for Min oscillations.

Natural membranes are crowded with many membrane proteins. To address the effect that molecular crowding has on the Min patterns, we added PEG5000-PE (PE phospholipid with a PEG moiety of molecular mass 5000 g/mol) at various concentrations into a DOPE SLB with 10% DOPG. We expressed both minD (10 nM linear P70a-minD) and minE (0.1 nM linear P70a-minE) at optimal concentrations in the QCMD module. As we increased the amount of PEG5000-PE in the SLB, we observed an increase in the amplitude of the early oscillations (Fig. 5j). Membrane molecular crowding accelerates the binding of MinD to the SLB, which can be reasoned by the fact molecular crowding facilitates the formation of MinD multimers 76-79. Molecular crowding decreased the total reaction duration and, in the 0.27% PEG5000-PE case, caused a 2-hour long transient disappearance of oscillations after the largeamplitude oscillations in the first hour. It is important to note that producing mass oscillations across the entire sensor requires that the MinD proteins collectively bind and unbind from the SLB in-phase and the transient disappearance of the oscillations might indicate that the

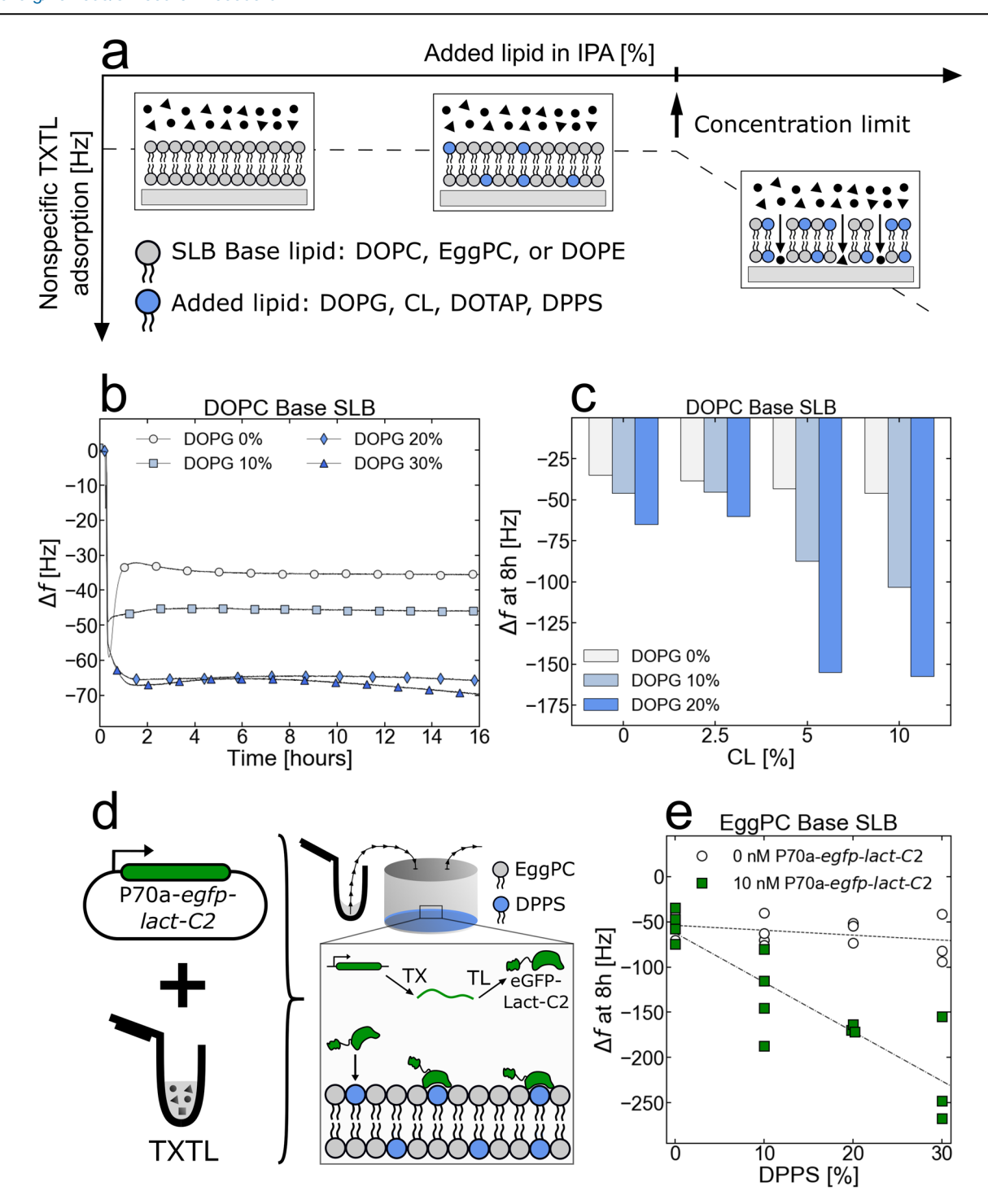


Fig. 4 | Phospholipids that cannot form stable SLBs in normal TXTL conditions can be added to 'base lipid' SLBs such as DOPC, EggPC, and DOPE SLBs.

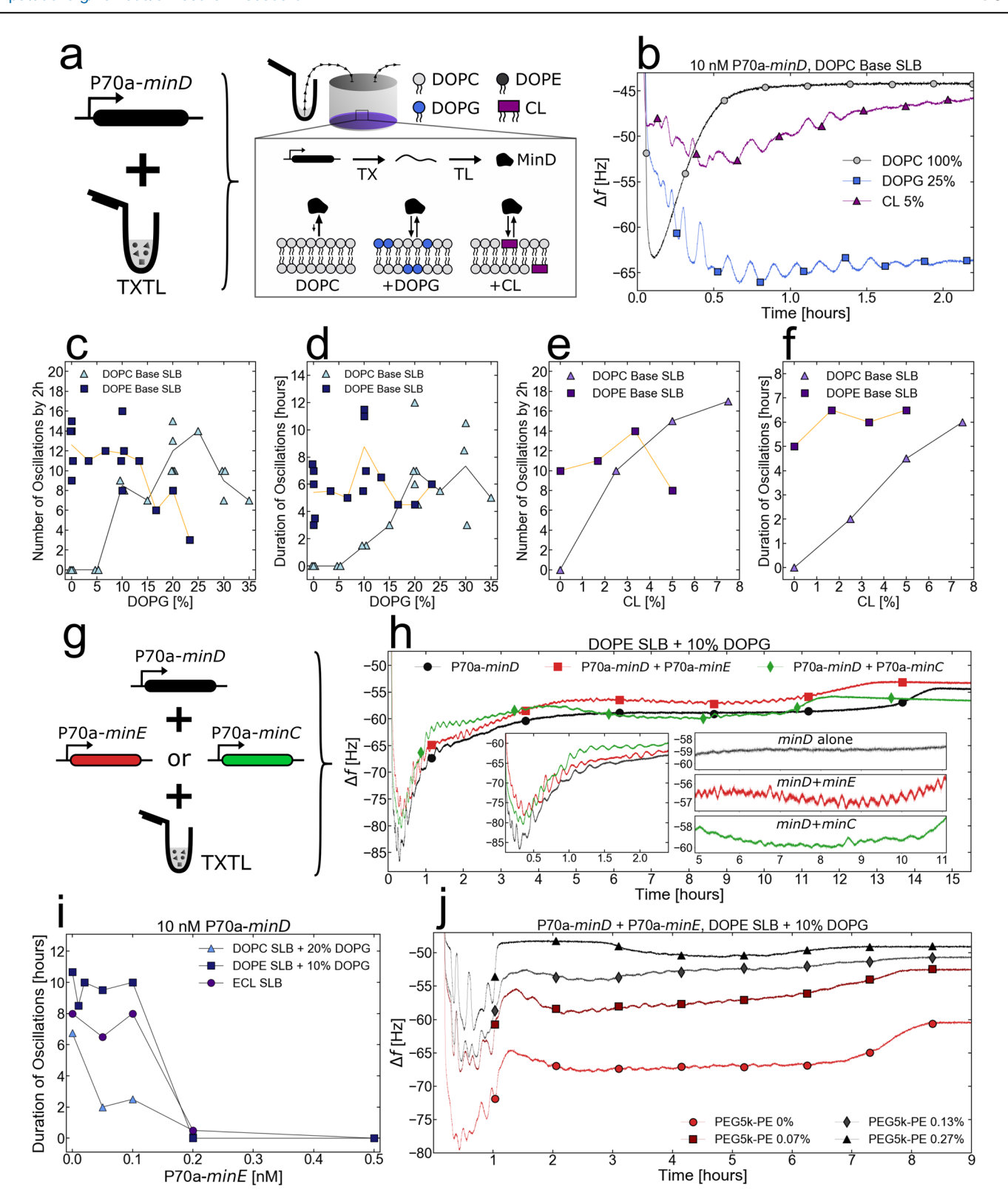
a Graphical illustration of the 'added lipid' concentration limit. Although phospholipids with various headgroups can be added to base SLBs, there is an observed limit to the added lipid concentration in the phospholipid-IPA mix before the SLBsensor system incurs nonspecific adsorption from a blank TXTL reaction.

b Adsorption kinetics of a blank TXTL reaction (P70a-T7rnap, 0.15 nM) in contact with DOPC/DOPG SLBs of different ratios. c The frequency change after 8 hours of a

blank TXTL reaction (P70a-*T7rnap*, 0.15 nM) incubating over a DOPC Base SLB as a function of added CL and DOPG. **d** Cell-free synthesis of eGFP-Lact-C2 (plasmid P70a-*egfp-lact-C2*, 5 nM) into the QCMD module. The in situ synthesized eGFP-Lact-C2 interacts with the DPPS phospholipids. **e** The frequency change after 8 h of either a blank (no DNA added) or eGFP-Lact-C2 (P70a-*egfp-lact-C2*, 5 nM) TXTL reaction being in contact with EggPC/DPPS SLBs fabricated with varying SALB DPPS concentrations. All of the collected experiments are shown in this plot as individual data points.

Min patterns are exhibiting energetically costly chaotic dynamics^{64,80,81} during which the MinDE system is assessing a more ordered state^{82,83}. This result emphasizes the strength of a tool (such as QCMD) that measures the total mass of a pattern-forming system. With the amplitude of the oscillations and the duration of the reactions, we could simultaneously assess the relative correlation lengths and the energy efficiency of

the pattern-forming system as a function of the randomly distributed SLB impurities (PEG) and morphogen concentrations. In future studies, it would be particularly interesting to see how adding impurities of controlled size and position on the sensor affects the energetic efficiency and coherence of MinCDE patterns or other membrane-associated dynamical pattern-forming systems.



Type II Zorya antiphage defense system is membrane associated Recently, a plethora of novel microbial defense systems have been discovered in genomic defense islands^{84,85} and in phages⁸⁶. Yet, their mechanisms of immunity largely remain unknown. One of such defense systems, type II Zorya, consists of ZorA, ZorB, and ZorE proteins that together protect their host *E. coli* from phage infection via an unknown mechanism⁸⁴. ZorA and ZorB are likely IIMPs, as they contain predicted membrane-interacting domains (Fig. 6a) and are homologous to the

flagellar motor proteins MotA and MotB⁸⁴. In a recent cryo-EM study, the type I ZorA and ZorB proteins have been studied using cryo-EM and it has been determined that ZorA has three transmembrane domains, while ZorB has one⁸⁷. Here, we demonstrated that the native Zorya system protects *E. coli* ATCC 8739 against phages T7 and PhiX174 (Fig. S31a). However, tagging the individual Zorya proteins for determining their localization and for subsequent purification disrupted their protective function (Fig. S31b–d), making this novel defense system particularly challenging to study.

Fig. 5 | In situ TXTL synthesis of Min proteins induces coherent long-range mass oscillations across the SLB-Sensor system. a Cell-free synthesis of MinD (linear P70a-minD) into the QCMD modules on top of SLBs. The cartoon shows a very simplified model of the synthesized MinD binding kinetics when the reaction is in contact with either a pure DOPC SLB, a DOPC/DOPG SLB, or a DOPC/CL SLB.

b Adsorption kinetics of MinD with either a pure DOPC SLB, a DOPC/DOPG SLB, or a DOPC/CL SLB. The curves are labeled with a few symbols, the lines are experimental points. c Number of oscillation peaks within the first 2 hours as a function of the relative DOPG concentration during SALB for a DOPE and DOPC Base SLB. d Duration of oscillations as a function of the relative DOPG concentration during SALB for a DOPE and DOPC Base SLB. e Number of oscillation peaks within the first 2 hours as a function of the relative CL concentration during SALB for a DOPE and DOPC Base SLB. f Duration of oscillations as a function of the relative CL concentration during SALB for a DOPE Base SLB. f Duration of oscillations as a function of the relative CL concentration during SALB for a DOPE Base SLB. g Cell-free

synthesis of MinD with either MinE (linear P70a-minE) or MinC (linear P70a-minC) into the QCMD modules on top of SLBs. **h** Adsorption kinetics of MinD (P70a-minD, 10 nM), MinDE (P70a-minD, 10 nM and P70a-minE, 0.1 nM), and MinCD (P70a-minD, 10 nM and P70a-minC, 5 nM), on a 10% mol ratio DOPG/DOPE SLB. The left inlet shows a close-up of the oscillations during the first 2.4 hours. The right inlet shows a close-up of the oscillations between t = 5 hours and t = 11 hours. The curves are labeled with a few symbols, the lines are experimental points. **i** Duration of oscillations as a function of P70a-minE concentration in the TXTL reaction for a DOPG/DOPE SLB, a DOPG/DOPC SLB, and an E. coli lipids (ECL) SLBs. **j** Adsorption kinetics of a MinDE (P70a-minD, 10 nM and P70a-minE, 0.1 nM) on a 10% mol ratio DOPG/DOPE SLB with a range of PEG5k-PE added during SALB. The curves are labeled with a few symbols, the lines are experimental points. Each measurement is represented as an individual data point.

To overcome these limitations, we used the TXTL/QCMD approach to unravel the interactions of the Zorya proteins with lipid bilayers and to shed light on its mechanism of immunity.

ZorA, ZorB, and ZorE were synthesized through the T7 transcriptional activation cascade (Fig. 6a). The interaction of ZorA with SLBs was enhanced when CL was added to DOPE SLBs (Fig. 6b). However, adding DOPG to DOPE SLBs did not result in improved ZorA interaction (Fig. S32). Expectedly, ZorA did not interact with a DOPC SLB suggesting a preference for bacterial lipids (Fig. S33). When ZorA and ZorB were synthesized together, they produced a larger QCMD frequency shift than either of them alone, which indicates that they form a complex at the membrane (Fig. 6c, d). This is consistent with the cryo-EM result of type I ZorA and ZorB forming 5:2 ZorAB complexes similar to MotAB⁸⁷, but additionally demonstrates that each protein can be incorporated in the bilayer on its own. On an ECL SLB, ZorA produces a small frequency shift with or without ZorB (Fig. S34). The kinetics of such shift is fast, indicating that the concentration of CL in the ECL SLB is small compared to the one tested in DOPE SLBs.

Although ZorE is not predicted to have membrane-interacting domains⁸⁴, ZorE protein interacted with a pure DOPE SLB but not with a pure DOPC SLB (Fig. 6e). As with ZorAB, ZorE interacted more strongly with a DOPE/CL SLB than a pure DOPE SLB (Fig. 6f). To determine the strength of the interaction with the SLBs, we flushed Tris NaCl though the QCMD chamber above the SLBs at the end of the TXTL reaction. We observed that the ZorE frequency change was preserved only when CL was present in the SLB. In the condition with a pure DOPE SLB, it appears that all the synthesized ZorE proteins interacting with the SLB have been removed during flush (Fig. S35). This suggests that ZorE interacts weakly on the surface with a pure DOPE membrane but interacts irreversibly with membranes containing cardiolipin. Finally, the co-synthesis of ZorE with ZorAB did not result in a stronger interaction with a DOPE/CL SLB than ZorAB alone (Fig. 6g).

Overall, our results suggest that the ZorABE proteins likely localize at the poles of *E. coli* where cardiolipin is most dense (Fig. 6h). ZorE likely diffuses along the surface of the inner membrane and associates with the membrane upon finding cardiolipin-rich domains. Considering that Zorya protects *E. coli* from T7 and that T7 preferably binds *E. coli* cells at the poles⁸⁸, it is possible that the ZorA and ZorB proteins disrupt the membrane potential that T7 uses to inject the first segment of its genome into the cell⁸⁹. Alternatively, ZorAB may sense membrane depolarization caused by T7 infection and activate ZorE, which contains a predicted HNH domain (Fig. 6a), as a putative downstream effector to enact immunity.

Discussion

The QCMD-TXTL approach for characterizing IIMPs' interactions with lipid bilayers has several advantages compared to the current methods (Table 1). The approach is fast, non-disruptive, and reproducible. It enables assaying single or concurrently in situ synthesized IIMPs on membranes with arbitrarily complex lipid compositions on physical scales that tolerate the formation of large dynamical patterns. The QCMD-TXTL method proves to be useful for unraveling basic underpinning details about how

IIMPs interact with different lipids and assemble at or into membranes. This method also provides information for engineering synthetic membranes capable of hosting IIMPs that naturally reside in different lipid environments. Taken altogether, these features make the QCMD-TXTL approach a highly favorable method for characterizing IIMPs membranes interactions. We anticipate that it could be useful for the bottom-up engineering of systems such as synthetic cells^{43,90–93}

In the field of *E. coli* cell-free expression systems, it is established that *E.* coli inner membrane proteins integrate into lipid membranes without secretion mechanisms via a process coupled to translation 94,95. This assumption is supported by the fact that IIMPs also integrate into lipid membranes when they are synthesized with the PURE system deprived of any secretion components⁹⁶. In lysate-based TXTL systems, it is not clear whether soluble parts of the secretion mechanism present in the lysate (e.g., SecA is present in E. coli lysates³⁵) help IIMPs integrate into membranes. In this work, we used an E. coli TXTL system, commercially available under the name of myTXTL (Arbor Biosciences). Other TXTL systems could be used if protein synthesis yields are large enough, which should be on the order of at least 100 nM based on our measurements and estimations (Fig. S11). We anticipate that most of the IIMPs from bacteria could be assayed using TXTL systems from E. coli or other bacteria, many of which have been reported in the literature⁹⁷. Studying IIMPs from higher organisms with the QCMD-TXTL method remains to be investigated and is likely to be dependent on the complexity of the post-translation modifications of each IIMP. The scope of the IIMPs assayed in this work was chosen to demonstrate (i) that the QCMD-TXTL method corroborates many observations previously reported, (ii) and that novel insights and discoveries into the IIMPs-membranes' interactions can be rapidly obtained. For instance, deciphering the Zorya system supports that many other novel defense systems could be deciphered using this approach.

The QCMD provides two signals, the change in frequency and the dissipation. In our work, we only used the change in frequency change Δf as it is proportional to the mass added to the SLB. The dissipation term gives information about the viscoelastic changes of the lipid bilayer. As opposed to the frequency change, however, the dissipation term is much more difficult to understand and has not been subject to a comprehensive characterization in the literature. Extensive studies based on model systems would be necessary to make dissipation a truly interpretable term.

The preparation of the SLBs was performed using SALB in all of our experiments. Other works have used standard characterization techniques to demonstrate that SALB results in homogenous and fluid SLBs without any pervasive defects, such as the abundant micelles on the sensor surface instead of an SLB^{29,31,98,99}. It is critical that the concentration of the lipids used during SALB is above the minimal concentration for complete coverage for TXTL. Using a SALB concentration two-fold larger than the minimal concentration does not appear to affect the kinetics of the TXTL experiments (Fig. 2c–e). However, previous works have shown that using lipid concentrations that are 16-fold larger than the minimum results in the formation of lower-quality SLBs likely due to the aggregation of micelles⁹⁸, which accentuates the importance of determining the minimal

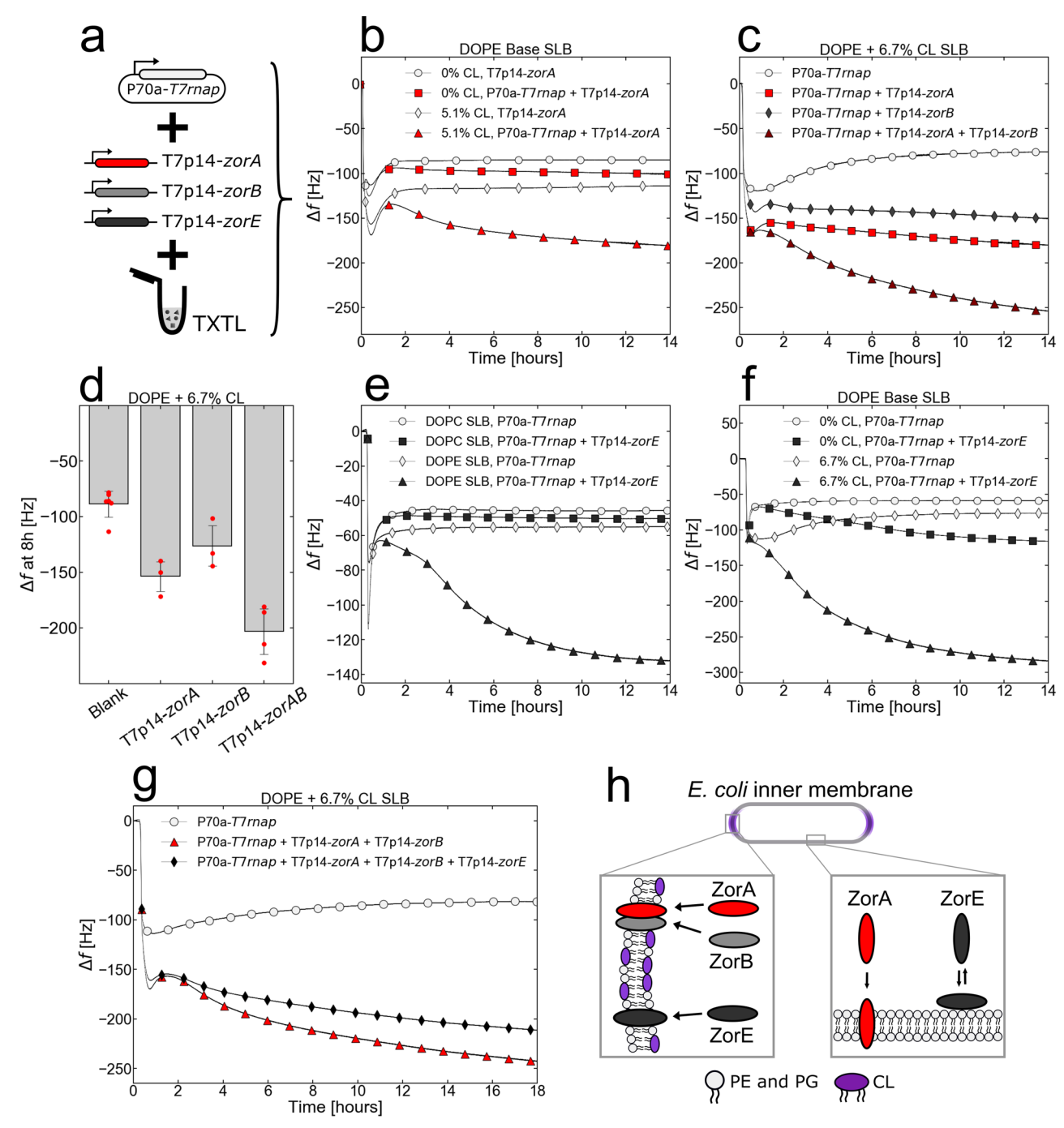


Fig. 6 | Type II Zorya defense proteins interact with cardiolipin-rich lipid membranes. a ZorA, ZorB, and ZorE were synthesized via the T7 transcriptional activation cascade (plasmid P70a-*T7rnap*, 0.15 nM, linear T7p14-*zorA*, T7p14-*zorB*, T7p14-*zorC*, 10 nM). The TXTL reactions were immediately pushed into the QCMD modules with SLBs on the sensor. **b** Adsorption kinetics of the blank (P70a-*T7rnap*, 0.15 nM) and ZorA (P70a-*T7rnap*, 0.15 nM and T7p14-*zorA*, 10 nM) conditions with either a pure DOPE or DOPE + 5.1% CL SLBs. **c** The adsorption kinetics of the blank (P70a-*T7rnap*, 0.15 nM), ZorA alone (P70a-*T7rnap*, 0.15 nM and T7p14-*zorA*, 10 nM), ZorB alone (P70a-*T7rnap*, 0.15 nM and T7p14-*zorB*, 10 nM), and ZorA and ZorB together (P70a-*T7rnap*, 0.15 nM, T7p14-*zorA*, 10 nM and T7p14-*zorB*, 10 nM) with a DOPE + 6.7% CL SLB. **d** The frequency changes after 8 hours of TXTL incubation, for the cases described in **c**. The bar plot level and error bars represent the mean and standard deviation of at least 3 replicates. **e** The

adsorption kinetics of the blank (P70a-*T7rnap*, 0.15 nM) and ZorE (P70a-*T7rnap*, 0.15 nM and T7p14-*zorE*, 10 nM) conditions with either a pure DOPC or pure DOPE SLBs. **f** The adsorption kinetics of the blank (P70a-*T7rnap*, 0.15 nM) and ZorE (P70a-*T7rnap*, 0.15 nM and T7p14-*zorE*, 10 nM) conditions with either a pure DOPE or DOPE + 6.7% CL SLBs. **g** The adsorption kinetics of the blank (P70a-*T7rnap*, 0.15 nM), ZorAB (P70a-*T7rnap*, 0.15 nM, T7p14-*zorA*, 10 nM, and T7p14-*zorB*, 10 nM), and ZorABE (P70a-*T7rnap*, 0.15 nM, T7p14-*zorA*, 10 nM, T7p14-*zorB*, 10 nM, and T7p14-*zorE*, 5 nM) conditions with a DOPE + 6.7% CL SLB. **h** An illustration of the hypothetical localization of the Zorya proteins in the host *E. coli* inner membrane. All Zorya proteins preferentially interact with the CL-rich polar regions of the inner membrane. In addition, ZorA likely has a weak interaction with the equatorial region of the inner membrane and ZorE likely has a reversible interaction with the equatorial region of the inner membrane.

Table 1 | Comparison of techniques for cell-free synthesized IIMP characterization

	Techniques for characterizing IIMPs with TXTL				
	SDS PAGE	Microscopy	AFM	SPR	QCM ^a
Label-free	✓	Χ	✓	✓	✓
Real-time TXTL	Х	√ 106	X	√ 107	1
Spatially resolved	Х	√ ¹⁰⁸	✓ ¹⁰⁹	X ^b 110	Х
IIMPs interactions	✓ ¹¹¹	√ ¹¹²	✓ ¹¹³	√ 114	1
SLB complexity ^c	√ 31	✓31	√ 31	√ 31,115	1
Sensitivity	100 ng ¹¹⁶	SM ^{d117}	SM ^{d118}	1 ng ¹¹⁹	1 ng
Penetration depth	N/A	N/A	10 nm ¹²⁰	200 nm ¹²¹	250 nm ¹²²
Preparation time	2 d ¹²³	3 h ¹²⁴	1 d ²³	1 d ^{e 125}	3 h

^aThe information for QCMD is from this study.

concentration for each lipid type used in SALB. We demonstrated that blank TXTL reactions (no DNA added) resulted in replicable kinetics that could be routinely used as negative controls for lipid-protein interaction experiments. It would be of interest to also understand what exactly occurs between the biomolecules in the TXTL reaction and the lipid bilayer. We have demonstrated that the lipids are not being expelled from the SLB at a noticeable rate during TXTL incubation (Fig. S13), but additional measurements that could determine the packing and curvature of the SLB would assist in understanding how lipid bilayers respond to insertion or binding of TXTL biomolecules and TXTL-synthesized IIMPs. Also, the characterization of the electrostatic interactions between TXTL and SLBs is of significance, considering that the addition of charged lipids changed the kinetics of blank TXTL reactions in the QCMD.

We focused our work on using planar SLBs formed on the QCMD sensor. We showed that this configuration enables probing IIMPs' interactions with membranes over a wide variety of lipids, including lipids localized in vivo, like cardiolipin. This configuration does not enable looking at specific variables found in living systems, such as membrane curvature for example. Instead of making flat SLBs, vesicles could be attached to the sensor, which has been done previously without TXTL 100. We anticipate that dynamical patterns, such as the Min system, would be harder to achieve in this configuration, which would also require passivating the sensor to prevent nonspecific adsorption. Alternatively, SLBs can be fabricated on top of silica nanoparticles of controlled radii to mimic membrane curvature 101.

Methods Reagents

All the phospholipids were obtained from Avanti Polar Lipids in powder form. The phospholipids were dissolved in IPA (isopropyl alcohol, ThermoFisher Scientific, A416S-4) at the following stock concentrations: EggPC -100 mg/mL (840051 P), DOPC (1,2-dioleoyl-sn-glycero-3-phosphocholine)—100 mg/mL (850375 P), ECL (100500 P)—20 mg/mL, DOPE (1,2dioleoyl-sn-glycero-3-phosphoethanolamine)—25 mg/mL (850725 P), DOPG (1,2-dioleoyl-sn-glycero-3-phospho-(1'-rac-glycerol))—10 mg/mL (840475 P), CL (1',3'-bis[1,2-distearoyl-sn-glycero-3-phospho]-glycerol)— 5 mg/mL (710334 P), DOTAP (1,2-dioleoyl-3-trimethylammonium-propane)—10 mg/mL (890890 P), DPPS (1,2-distearoyl-sn-glycero-3-phospho-L-serine) - 50 mg/mL (840029 P), PEG5000-PE (1,2-dipalmitoyl-snglycero-3-phosphoethanolamine-N-[methoxy(polyethylene glycol)-5000]) -0.5 mg/mL (880200 P). To prepare the working IPA-lipid mixes, an appropriate volume of the stock phospholipids was diluted in IPA to the desired concentration, vortexed at medium-high speed for ten seconds, and immediately used for SALB.

Oligos

All of the following oligos have been ordered from IDT.

 $\label{eq:minC-s1} \mbox{MinC-s1:} \ \ \mbox{CTTTAAGAAGGAGGTACCAatgTCAAACACGCC} \\ \mbox{AATCGAG}$

 $\label{lem:minC-as1:} MinC-as1: CGGCGGGCTTTGCTCGAGTTTGACCGTTCAACCGTTAAATtga$

 $\label{lem:minD-s1:minD-s1:} MinD-s1: CTTTAAGAAGGAGGGTACCAatgGCACGCATTAT\\ TGTTGTTACTTCG$

MinD-as1: CGGCGGGCTTTGCTCGAGttaTCCTCCGAACAAGCGTTTGA

MinE-s1: CTTTAAGAAGGAGGGTACCAatgGCATTACTCGAT TTCTTTCTCTCG

MinE-as1: CGGCGGGCTTTGCTCGAGttaTTTCAGCTCTTCTGC
TTCCGG

ZorA-s1: CTTTAAGAAGGAGAGGTACCAatgttagcgcagctttttgagc ZorA-as1: CGGCGGGCTTTGCTCGAGgatcgattaccctcgatgtttattagcag ZorB-s1: CTTTAAGAAGGAGGTACCAatggataagattatagggaaaca attaccta

 $Zor B-as 1: \ CGGCGGGCTTTGCTCGAGttactcctgaataatctttctaatctgcaactcg$

 $Zor E-s1: \ CTTTAAGAAGGAGGTACCA at gaa attatct at cga cattt caa gaactt at t caa$

ZorE-as1: CGGCGGGCTTTGCTCGAGttacaattttgctggcgtaaaggct T7p14-UTR1-s1: GATCGAGATCTCGATCCCGCGAAATTAATA CGACTCACTATAGGGAGACCACAACG

 $\label{eq:GTTTCCTTAGAAATAATTTTGTTTAACTTTAAGAAGGA-GAGGTACCAATG} GAGGTACCAATG$

P70a-UTR1-s1: GTTCCGCTGGGCATGCTGAGCTAACACCGTG CGTGTTGACAATTTTACCTCTGGCGG

TGATAATGGTTGCAGCTAGCAATAATTTTGTTTAACTTTAA GAAGGAGGGTACCA

ATC

T500-as1: GTCGACACAGAAAAGCCCGCCTTTCGGCGGGCTTTGCTCGAG

Cell-free transcription-translation

Cell-free gene expression was carried out using an *E. coli* TXTL system described previously²⁷, with one modification. We used the strain BL21- Δ recBCD Rosetta2 in which the recBCD gene set is knocked out to prevent the degradation of linear DNA¹⁰². The preparation and usage of the TXTL system were the same as reported before^{27,103}. Briefly, *E. coli* cells were grown in a 2xYT medium supplemented with phosphates. Cells were pelleted, washed, and lysed with a cell press. After centrifugation, the supernatant was recovered and preincubated at 37 °C for 80 min. After a second centrifugation step, the supernatant was dialyzed for 3 h at 4 °C. After final centrifugation; the supernatant was aliquoted and stored at -80 °C. The TXTL reactions comprised the cell lysate, the energy and amino acid mixtures, maltodextrin (30 mM) and ribose (30 mM), magnesium (2–5 mM) and potassium

^bSPR can have spatial resolution, but this modality is not used for IIMP characterization.

The supported lipid bilayer (SLB) complexity refers to whether any type of lipid compositions can be achieved.

dSingle molecule (SM).

Potentially, the preparation time of SPR can be reduced to the same time as QCM experiments, but no studies utilizing the SALB-TXTL approach with SPR have been reported.

(50–100 mM), PEG8000 (1–2 wt%), water and the DNA to be expressed. The TXTL reactions were incubated at 30 °C in QCMD chambers (40 μL reactions). The TXTL reactions were incubated at 30 °C on 96 well plates (2 μL reactions) for the measurement of the kinetics of deGFP synthesis.

Reporter protein quantification

deGFP, AH-eGFP, and LactC2-eGFP were quantified on an Agilent Biotek H1M plate reader using a calibration curve. The calibration curve was determined using pure eGFP (Cell Biolabs, STA-201) diluted with an empty TXTL reaction at various concentrations.

DNA preparation

All the DNA sequences are reported in the Supplementary Data 2. We either used plasmids or linear DNAs. DNAs were obtained either by PCR or purchased (Twist Biosciences, IDT). DNA stock solutions were quantified with a spectrophotometer (ThermoFisher Scientific, NanoDrop 2000). Genes were expressed either from the strong *E. coli* promoter P70a or the T7 transcriptional activation cascade^{25–27}.

QCMD sensors and modules preparation

A QSense Analyzer (Biolin Scientific, Gothenburg, Sweden) was used for the experiments. The QSense Analyzer has four channels that can be used independently and concurrently. The preparation of the instrument for an experiment consisted of a 400 $\mu L/min$ flush of at least 20 mL of a 1% wt SDS solution, then 20 mL of autoclaved deionized water, and then air until the tubing was empty. After the four QCMD modules were dried, they were disconnected from the QSense Analyzer mount and opened. After removing the sensors (Biolin Scientific, QSX303), the QCMD modules were dried with nitrogen. The sensors were dried with nitrogen as well and plasma-cleaned (Harrick Plasma, PDG-32) at low RF power for 10 minutes. The plasma-cleaned sensors were then reinserted into the dry QCMD modules. The QCMD modules were closed and connected to the QSense Analyzer mount. Using the QSoft software, the bare sensors were calibrated and the QCMD modules were ready.

QCMD SLB preparation and TXTL reaction

The QCMD modules were maintained at 29 °C throughout the whole experiment. First, a Tris NaCl Buffer (10 mM Tris, 150 mM NaCl, 7.5 pH) was flushed at 100 μ L/min through all the modules until the resonance frequency of the sensors stabilized, which took 40–60 minutes. Next, IPA was flushed until signal stabilization, which takes around 20 minutes and produces a change in frequency of ~ -75 to -80 Hz. We then flushed the IPA-lipid mixes at 100 μ L/min for 20 minutes. After stabilization, the signal varies by -5 to -10 Hz, depending on the lipids used, usually within 5–10 minutes, except for ECL which requires the full duration of the flush. Next, we flushed the Tris NaCl buffer at 100 μ L/min until signal stabilization to complete the formation of the SLB. This step takes up to 40 minutes and produces a change of frequency of the order of 30–50 Hz, depending on the lipids used. Finally, we pushed the TXTL reactions (up to four different conditions, one per module) at 25 μ L/min. The pumps were stopped and the TXTL reactions were incubated in contact with the SLB-sensor system for 3–20 h.

QCMD data analysis

The analysis of QSense Analyzer data was performed on the 7th overtone of the resonance of the sensor due to its lowest sensitivity to variations in the mounting of the sensor, following the manufacturer's recommendation. The frequency at the end of the second Tris NaCl flush during the SLB preparation was reset as $\Delta f = 0$. The frequency output of the seventh harmonic was divided by 7 to reflect the effect the TXTL reactions had on the fundamental frequency changes of the sensor. Example python code: https://zenodo.org/records/12752763.

Zorya knockout mutants

Zorya genes *zorABE* were deleted from the genome of *Escherichia coli* DSM 1576 (ATCC 8739) using lambda red recombination as described¹⁰⁴. The

genes were deleted in the region of the chromosome between 4,265,744 and 4,269,528 bp (NCBI Ref. CP000946).

Plaque assay

Double layer plaque assay was used to determine phage titers. *E. coli* were cultivated in LB medium until the OD $_{600}$ of 0.55 before centrifugation. The pellet was resuspended in cold LB, mixed with soft agar, and the appropriate phage dilution. This mixture was added to an agar plate and solidified. Subsequently, phage dilutions were directly spotted on the plate. The plates were incubated at 37 °C until visible plaques developed within 4 to 18 hours.

Statistics and reproducibility

The QCMD collects four measurements at a time. Because of this speed of new data collection, we prioritized the replication of the most critical experiments. For these experiments, we collected at least three independent replicates and either showed each data point and, in some cases, also the mean and standard deviation of the replicates. For the experiments that served to assist the main message we sometimes did not collect replicates due to the throughput of the QCMD. However, those experiments are meant to identify trends and thus are always presented as comparisons to data for which replicates have been collected (example: Fig. 4b).

Reporting summary

Further information on research design is available in the Nature Portfolio Reporting Summary linked to this article.

Data availability

The data used in Figs. 2–6 and Supplementary Figs. S1–S35 are provided as source data files in Supplementary Data 1. Plasmids and strains used in this study are listed in Supplementary Data 2. All experimental data are stored on UMN DRUM and can be accessed here: https://hdl.handle.net/11299/264081.

Code availability

The data analysis of the QCMD data in this study were performed with Python. The analysis is the same for all QCMD files and an example of code can be accessed on Zenodo (https://zenodo.org/records/12752763)¹⁰⁵.

Received: 26 January 2024; Accepted: 6 August 2024; Published online: 17 August 2024

References

- Sukharev, S. I., Blount, P., Martinac, B. & Kung, C. Mechanosensitive channels of escherichia coli: the MscL gene, protein, and activities. *Annu. Rev. Physiol.* 59, 633–657 (1997).
- Saidijam, M. et al. Active membrane transport and receptor proteins from bacteria. Biochem. Soc. Trans. 33, 867–872 (2005).
- Wettmann, L. & Kruse, K. The Min-protein oscillations in Escherichia coli: an example of self-organized cellular protein waves. *Philos. Trans. R. Soc. B Biol. Sci.* 373, 20170111 (2018).
- Errington, J., Daniel, R. A. & Scheffers, D.-J. Cytokinesis in bacteria. *Microbiol. Mol. Biol. Rev.* 67, 52–65 (2003).
- Shi, H., Bratton, B. P., Gitai, Z. & Huang, K. C. How to build a bacterial cell: MreB as the foreman of E. coli construction. *Cell* 172, 1294–1305 (2018).
- Thorn, K. Genetically encoded fluorescent tags. Mol. Biol. Cell 28, 848–857 (2017).
- Litschel, T. & Schwille, P. Protein reconstitution inside giant unilamellar vesicles. Annu. Rev. Biophys. 50, 525–548 (2021).
- Skrzypek, R., Iqbal, S. & Callaghan, R. Methods of reconstitution to investigate membrane protein function. *Methods* 147, 126–141 (2018).
- Garenne, D. & Noireaux, V. Cell-free transcription-translation: engineering biology from the nanometer to the millimeter scale. Curr. Opin. Biotechnol. 58, 19–27 (2019).

- Silverman, A. D., Karim, A. S. & Jewett, M. C. Cell-free gene expression: an expanded repertoire of applications. *Nat. Rev. Genet.* 21, 151–170 (2020).
- 11. Garenne, D. et al. Cell-free gene expression. *Nat. Rev. Methods Prim.* **1**, 1–18 (2021).
- Schwarz, D. et al. Preparative scale cell-free expression systems: New tools for the large scale preparation of integral membrane proteins for functional and structural studies. *Methods* 41, 355–369 (2007).
- Lyukmanova, E. N. et al. Lipid–protein nanodiscs for cell-free production of integral membrane proteins in a soluble and folded state: Comparison with detergent micelles, bicelles and liposomes. *Biochim. Biophys. Acta. Biomembr.* 1818, 349–358 (2012).
- Kai, L. et al. Co-translational stabilization of insoluble proteins in cellfree expression systems. Methods Mol. Biol. 1258, 125–143 (2015).
- Mezhyrova, J., Mörs, K., Glaubitz, C., Dötsch, V. & Bernhard, F. Applications of cell-free synthesized membrane protein precipitates. *Methods Mol. Biol.* 2406, 245–266 (2022).
- Roos, C. et al. Co-translational association of cell-free expressed membrane proteins with supplied lipid bilayers. *Mol. Membr. Biol.* 30, 75–89 (2013).
- Katzen, F., Peterson, T. C. & Kudlicki, W. Membrane protein expression: no cells required. *Trends Biotechnol.* 27, 455–460 (2009).
- Rajesh, S., Knowles, T. & Overduin, M. Production of membrane proteins without cells or detergents. N. Biotechnol. 28, 250–254 (2011).
- Li, M. J., Atkins, W. M. & McClary, W. D. Preparation of lipid nanodiscs with lipid mixtures. Curr. Protoc. Protein Sci. 98, e100 (2019).
- Stano, P. Gene expression inside liposomes: from early studies to current protocols. *Chem. Eur. J.* 25, 7798–7814 (2019).
- Rodahl, M. & Kasemo, B. A simple setup to simultaneously measure the resonant frequency and the absolute dissipation factor of a quartz crystal microbalance. Rev. Sci. Instrum. 67, 3238–3241 (1996).
- Kanazawa, K. Keiji & Gordon, J. G. Frequency of a quartz microbalance in contact with liquid. *Anal. Chem.* 57, 1770–1771 (1985).
- Chalmeau, J., Monina, N., Shin, J., Vieu, C. & Noireaux, V. α-Hemolysin pore formation into a supported phospholipid bilayer using cell-free expression. *Biochim. Biophys. Acta Biomembr.* 1808, 271–278 (2011).
- Coutable, A. et al. A comparative study of α-hemolysin expression in supported lipid bilayers of synthetic and enriched complex bacterial lipid. Bio. Nano. Science 4, 104–110 (2014).
- Garenne, D., Thompson, S., Brisson, A., Khakimzhan, A. & Noireaux,
 V. The all-E. coliTXTL toolbox 3.0: new capabilities of a cell-free synthetic biology platform. Synth. Biol. 6, ysab017 (2021).
- Shin, J.& Noireaux, V. An E. coli cell-free expression toolbox: application to synthetic gene circuits and artificial cells. ACS Synth. Biol. 1, 29–41 (2012).
- Garamella, J., Marshall, R., Rustad, M. & Noireaux, V. The All E. coli TX-TL toolbox 2.0: a platform for cell-free synthetic biology. ACS Synth. Biol. 5, 344–355 (2016).
- Contreras, F.-X., Ernst, A. M., Wieland, F. & Brügger, B. Specificity of intramembrane protein–lipid interactions. *Cold Spring Harb. Perspect. Biol.* 3, a004705 (2011).
- Tabaei, S. R., Choi, J.-H., Haw Zan, G., Zhdanov, V. P. & Cho, N.-J. Solvent-assisted lipid bilayer formation on silicon dioxide and gold. *Langmuir* 30, 10363–10373 (2014).
- Tabaei, S. R. et al. Biomembrane fabrication by the solvent-assisted lipid bilayer (SALB) method. J. Vis. Exp. e53073, https://doi.org/10. 3791/53073. (2015).
- Ferhan, A. R. et al. Solvent-assisted preparation of supported lipid bilayers. *Nat. Protoc.* 14, 2091–2118 (2019).
- Rowlett, V. W. et al. Impact of membrane phospholipid alterations in Escherichia coli on cellular function and bacterial stress adaptation.
 J. Bacteriol. 199, https://doi.org/10.1128/jb.00849-16 (2017).
- Gillissen, J. J., Tabaei, S. R. & Cho, N. J. A phenomenological model of the solvent-assisted lipid bilayer formation method. *Phys. Chem. Chem. Phys.* 18, 24157–24163 (2016).

- Bonet, N. F., Cava, D. G. & Vélez, M. Quartz crystal microbalance and atomic force microscopy to characterize mimetic systems based on supported lipids bilaver. Front. Mol. Biosci. 9, 935376 (2022).
- Garenne, D., Beisel, C. L. & Noireaux, V. Characterization of the all-E. coli transcription-translation system myTXTL by mass spectrometry. *Rapid Commun. Mass Spectrom.* 33, 1036–1048 (2019).
- Galdiero, S. & Gouaux, E. High resolution crystallographic studies of α-hemolysin–phospholipid complexes define heptamer–lipid head group interactions: Implication for understanding protein–lipid interactions. *Protein Sci.* 13, 1503–1511 (2004).
- Noireaux, V. & Libchaber, A. A vesicle bioreactor as a step toward an artificial cell assembly. *Proc. Natl Acad. Sci.* 101, 17669–17674 (2004).
- Song, L. et al. Structure of staphylococcal α-hemolysin, a heptameric transmembrane pore. Science 274, 1859–1865 (1996).
- Sukharev, S. I., Schroeder, M. J. & McCaslin, D. R. Stoichiometry of the large conductance bacterial mechanosensitive channel of E. coli. a biochemical study. *J. Membr. Biol.* 171, 183–193 (1999).
- 40. Berube, B. J. & Wardenburg, J. B. Staphylococcus aureus α-toxin: nearly a century of intrigue. *Toxins* **5**, 1140–1166 (2013).
- 41. Ishihama, Y. et al. Protein abundance profiling of the Escherichia coli cytosol. *BMC Genomics* **9**, 102 (2008).
- 42. Hung, W.-C., Lee, M.-T., Chen, F.-Y. & Huang, H. W. The condensing effect of cholesterol in lipid bilayers. *Biophys. J.* **92**, 3960–3967 (2007).
- Garenne, D. & Noireaux, V. Membrane functions genetically programmed in synthetic cells: a barrier to conquer. *Curr. Opin. Syst. Biol.* 24, 9–17 (2020).
- Margheritis, E., Kappelhoff, S. & Cosentino, K. Pore-forming proteins: from pore assembly to structure by quantitative singlemolecule imaging. *Int. J. Mol. Sci.* 24, 4528 (2023).
- Thompson, J. R., Cronin, B., Bayley, H. & Wallace, M. I. Rapid assembly of a multimeric membrane protein pore. *Biophys. J.* 101, 2679–2683 (2011).
- Powl, A. M., East, J. M. & Lee, A. G. Importance of direct interactions with lipids for the function of the mechanosensitive channel MscL. *Biochemistry* 47, 12175–12184 (2008).
- Grage, S. L. et al. Bilayer-mediated clustering and functional interaction of MscL channels. *Biophys. J.* 100, 1252–1260 (2011).
- Flegler, V. J., Rasmussen, T. & Böttcher, B. How functional lipids affect the structure and gating of mechanosensitive MscS-like channels. *Int. J. Mol. Sci.* 23, 15071 (2022).
- Sohlenkamp, C. & Geiger, O. Bacterial membrane lipids: diversity in structures and pathways. FEMS Microbiol. Rev. 40, 133–159 (2016).
- Akutsu, H. Structure and dynamics of phospholipids in membranes elucidated by combined use of NMR and vibrational spectroscopies. *Biochim. Biophys. Acta Biomembr.* 1862, 183352 (2020).
- 51. Coones, R. T., Green, R. J. & Frazier, R. A. Investigating lipid headgroup composition within epithelial membranes: a systematic review. *Soft Matter* **17**, 6773–6786 (2021).
- Vorobyov, I. & Allen, T. W. On the role of anionic lipids in charged protein interactions with membranes. *Biochim. Biophys. Acta Biomembr.* 1808, 1673–1683 (2011).
- Yeung, T. et al. Membrane phosphatidylserine regulates surface charge and protein localization. Science 319, 210–213 (2008).
- Leventis, P. A. & Grinstein, S. The distribution and function of phosphatidylserine in cellular membranes. *Annu. Rev. Biophys.* 39, 407–427 (2010).
- Del Vecchio, K. & Stahelin, R. V. Investigation of the phosphatidylserine binding properties of the lipid biosensor, Lactadherin C2 (LactC2), in different membrane environments. *J. Bioenerg. Biomembr.* 50, 1–10 (2018).
- Raskin, D. M. & de Boer, P. A. J. Rapid pole-to-pole oscillation of a protein required for directing division to the middle of Escherichia coli. *Proc. Natl. Acad. Sci.* 96, 4971–4976 (1999).

- Litschel, T., Ramm, B., Maas, R., Heymann, M. & Schwille, P. Beating vesicles: encapsulated protein oscillations cause dynamic membrane deformations. *Angew. Chem. Int. Ed.* 57, 16286–16290 (2018).
- Godino, E. et al. De novo synthesized Min proteins drive oscillatory liposome deformation and regulate FtsA-FtsZ cytoskeletal patterns. Nat. Commun. 10, 4969 (2019).
- Kohyama, S., Merino-Salomón, A. & Schwille, P. In vitro assembly, positioning and contraction of a division ring in minimal cells. *Nat. Commun.* 13, 6098 (2022).
- Fu, M. et al. Mechanochemical feedback loop drives persistent motion of liposomes. *Nat. Phys.* 19, 1211–1218 (2023).
- Loose, M., Fischer-Friedrich, E., Ries, J., Kruse, K. & Schwille, P. Spatial regulators for bacterial cell division self-organize into surface waves in vitro. Science 320, 789–792 (2008).
- Vecchiarelli, A. G., Li, M., Mizuuchi, M. & Mizuuchi, K. Differential affinities of MinD and MinE to anionic phospholipid influence Min patterning dynamics in vitro. *Mol. Microbiol.* 93, 453–463 (2014).
- Ramm, B. et al. The MinDE system is a generic spatial cue for membrane protein distribution in vitro. Nat. Commun. 9, 3942 (2018).
- Meindlhumer, S. et al. Directing Min protein patterns with advective bulk flow. Nat. Commun. 14, 450 (2023).
- Park, K.-T. et al. The min oscillator uses MinD-dependent conformational changes in MinE to spatially regulate cytokinesis. Cell 146, 396–407 (2011).
- Park, K.-T., Villar, M. T., Artigues, A. & Lutkenhaus, J. MinE conformational dynamics regulate membrane binding, MinD interaction, and Min oscillation. *Proc. Natl. Acad. Sci.* 114, 7497–7504 (2017).
- Halatek, J., Brauns, F. & Frey, E. Self-organization principles of intracellular pattern formation. *Philos. Trans. R. Soc. B Biol. Sci.* 373, 20170107 (2018).
- Halatek, J. & Frey, E. Rethinking pattern formation in reaction–diffusion systems. *Nat. Phys.* 14, 507–514 (2018).
- Shih, Y.-L. et al. Active transport of membrane components by selforganization of the min proteins. *Biophys. J.* 116, 1469–1482 (2019).
- Palanisamy, N., Öztürk, M. A., Akmeriç, E. B. & Di Ventura, B.
 C-terminal eYFP fusion impairs Escherichia coli MinE function. Open Biol. 10, 200010 (2020).
- Renner, L. D. & Weibel, D. B. MinD and MinE interact with anionic phospholipids and regulate division plane formation in Escherichia coli*. J. Biol. Chem. 287, 38835–38844 (2012).
- Wu, F., van Schie, B. G. C., Keymer, J. E. & Dekker, C. Symmetry and scale orient Min protein patterns in shaped bacterial sculptures. *Nat. Nanotechnol.* 10, 719–726 (2015).
- Mileykovskaya, E. & Dowhan, W. Visualization of phospholipid domains in Escherichia coli by using the cardiolipin-specific fluorescent dye 10-N-nonyl acridine orange. *J. Bacteriol.* 182, 1172–1175 (2000).
- Renner, L. D. & Weibel, D. B. Cardiolipin microdomains localize to negatively curved regions of Escherichia coli membranes. *Proc. Natl Acad. Sci.* 108, 6264–6269 (2011).
- Oliver, P. M. et al. Localization of anionic phospholipids in escherichia coli cells. J. Bacteriol. 196, 3386–3398 (2014).
- 76. Rivas, G., Fernandez, J. A. & Minton, A. P. Direct observation of the self-association of dilute proteins in the presence of inert macromolecules at high concentration via tracer sedimentation equilibrium: theory, experiment, and biological significance. *Biochemistry* **38**, 9379–9388 (1999).
- Rivas, G., Fernández, J. A. & Minton, A. P. Direct observation of the enhancement of noncooperative protein self-assembly by macromolecular crowding: Indefinite linear self-association of bacterial cell division protein FtsZ. *Proc. Natl Acad. Sci.* 98, 3150–3155 (2001).
- Ellis, J. R. Protein misassembly: macromolecular crowding and molecular chaperones. In: *Madame Curie Bioscience Database* [Internet] (Landes Bioscience, 2013).

- Heermann, T., Steiert, F., Ramm, B., Hundt, N. & Schwille, P. Masssensitive particle tracking to elucidate the membrane-associated MinDE reaction cycle. *Nat. Methods* 18, 1239–1246 (2021).
- Caspi, Y. & Dekker, C. Mapping out Min protein patterns in fully confined fluidic chambers. *eLife* 5, e19271 (2016).
- Kuramoto, Y. Chemical Turbulence. In: Chemical oscillations, waves, and turbulence (ed. Kuramoto, Y.) 111–140. https://doi.org/10.1007/ 978-3-642-69689-3_7. (Springer, Berlin, Heidelberg, 1984).
- Lan, G., Sartori, P., Neumann, S., Sourjik, V. & Tu, Y. The energy–speed–accuracy trade-off in sensory adaptation. *Nat. Phys.* 8, 422–428 (2012).
- 83. Zhang, D., Zhang, C., Ouyang, Q. & Tu, Y. Free energy dissipation enhances spatial accuracy and robustness of self-positioned Turing pattern in small biochemical systems. *J. R. Soc. Interface* **20**, 20230276 (2023).
- 84. Doron, S. et al. Systematic discovery of antiphage defense systems in the microbial pangenome. *Science* **359**, eaar4120 (2018).
- Gao, L. et al. Diverse enzymatic activities mediate antiviral immunity in prokaryotes. Science 369, 1077–1084 (2020).
- Rousset, F. et al. Phages and their satellites encode hotspots of antiviral systems. Cell Host Microbe 30, 740–753.e5 (2022).
- 87. Hu, H. et al. Structure and mechanism of Zorya anti-phage defense system. Preprint at https://doi.org/10.1101/2023.12.18.572097 (2023).
- 88. Edgar, R. et al. Bacteriophage infection is targeted to cellular poles. *Mol. Microbiol.* **68**, 1107–1116 (2008).
- Kemp, P., Gupta, M. & Molineux, I. J. Bacteriophage T7 DNA ejection into cells is initiated by an enzyme-like mechanism. *Mol. Microbiol.* 53, 1251–1265 (2004).
- Noireaux, V. & Liu, A. P. The new age of cell-free biology. Annu. Rev. Biomed. Eng. 22, 51–77 (2020).
- Blanken, D., Foschepoth, D., Serrão, A. C. & Danelon, C. Genetically controlled membrane synthesis in liposomes. *Nat. Commun.* 11, 4317 (2020).
- 92. Robinson, A. O., Venero, O. M. & Adamala, K. P. Toward synthetic life: biomimetic synthetic cell communication. *Curr. Opin. Chem. Biol.* **64**, 165–173 (2021).
- Peruzzi, J. A., Galvez, N. R. & Kamat, N. P. Engineering transmembrane signal transduction in synthetic membranes using two-component systems. *Proc. Natl Acad. Sci.* 120, e2218610120 (2023).
- Klammt, C., Schwarz, D., Dötsch, V. & Bernhard, F. Cell-free production of integral membrane proteins on a preparative scale. In vitro transcription and translation protocols (ed. Grandi, G.) 57–78 (Humana Press, Totowa, NJ, 2007).
- Rues, R.-B., Henrich, E., Boland, C., Caffrey, M. & Bernhard, F. Cellfree production of membrane proteins in Escherichia coli lysates for functional and structural studies. In *Heterologous Expression of Membrane Proteins: Methods and Protocols* (ed. Mus-Veteau, I.) 1–21 (Springer, New York, NY, 2016).
- Kuruma, Y. & Ueda, T. The PURE system for the cell-free synthesis of membrane proteins. *Nat. Protoc.* 10, 1328–1344 (2015).
- Gregorio, N. E., Levine, M. Z. & Oza, J. P. A user's guide to cell-free protein synthesis. *Methods Protoc.* 2, 24 (2019).
- Tabaei, S. R., Jackman, J. A., Kim, S.-O., Zhdanov, V. P. & Cho, N.-J. Solvent-assisted lipid self-assembly at hydrophilic surfaces: factors influencing the formation of supported membranes. *Langmuir* 31, 3125–3134 (2015).
- Hohner, A. O., David, M. P. C. & Rädler, J. O. Controlled solventexchange deposition of phospholipid membranes onto solid surfaces. *Biointerphases* 5, 1–8 (2010).
- Patel, A. R., Kanazawa, K. K. & Frank, C. W. Antibody binding to a tethered vesicle assembly using QCM-D. Anal. Chem. 81, 6021–6029 (2009).
- Lee, Y. K., Lee, H. & Nam, J.-M. Lipid-nanostructure hybrids and their applications in nanobiotechnology. NPG Asia Mater. 5, e48–e48 (2013).

- Batista, A. C. et al. Differentially optimized cell-free buffer enables robust expression from unprotected linear DNA in exonucleasedeficient extracts. ACS Synth. Biol. 11, 732–746 (2022).
- Sun, Z. Z. et al. Protocols for implementing an Escherichia coli based TX-TL cell-free expression system for synthetic biology. *J. Vis. Exp.* 16, e50762 (2013).
- Datsenko, K. A. & Wanner, B. L. One-step inactivation of chromosomal genes in Escherichia coli K-12 using PCR products. *Proc. Natl. Acad. Sci.* 97, 6640–6645 (2000).
- Khakimzhan, A. K. et al. QCMD-TXTL Example code (Fig. 5j PEG-PE range MinDE). (2024).
- Garamella, J., Majumder, S., Liu, A. P. & Noireaux, V. An adaptive synthetic cell based on mechanosensing, biosensing, and inducible gene circuits. ACS Synth. Biol. 8, 1913–1920 (2019).
- Lee, K.-H. et al. Real-time monitoring of cell-free protein synthesis on a surface plasmon resonance chip. *Anal. Biochem.* 366, 170–174 (2007).
- Combs, C. A. Fluorescence microscopy: a concise guide to current imaging methods. *Curr. Protoc. Neurosci.* 50, 2.1.1–2.1.14 (2010).
- Müller, D. J. et al. Atomic force microscopy-based force spectroscopy and multiparametric imaging of biomolecular and cellular systems. *Chem. Rev.* 121, 11701–11725 (2021).
- Shumaker-Parry, J. S. & Campbell, C. T. Quantitative methods for spatially resolved adsorption/desorption measurements in real time by surface plasmon resonance microscopy. *Anal. Chem.* 76, 907–917 (2004).
- Wuu, J. J. & Swartz, J. R. High yield cell-free production of integral membrane proteins without refolding or detergents. *Biochim. Biophys. Acta* 1778, 1237–1250 (2008).
- 112. Godino, E. et al. Cell-free biogenesis of bacterial division proto-rings that can constrict liposomes. *Commun. Biol.* **3**, 1–11 (2020).
- Gao, T. et al. Characterizing diffusion dynamics of a membrane protein associated with nanolipoproteins using fluorescence correlation spectroscopy. *Protein Sci.* 20, 437–447 (2011).
- Salamon, Z., Macleod, H. A. & Tollin, G. Surface plasmon resonance spectroscopy as a tool for investigating the biochemical and biophysical properties of membrane protein systems. I: Theoretical principles. *Biochim. Biophys. Acta* 1331, 131–152 (1997).
- Rahim Ferhan, A., Kyeong Yoon, B., Jeon, W.-Y. & Cho, N.-J.
 Biologically interfaced nanoplasmonic sensors. *Nanoscale Adv.* 2, 3103–3114 (2020).
- Brunelle, J. L. & Green, R. Chapter Thirteen coomassie blue staining. Methods Enzymol. 541, 161–167 (2014).
- Lelek, M. et al. Single-molecule localization microscopy. Nat. Rev. Methods Prim. 1, 1–27 (2021).
- Frederix, P. L. T. M., Bosshart, P. D. & Engel, A. Atomic force microscopy of biological membranes. *Biophys. J.* 96, 329–338 (2009).
- Abbas, A., Linman, M. J. & Cheng, Q. Sensitivity comparison of surface plasmon resonance and plasmon-waveguide resonance biosensors. Sens. Actuators B Chem. 156, 169–175 (2011).
- Chyasnavichyus, M., Young, S. L., Geryak, R. & Tsukruk, V. V. Probing elastic properties of soft materials with AFM: data analysis for different tip geometries. *Polymer* 102, 317–325 (2016).
- Brockman, J. M., Nelson, B. P. & Corn, R. M. Surface plasmon resonance imaging measurements of ultrathin organic films. *Annu. Rev. Phys. Chem.* 51, 41–63 (2000).
- Dixon, M. C. Quartz crystal microbalance with dissipation monitoring: enabling real-time characterization of biological materials and their interactions. *J. Biomol. Tech.* 19, 151 (2008).

- Laemmli, U. K. Cleavage of structural proteins during the assembly of the head of bacteriophage T4. *Nature* 227, 680–685 (1970).
- Manzer, Z. A. et al. Cell-free synthesis of a transmembrane mechanosensitive channel protein into a hybrid-supported lipid bilayer. ACS Appl. Bio Mater. 4, 3101–3112 (2021).
- Shinoda, T. et al. Cell-free methods to produce structurally intact mammalian membrane proteins. Sci. Rep. 6, 30442 (2016).

Acknowledgements

The authors thank David Garenne for his help in the preparation of the TXTL system used in this work. This work and the materials are based on funding provided by the National Science Foundation (BBSRC-NSF/BIO 2017932 to V.N.) and the Deutsche Forschungsgemeinschaft SPP 2330 program (BE 6703/2-1 to C.L.B.).

Author contributions

A.K., Z.I., S.T., O.D., and P.F. performed the experiments. A.K., Z.I., S.T., O.D., P.F., C.L.B., and V.N. designed the experiments, analyzed the data, and wrote the manuscript. V.N. edited the manuscript.

Competing interests

The authors declare no competing interests.

Additional information

Supplementary information The online version contains supplementary material available at https://doi.org/10.1038/s42003-024-06690-9.

Correspondence and requests for materials should be addressed to Vincent Noireaux.

Peer review information Communications Biology thanks the anonymous reviewers for their contribution to the peer review of this work. Primary Handling Editors: Laura Rodríguez Pérez and Christina Karlsson Rosenthal

Reprints and permissions information is available at http://www.nature.com/reprints

Publisher's note Springer Nature remains neutral with regard to jurisdictional claims in published maps and institutional affiliations.

Open Access This article is licensed under a Creative Commons Attribution 4.0 International License, which permits use, sharing, adaptation, distribution and reproduction in any medium or format, as long as you give appropriate credit to the original author(s) and the source, provide a link to the Creative Commons licence, and indicate if changes were made. The images or other third party material in this article are included in the article's Creative Commons licence, unless indicated otherwise in a credit line to the material. If material is not included in the article's Creative Commons licence and your intended use is not permitted by statutory regulation or exceeds the permitted use, you will need to obtain permission directly from the copyright holder. To view a copy of this licence, visit http://creativecommons.org/licenses/by/4.0/.

© The Author(s) 2024

Cell-free expression with a quartz crystal microbalance enables rapid, dynamic, and label-free characterization of membrane-interacting proteins

Aset Khakimzhan¹, Ziane Izri¹, Seth Thompson¹, Oleg Dmytrenko², Patrick Fischer², Chase Beisel^{2,3}, Vincent Noireaux^{1,*}

*Corresponding author: Email: noireaux@umn.edu

Item	Title	Pages	
Figure S1	TXTL lysate does not contain living E. coli cells		
Figure S2	Synthesis of deGFP from linear templates with a P70a promoter or a T7 cascade		
Figure S3	SALB procedure with and without lipids during step III		
Figure S4	Nonspecific TXTL adsorption for model SLBs	5	
Figure S5	Measuring the interaction of blank TXTL reactions with SLBs	6	
Figure S6	MscL TXTL adsorption replicates with ECL SLB		
Figure S7	AH-eGFP TXTL adsorption replicates with EggPC SLB		
Figure S8	Specific adsorption of MscL and AH-eGFP into DOPC and DOPE SLBs		
Figure S9	Pre-synthesized MscL does not integrate into SLBs		
Figure S10	Pre-synthesized AH-eGFP does integrate into SLBs	11	
Figure S11	Post-QCMD fluorescence measurements	12	
Figure S12	Mass sensitivity of the QCMD	13	
Figure S13	Adsorption of blank, AH-eGFP, and MscL TXTL reactions onto ECL-EggPC SLBs	14	
Figure S14	Adsorption of blank and MscL TXTL reactions into DOPE-DOPC SLBs	15	
Figure S15	Quantification of lipid expulsion caused by TXTL reactions.	16	
Figure S16	Nonspecific TXTL adsorption into DOPG-DOPE SLBs	17	
Figure S17	Nonspecific TXTL adsorption into CL-DOPG-DOPC SLBs	18	
Figure S18	Nonspecific TXTL adsorption into CL-DOPE SLBs	19	
Figure S19	eGFP-LactC2 adsorption kinetics and approximate endpoint concentrations	20	
Figure S20	Modes and wavelengths of oscillations produced by MinD	21	
Figure S21	MinD adsorption kinetics in DOPG-DOPC SLBs	22	
Figure S22	MinD adsorption kinetics in DOPG-DOPE SLBs	23	
Figure S23	MinD adsorption kinetics in CL-DOPC SLBs	24	
Figure S24	MinD adsorption kinetics in CL-DOPE SLBs	25	
Figure S25	Effect of DOTAP on MinD adsorption kinetics on DOPC and DOPG-DOPC SLBs	26	
Figure S26	Effect of DOTAP on MinD adsorption kinetics in DOPE and DOPG-DOPE SLBs	27	
Figure S27	Number of oscillations in the first 2h in SLBs with added DOTAP	28	
Figure S28	Effect of P70a-minE concentration on MinDE adsorption kinetics on a DOPG-DOPE SLB	29	
Figure S29	Effect of P70a-minE concentration on MinDE adsorption kinetics on a DOPG-DOPC SLB	30	
Figure S30	Effect of P70a-minE concentration on MinDE adsorption kinetics on an ECL SLB	31	
Figure S31	Tagging of Zorya proteins disrupts E. coli defense against phages	32	
Figure S32	Effect of DOPG on ZorA TXTL adsorption kinetics on a DOPE SLB	33	
Figure S33	Comparison of ZorA adsorption kinetics with a DOPC and a DOPE SLB	34	
Figure S34	ZorAB TXTL adsorption kinetics with an ECL SLB	35	
Figure S35	ZorE adsorption kinetics with post-incubation Tris NaCl flush included in the graph	36	
Table S1	Working lipid concentrations during step III of SALB	37	

¹School of Physics and Astronomy, University of Minnesota, Minneapolis, MN 55455, USA ²Helmholtz Institute for RNA-based Infection Research (HIRI), Helmholtz-Centre for Infection Research (HZI), 97080 Würzburg, Germany

³Medical Faculty, University of Würzburg, 97080 Würzburg, Germany

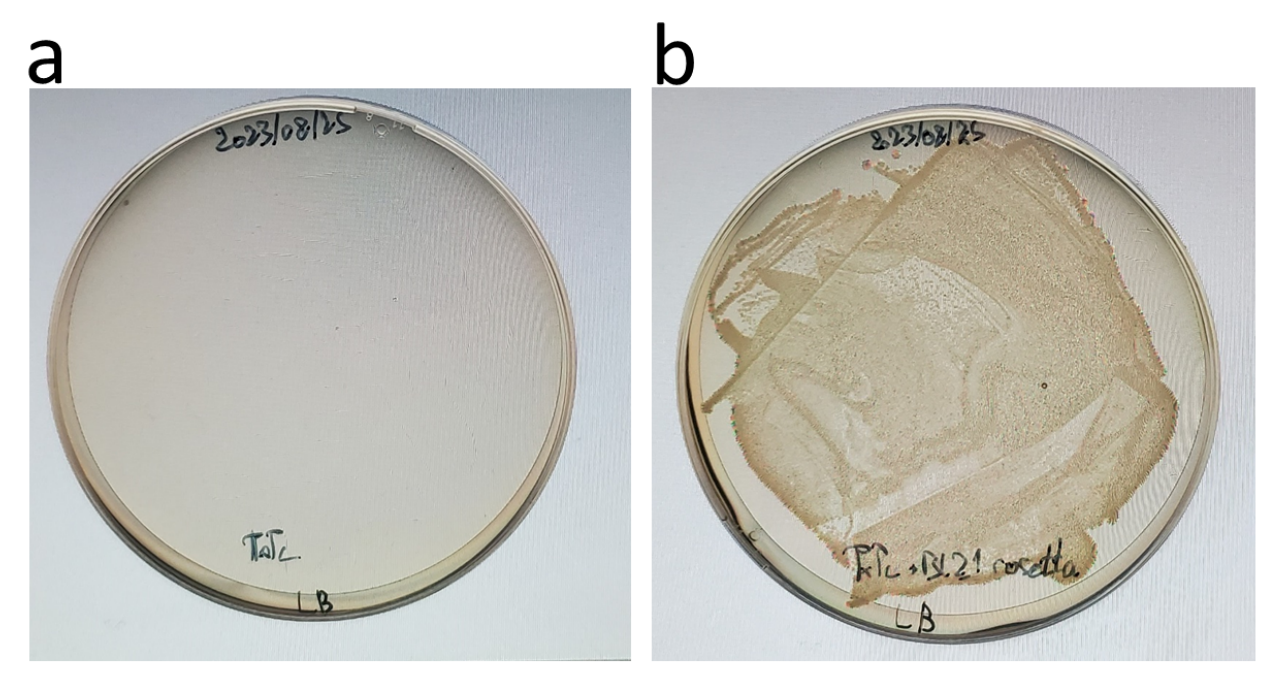


Figure S1. (a) Plating 45 μ l of a TXTL reaction onto an agar plate with no antibiotic shows no *E. coli* colonies. (b) Adding 5 μ l of BL21 Rosetta *E. coli* to 40 μ l of a TXTL reaction and then plating the mix onto an agar plate with no antibiotic shows many *E. coli* colonies.

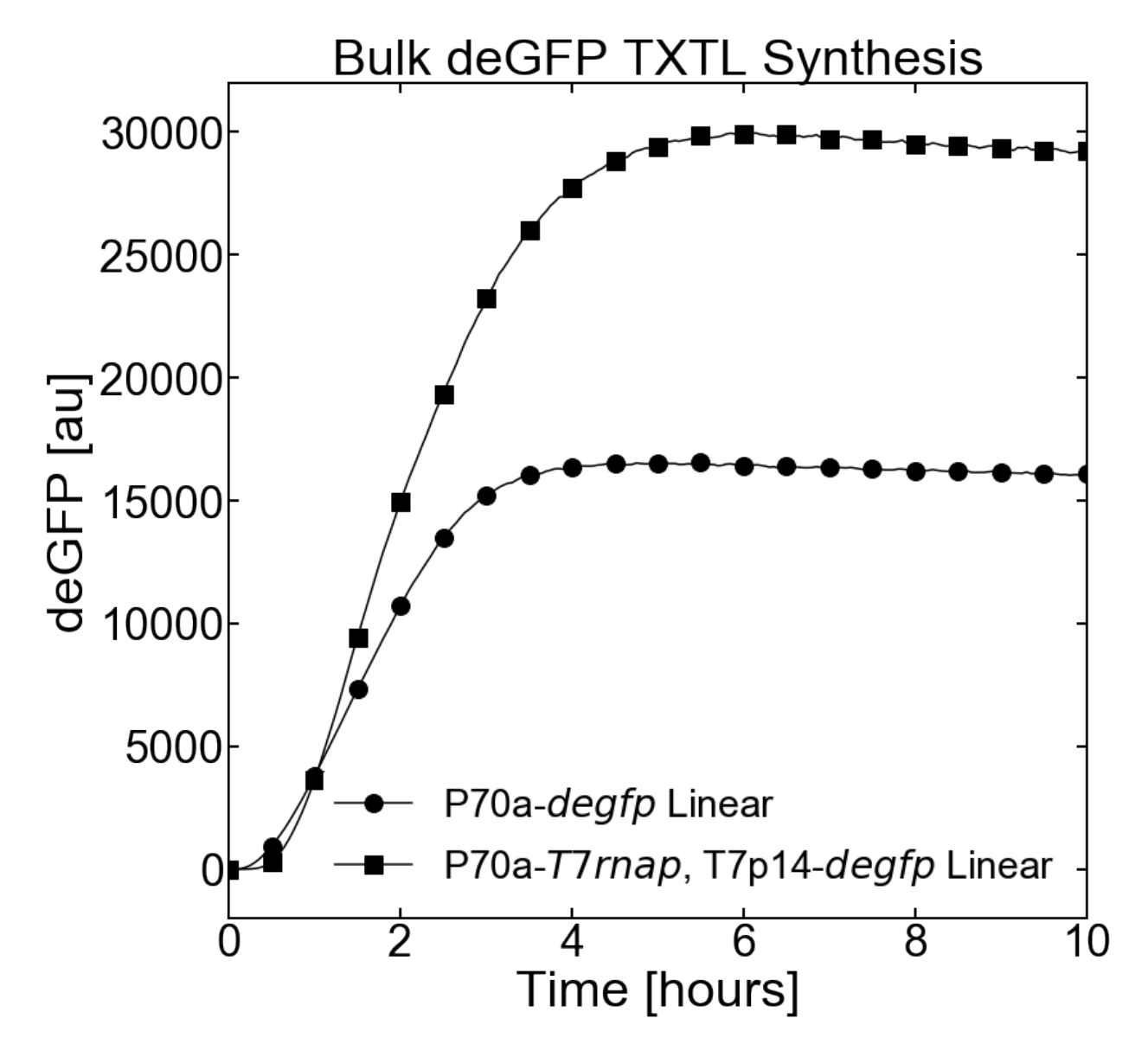


Figure S2. Batch mode TXTL of deGFP with the P70a promoter (P70a-*degfp*, 5nM) and with the T7 cascade (P70a-*T7rnap*, 0.15nM, T7p14-*degfp*, 5nM).

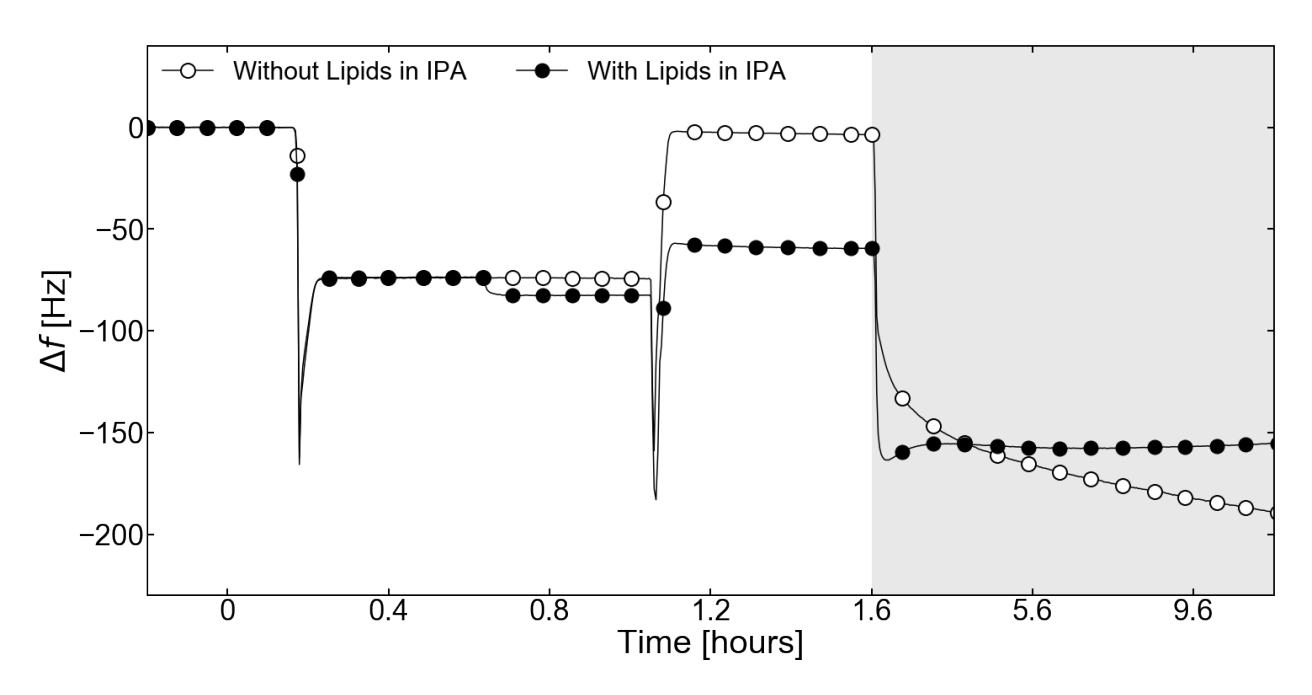


Figure S3. SALB protocol completed with ECL or without lipids added to the IPA-Lipid mix. Step III shows a return to $\Delta f = 0$ Hz, which indicates no SLB has been formed.

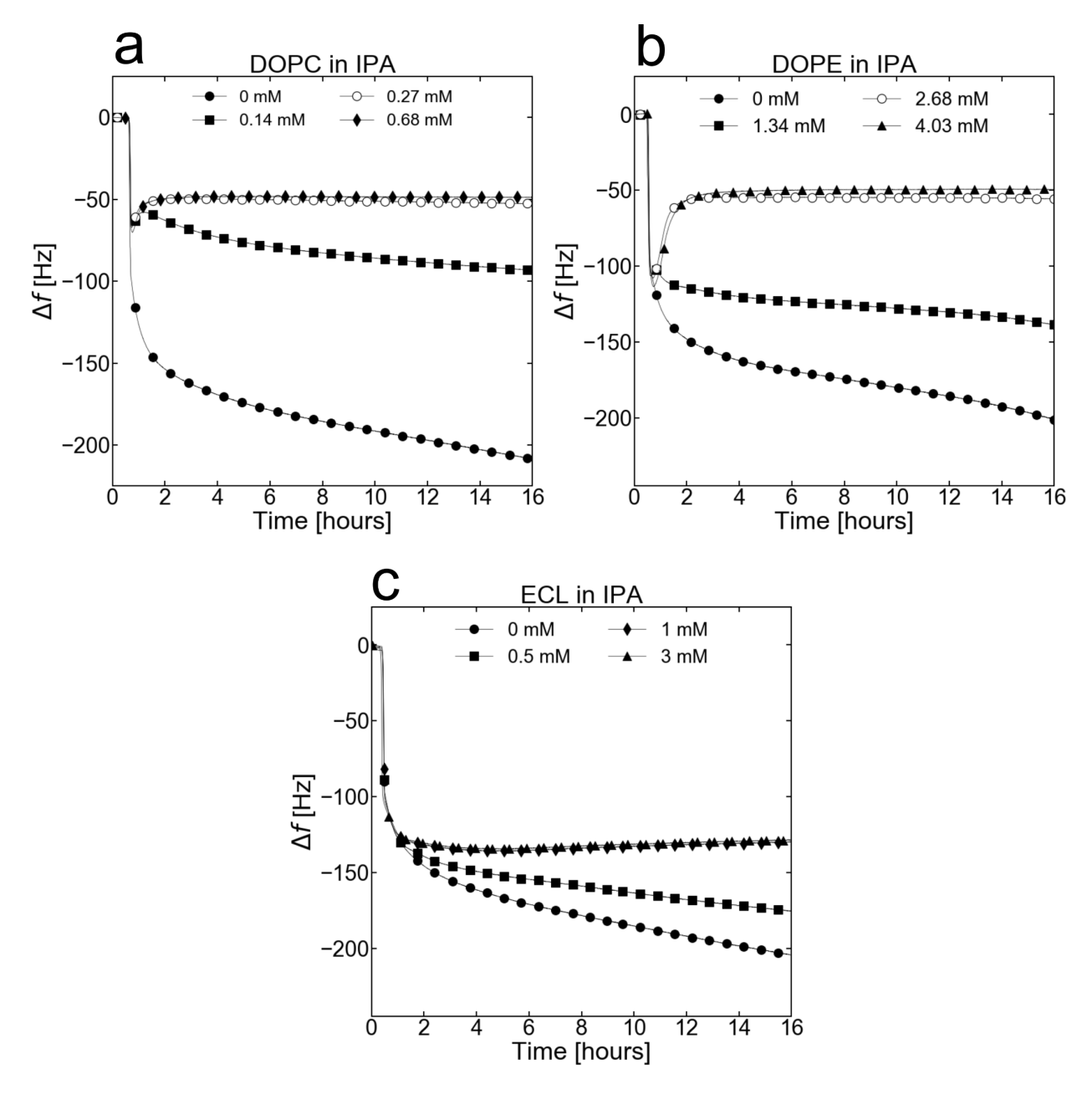


Figure S4. Adsorption kinetics of a blank TXTL reaction (P70a-*T7rnap*, 0.15 nM) on SLBs depending on the DOPC **(a)**, DOPE **(b)**, and ECL **(c)** phospholipids concentration in IPA during Step II of SALB.

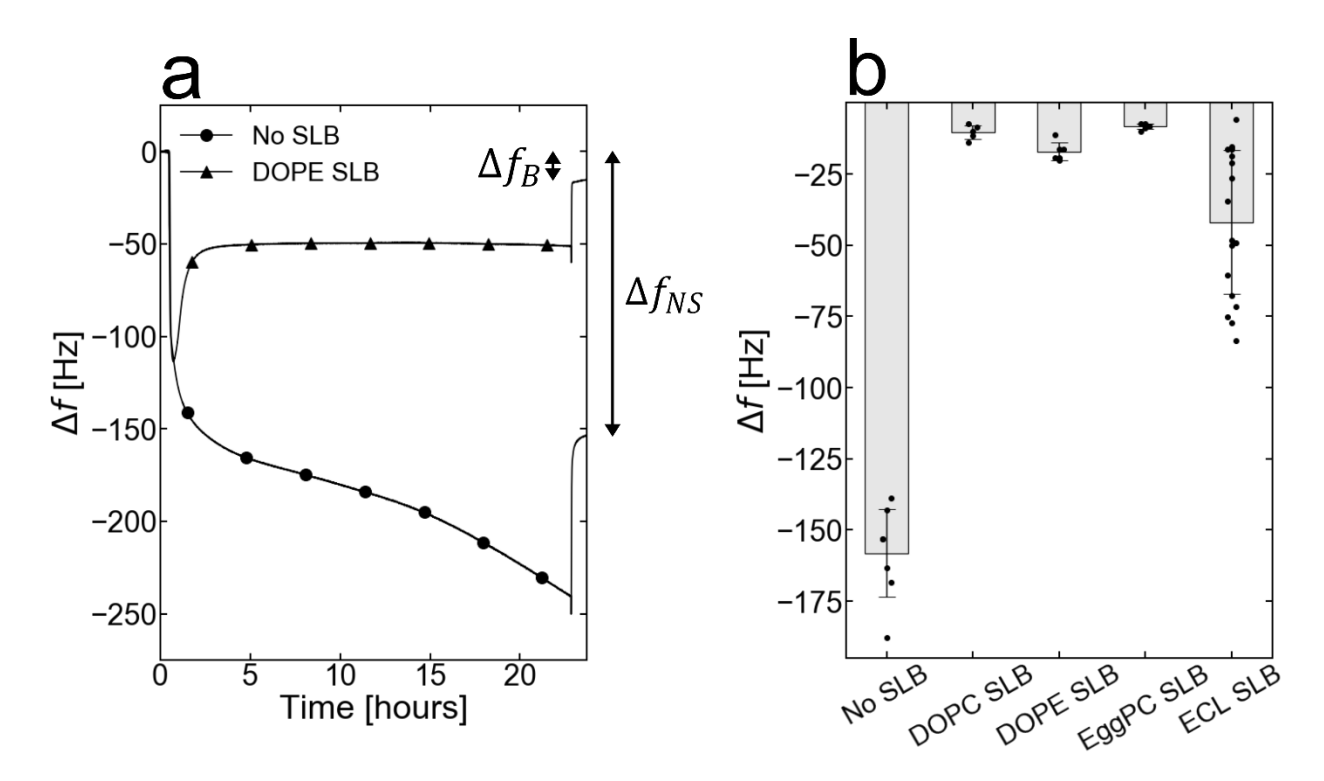


Figure S5. Measuring the interactions of blank TXTL reactions with SLBs. **(a)** Adsorption kinetics of blank TXTL reactions (P70a-*T7rnap*, 0.15 nM) in contact with either a bare sensor or with a DOPE SLB. The Tris NaCl buffer is flushed into the modules after the TXTL incubated for 22 hours. The difference in the frequency shift (Δf_B) between the Tris NaCl flush before TXTL and after the TXTL reaction quantifies the interaction strength of a blank TXTL reaction with the SLB. This value is compared to the difference obtained from nonspecific adsorption of TXTL to the bare sensor (Δf_{NS}). **(b)** Comparison of the mean Δf_B levels for the DOPC, DOPE, EggPC, and ECL SLBs to the Δf_{NS} levels obtained from bare sensors. The mean and the standard deviation are calculated from at least 5 replicates.

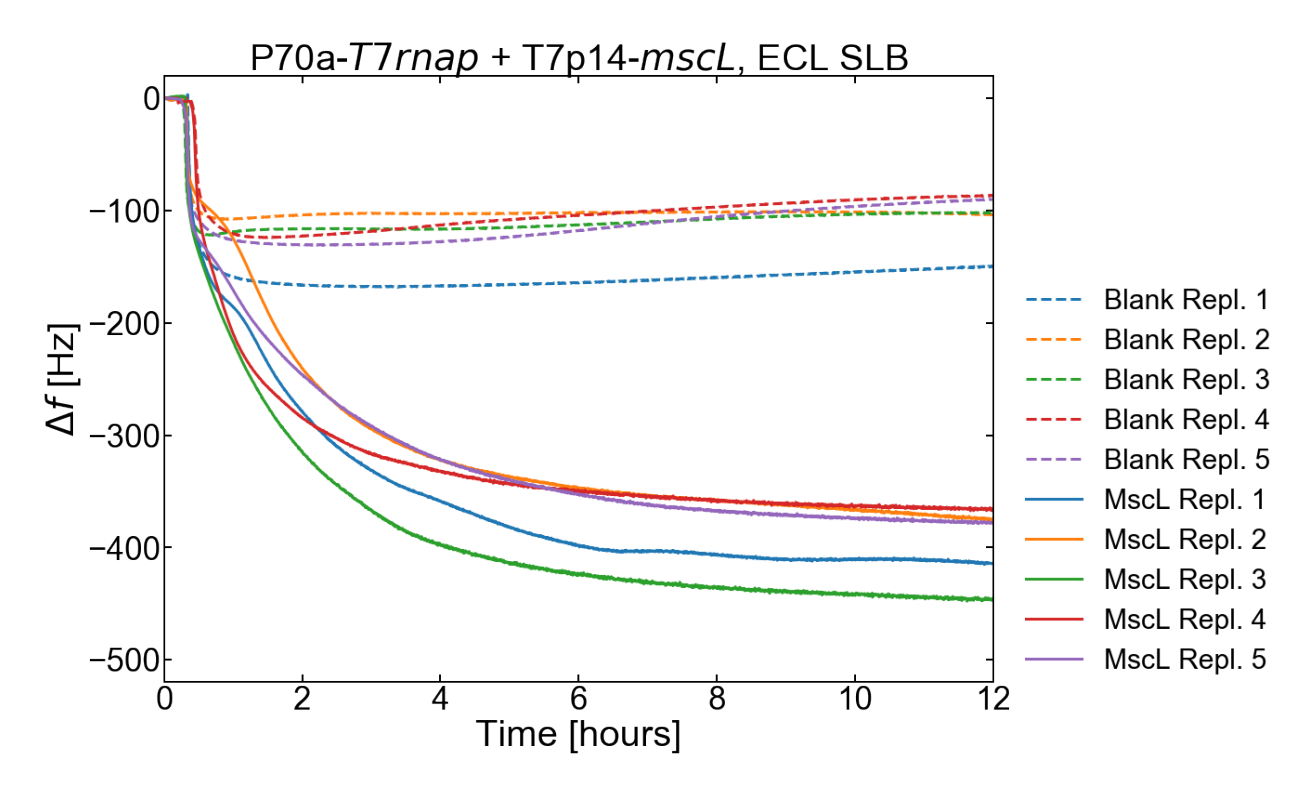


Figure S6. Replicates of the T7p14-*mscL* TXTL reaction (P70a-*T7rnap*, 0.15 nM, T7p14-*mscL*, 5 nM) incubated on an ECL SLB.

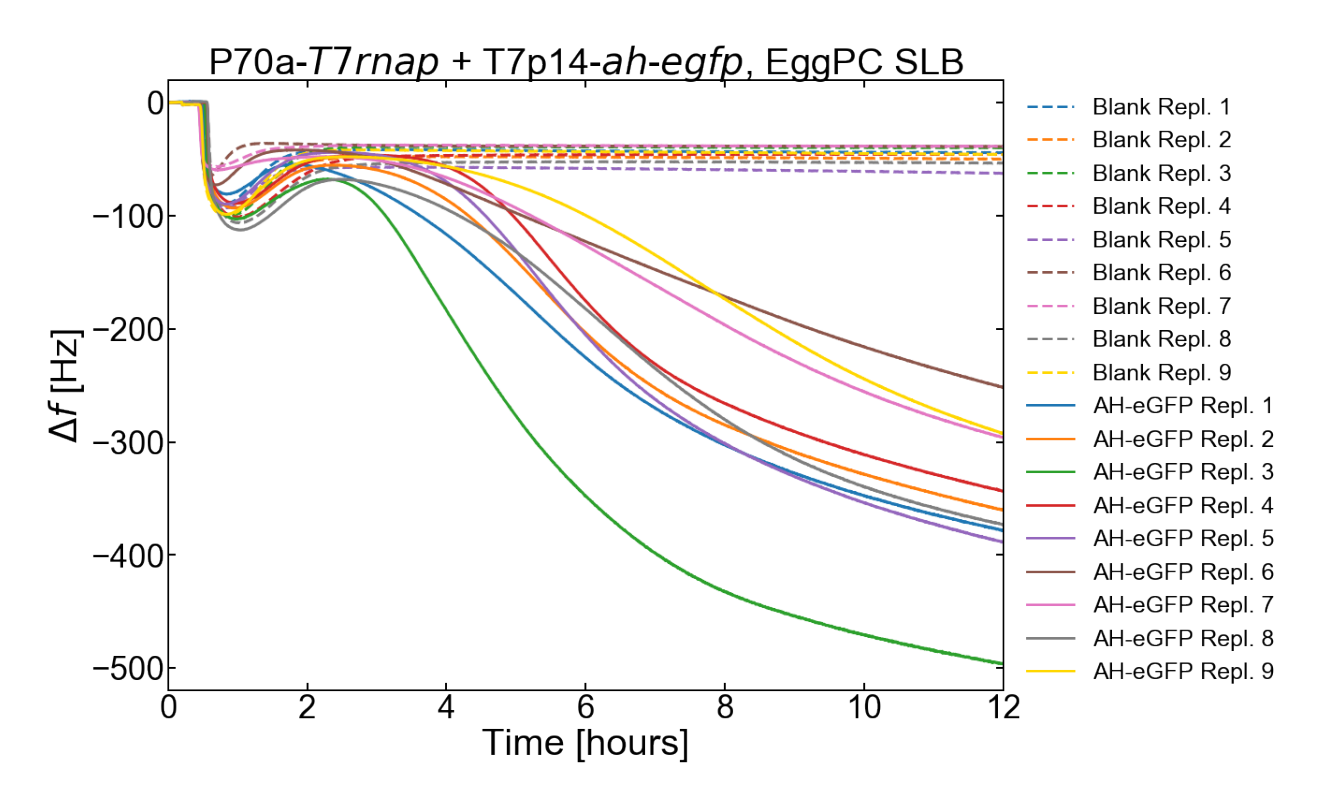


Figure S7. Replicates of the T7p14-*ah-eGFP* TXTL reaction (P70a-*T7rnap*, 0.15 nM, T7p14-*ah-egfp*, 5 nM) incubated on an EggPC SLB.

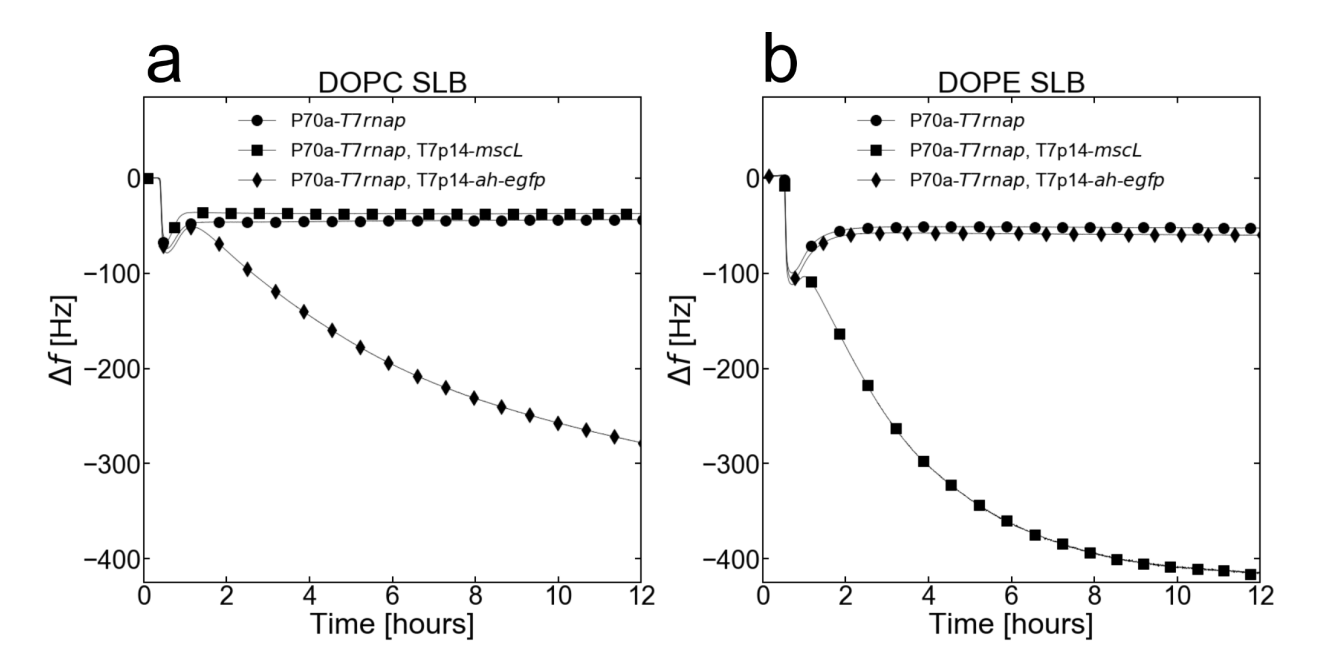


Figure S8. (a) and (b) Adsorption kinetics of either blank (P70a-*T7rnap*, 0.15 nM), AH-eGFP (P70a-*T7rnap*, 0.15 nM, T7p14-*ah-egfp*, 5 nM), or MscL (P70a-*T7rnap*, 0.15 nM, T7p14-*mscL*, 5 nM) TXTL reactions into a DOPC SLB and a DOPE SLB respectively.

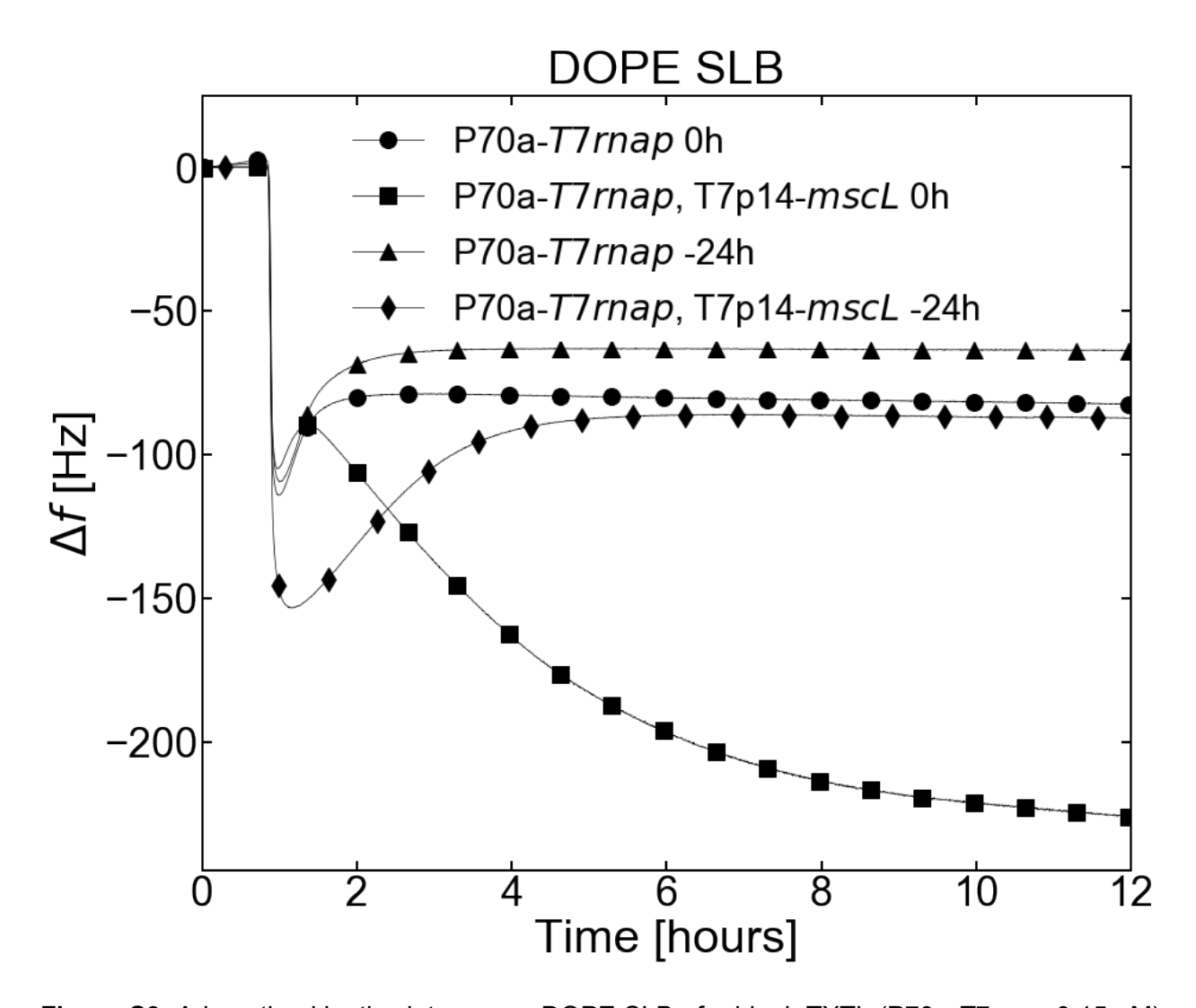


Figure S9. Adsorption kinetics into a pure DOPE SLB of a blank TXTL (P70a-*T7rnap*, 0.15 nM) and an MscL TXTL (P70a-*T7rnap*, 0.15 nM, T7p14-*mscL*, 5 nM) reactions that have either been freshly mixed (0 h) or that have been pre-incubated for 24 h (-24 h) before being flushed into the QCMD module.

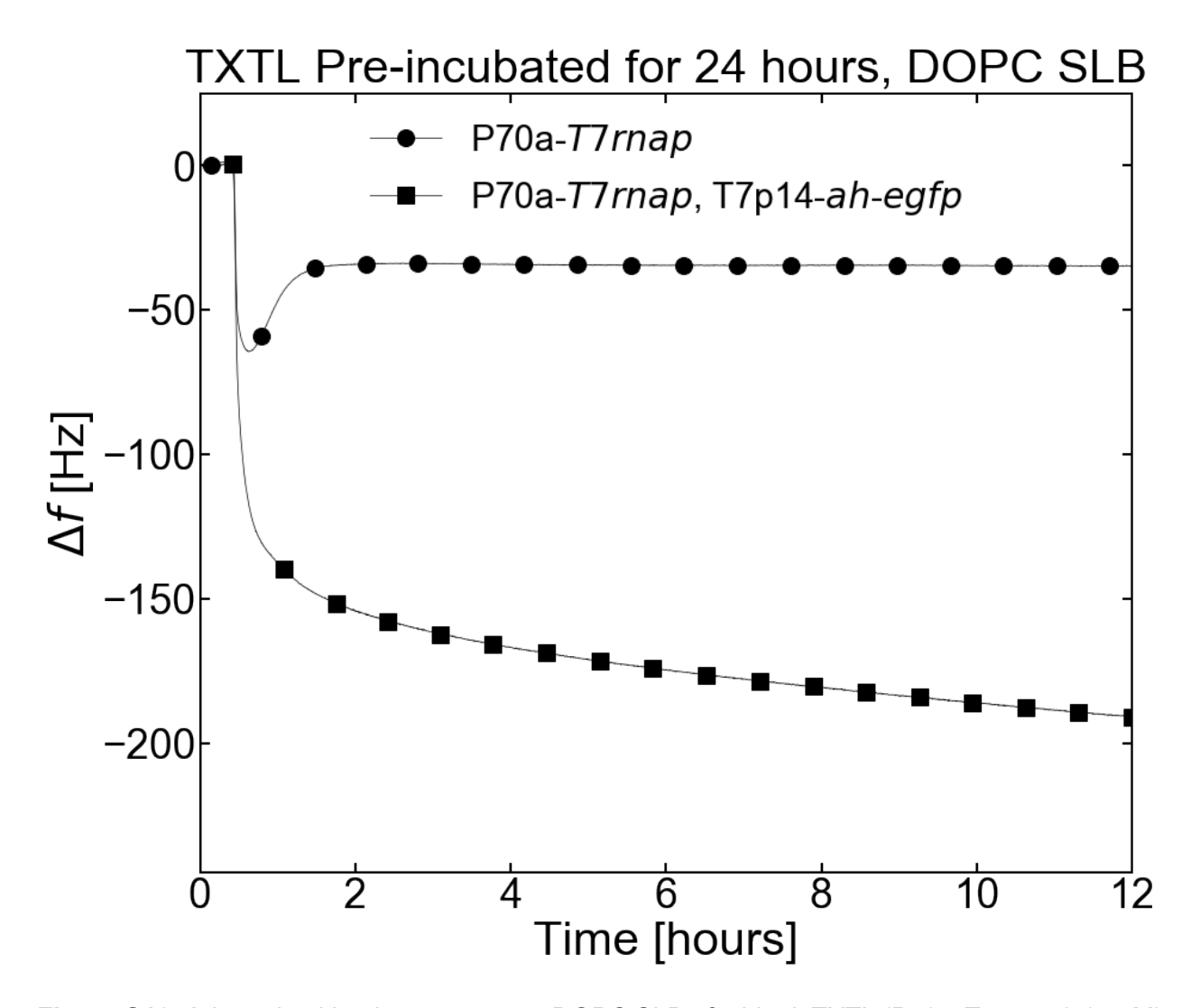


Figure S10. Adsorption kinetics onto a pure DOPC SLB of a blank TXTL (P70a-*T7rnap*, 0.15 nM) and an AH-eGFP TXTL (P70a-*T7rnap*, 0.15 nM, T7p14-*ah-egfp*, 5 nM), reactions that have been pre-incubated for 24 h before being flushed into the QCMD module.

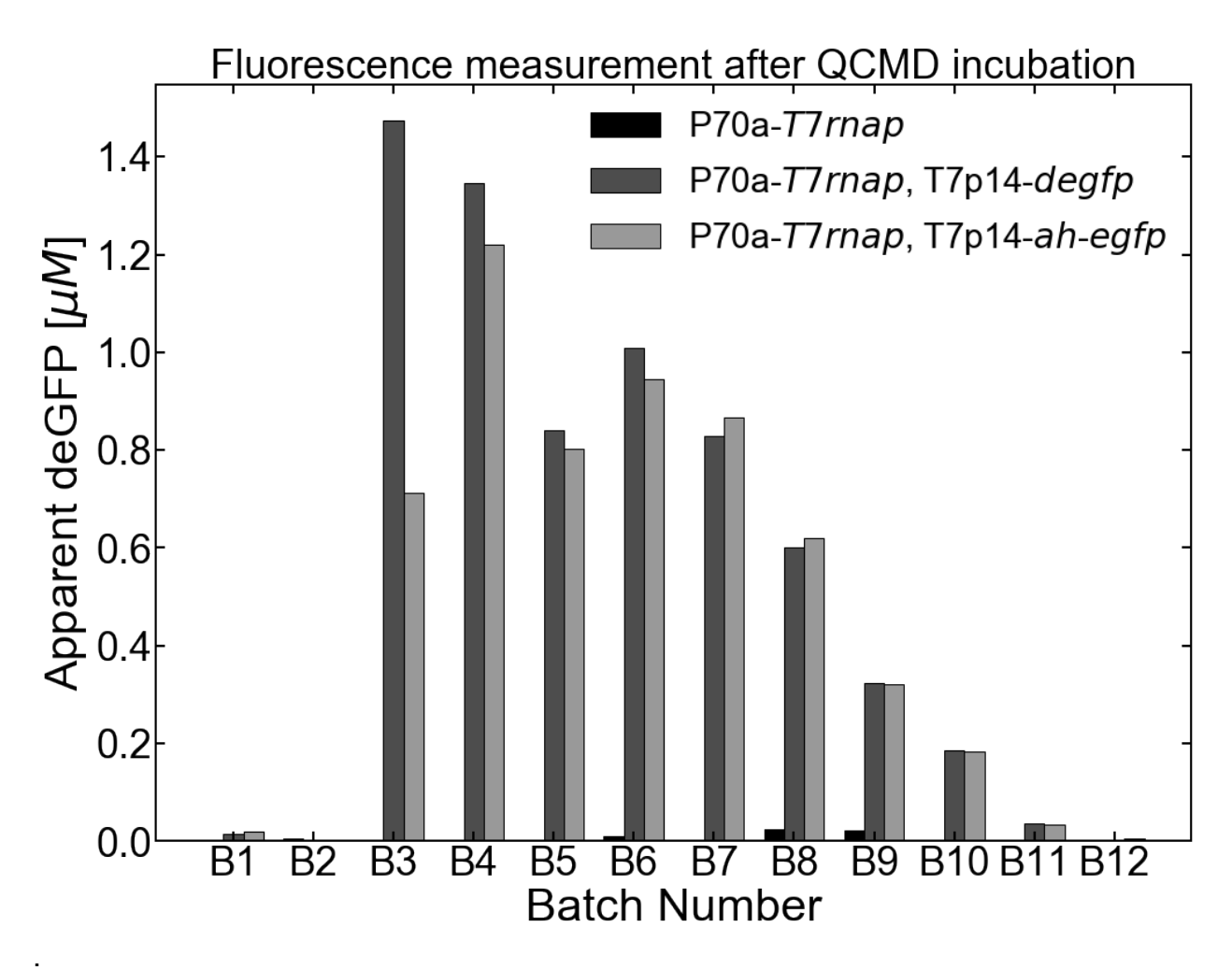


Figure S11. End-point measurement of either blank (P70a-*T7rnap*, 0.15 nM), AH-eGFP (P70a-*T7rnap*, 0.15 nM, T7p14-*ah-egfp*, 5 nM), or MscL (P70a-*T7rnap*, 0.15 nM, T7p14-*mscL*, 5 nM) TXTL reactions in the QCMD modules overnight. The TXTL is flushed out of the module in batches of 100 µl and the x-axis corresponds to the number of the batch.

Sensor dimensions

- Diameter 1.2 cm.
- Surface area = $1.131 \ 10^{-4} \ m^2$.

MscL dimensions

- MscL assembles into a pentamer.
- Molar mass of MscL monomer = 14957.2 g/mol.
- Mass of one monomer = $2.48 \cdot 10^{-20} \text{ g}$.
- Mass of one pentamer = $1.24 \cdot 10^{-19}$ g.
- Surface area of one pentamer: 140 nm² ¹.

Mass of closely packed MscL pentamers on the SLB

Hypothesis: close packing of circular MscL pentamers on SLB:

- The size ratio of closely packed circles is about 0.6.
- The number of MscL pentamers on the SLB is $0.6 * 1.131 \cdot 10^{-4} / (1.4 \cdot 10^{-16}) = 4.85 \cdot 10^{11}$.
- The maximum total mass of MscL on the SLB is 60.1 ng.
- For a 40-μl reaction (volume of each QCMD chamber), this corresponds to a concentration of 1.5 μg/ml or 0.1 μM of MscL proteins. Therefore, based on our deGFP and AH-eGFP quantifications (1-2 μM produced in QCMD chambers), about 20 times more proteins are produced in the QCMD chamber with respect to the membrane capacity.
- We assume a resolution of 5 Hz from the QCMD frequency signal.
- For MscL the drop is of about 300 Hz.
- We can detect 60 times less MscL, which corresponds to about 1 ng, based on maximum membrane coverage with MscL.
- It is unlikely that MscL reaches this level of packing on our SLBs, so this mass sensitivity is likely to be underestimated.

Figure S12. Estimation of the mass sensitivity of the QCMD.

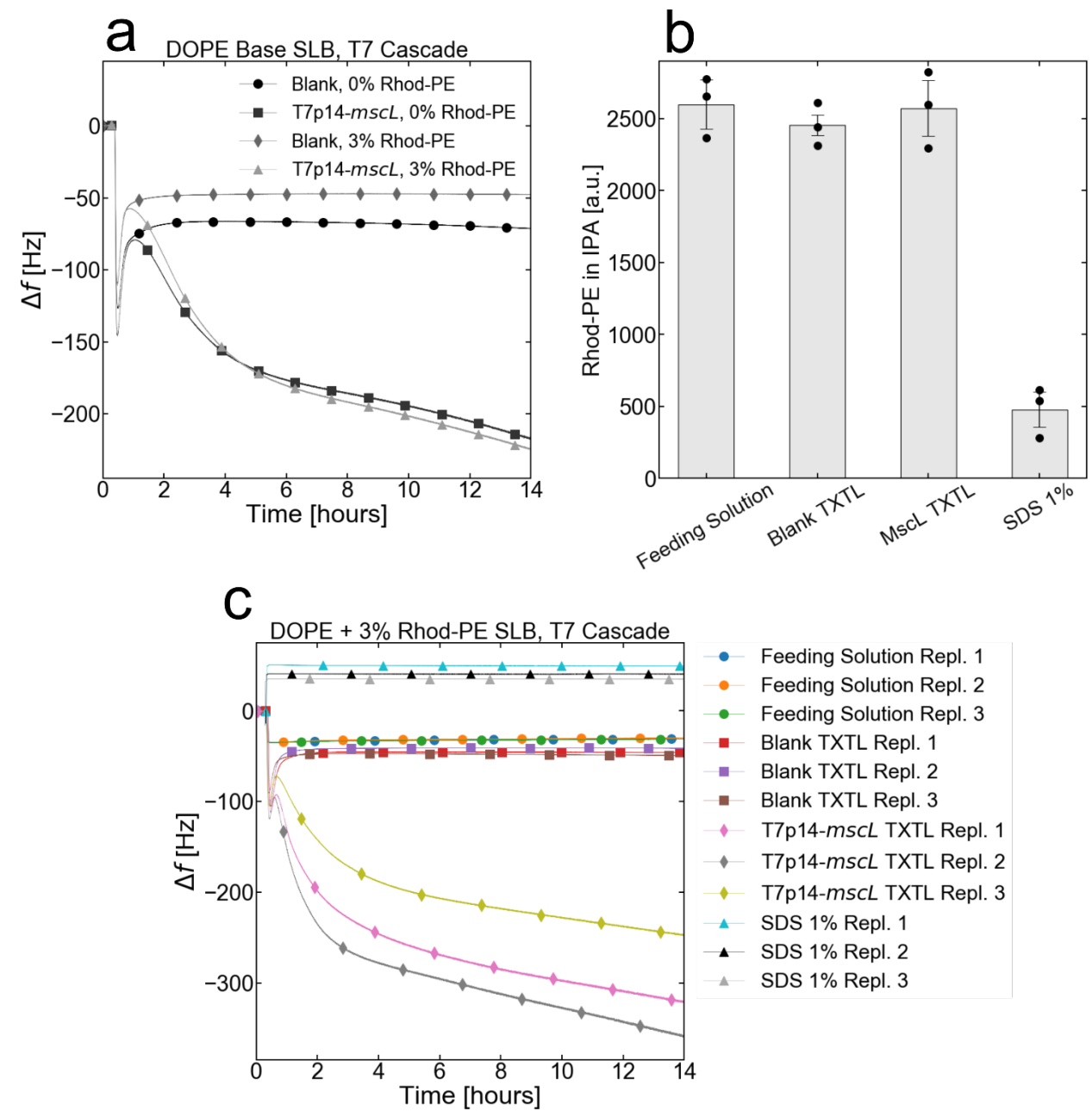


Figure S13. Quantification of lipid expulsion caused by TXTL reactions. **(a)** Adsorption kinetics of blank (P70a-*T7rnap*, 0.15 nM) and MscL (P70a-*T7rnap*, 0.15 nM, T7p14-*mscL*, 5 nM) TXTL reactions into DOPE and DOPE + Rhod-PE SLBs. **(b)** Quantification of IPA recovered Rhod-PE after overnight incubation of either a feeding solution (TXTL reaction without lysate), a blank TXTL reaction (P70a-*T7rnap*, 0.15 nM), an MscL TXTL reaction (P70a-*T7rnap*, 0.15 nM, T7p14-*mscL*, 5 nM), or 1% SDS. The mean and standard deviation are calculated from 3 replicates. **(c)** QCMD adsorption kinetics of the conditions from **(b)**.

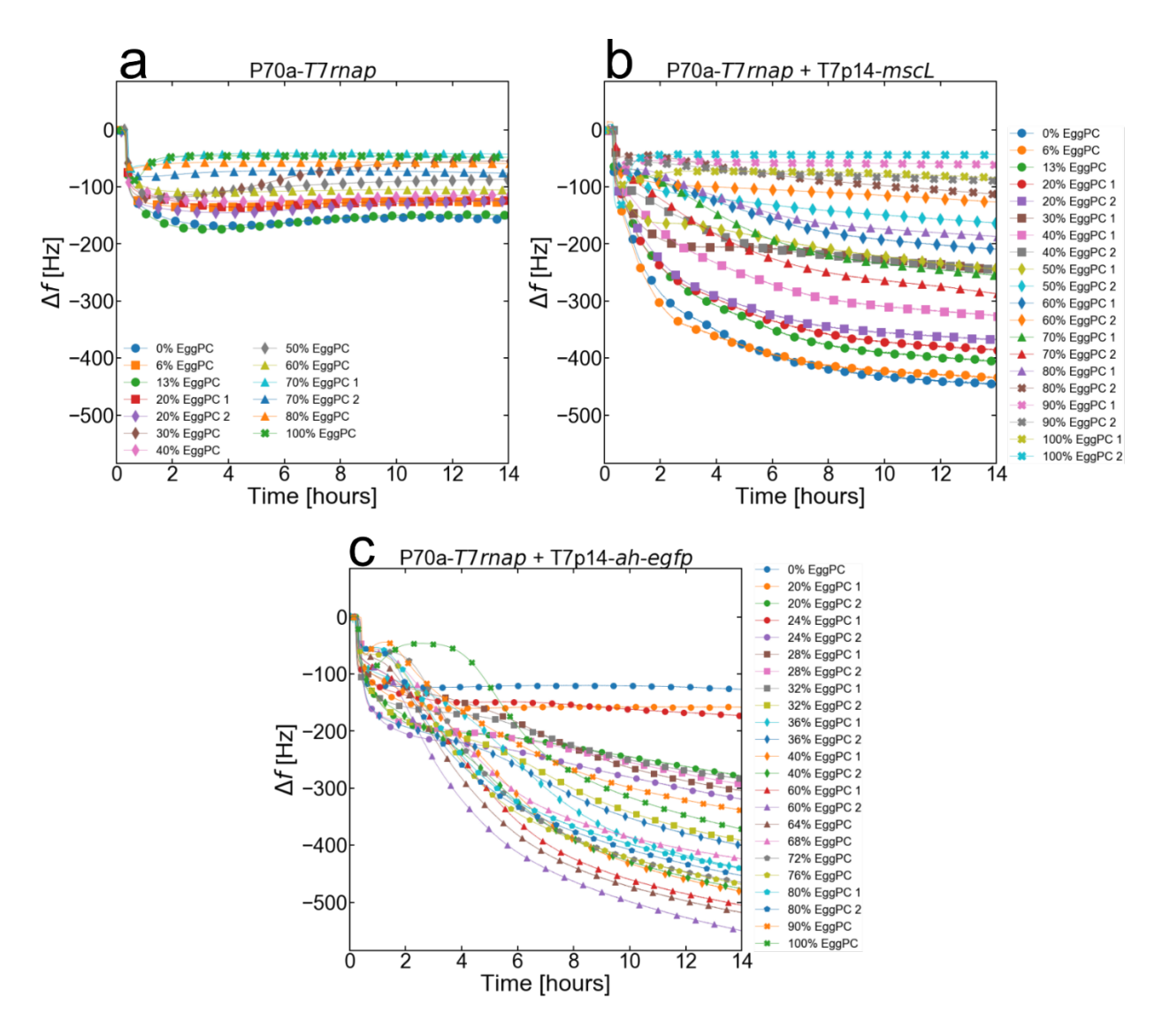


Figure S14. Adsorption kinetics of **(a)** a blank (P70a-*T7rnap*, 0.15 nM), **(b)** an MscL (P70a-*T7rnap*, 0.15 nM, T7p14-*mscL*, 5 nM), and **(c)** an AH-eGFP (P70a-*T7rnap*, 0.15 nM, T7p14-*ah-egfp*, 5 nM) TXTL reactions respectively into ECL – EggPC hybrid SLBs.

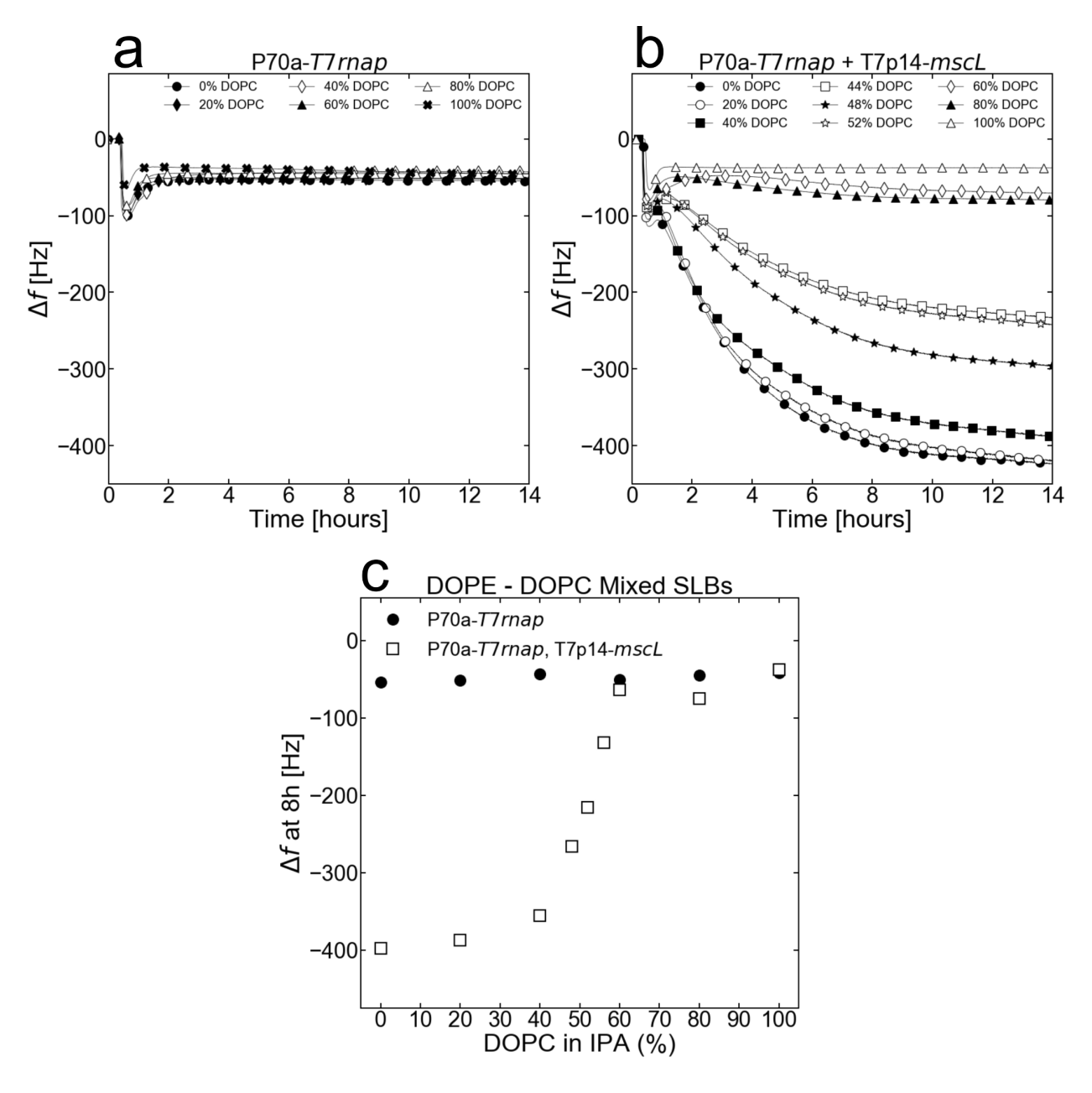


Figure S15. (a) and (b) Adsorption kinetics of blank (P70a-*T7rnap*, 0.15 nM) and MscL (P70a-*T7rnap*, 0.15 nM, T7p14-*mscL*, 5 nM) TXTL reactions respectively into DOPE – DOPC Mixed SLBs. (c) The frequency changes after 8 h of incubating either blank (P70a-*T7rnap*, 0.15 nM) or MscL (P70a-*T7rnap*, 0.15 nM, T7p14-*mscL*, 5 nM) TXTL reactions into DOPE – DOPC Mixed SLBs.

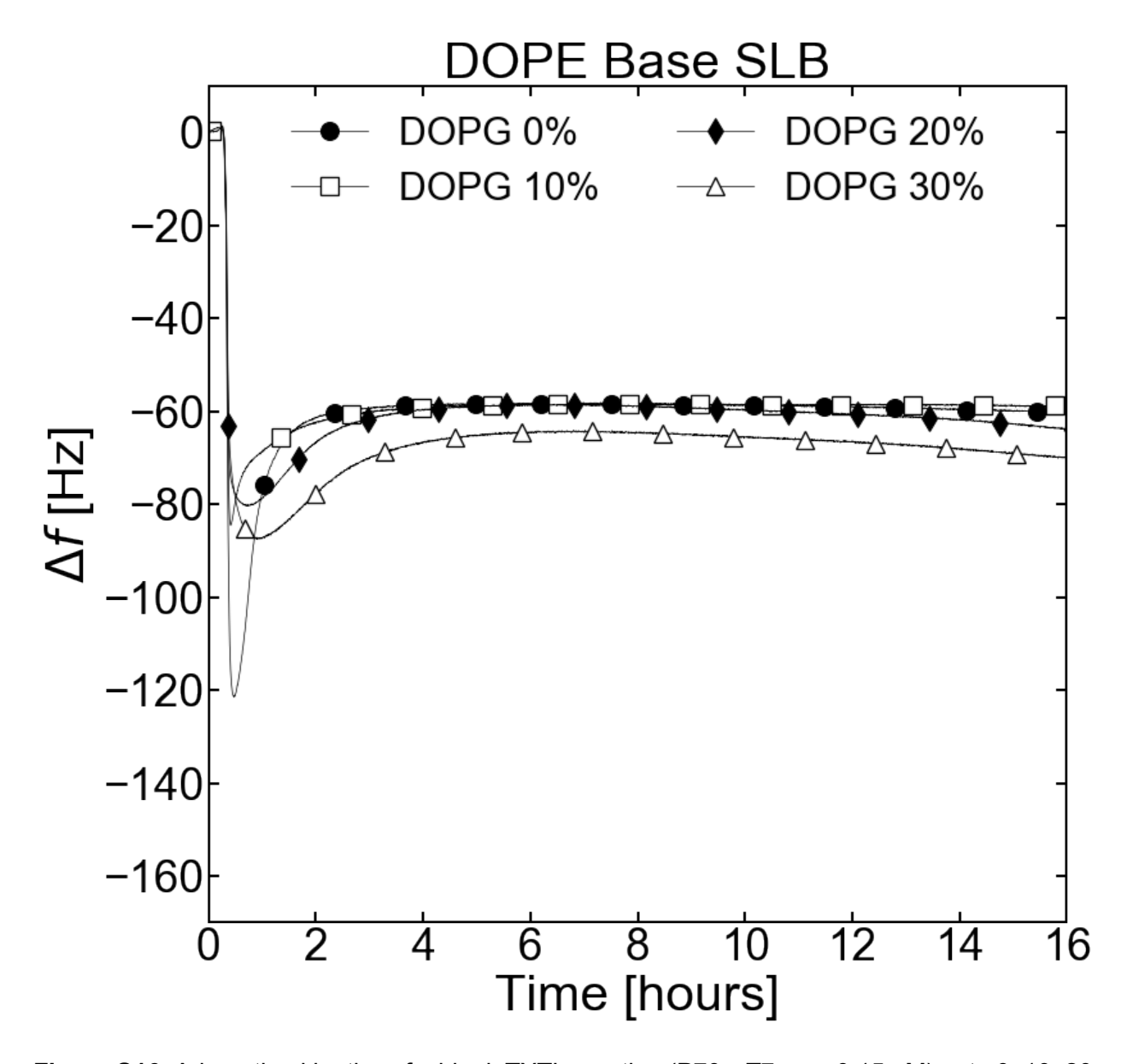


Figure S16. Adsorption kinetics of a blank TXTL reaction (P70a-T7rnap, 0.15 nM) onto 0, 10, 20, and 30% DOPG/DOPE SLBs

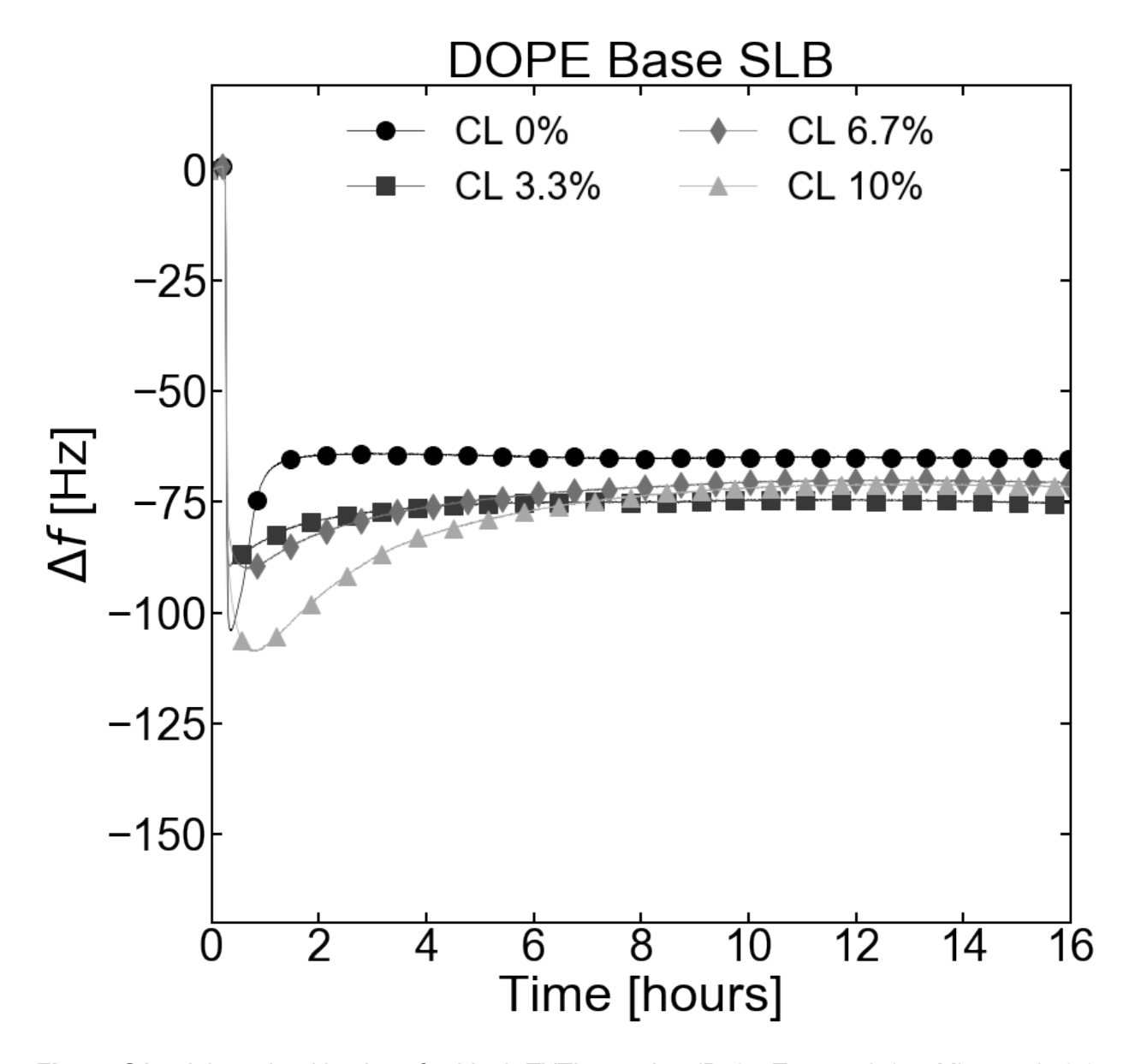


Figure S17. Adsorption kinetics of a blank TXTL reaction (P70a-T7rnap, 0.15 nM) onto 0, 3.3, 6.7, and 10% CL into a DOPE SLBs.

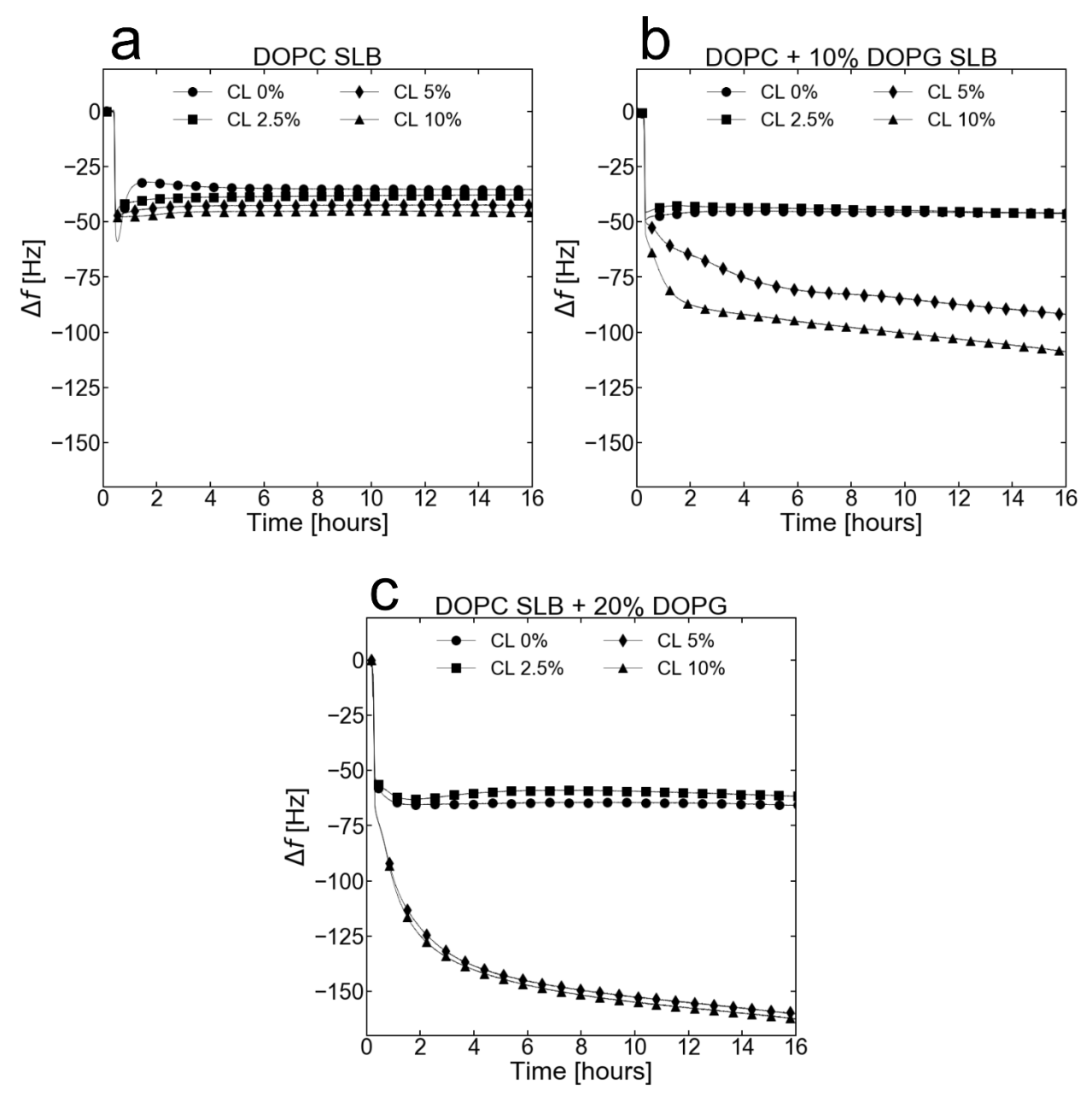


Figure S18. (a), (b), and (c) Adsorption kinetics of a blank TXTL reaction (P70a-*T7rnap*, 0.15 nM) onto a DOPC Base SLB as for different relative CL concentrations for a 0, 10, and 20% DOPG/DOPC mol. Ratio SLBs respectively.

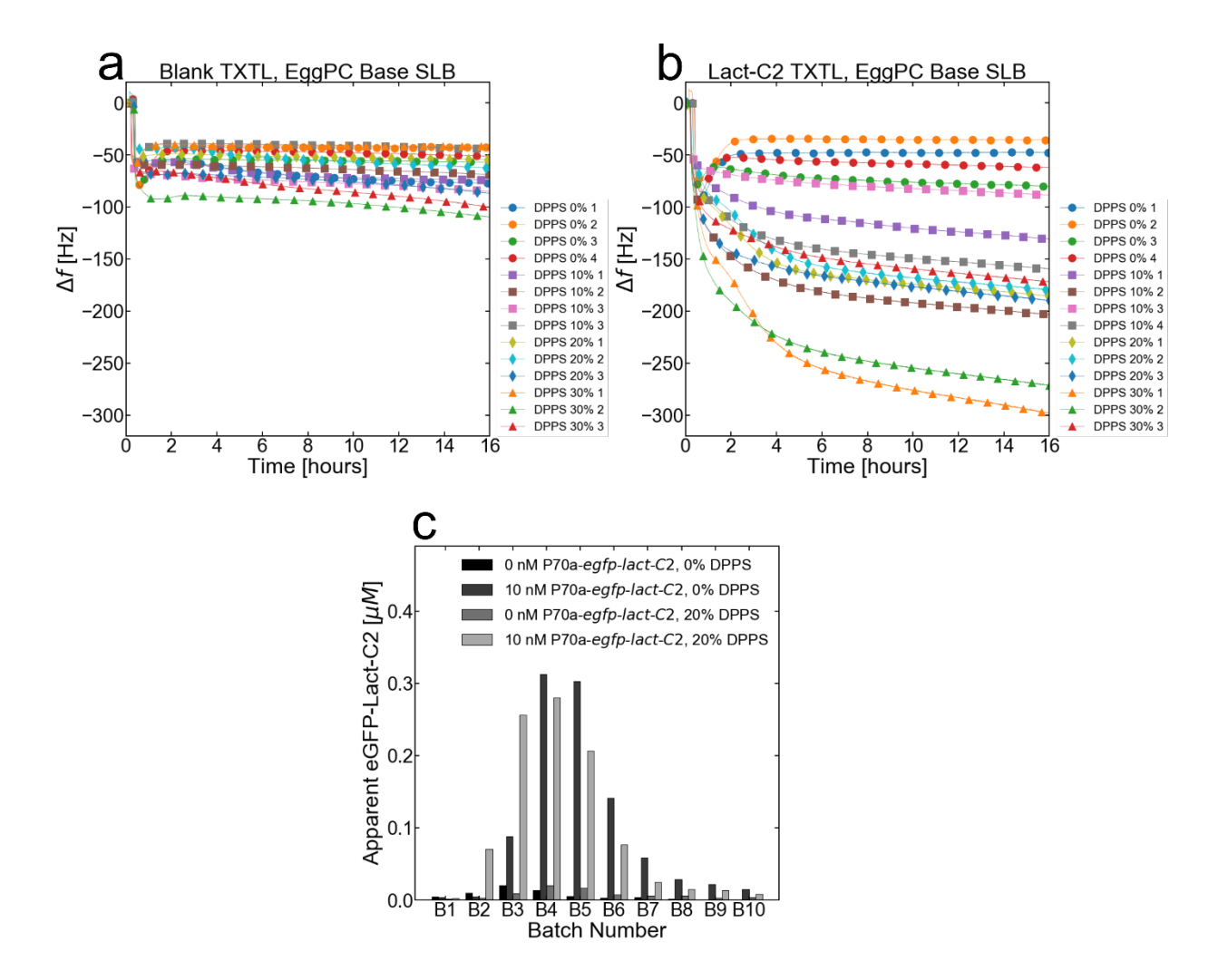


Figure S19. (a) and (b) Adsorption kinetics of either a blank (no DNA) and eGFP-Lact-C2 (P70a-egfp-lact-C2) TXTL reactions respectively incubated onto either a pure EggPC SLB or an EggPC SLB mixed with DPPS. (c) End-point measurement of TXTL expression with and without 20% DPPS in an EggPC SLB.

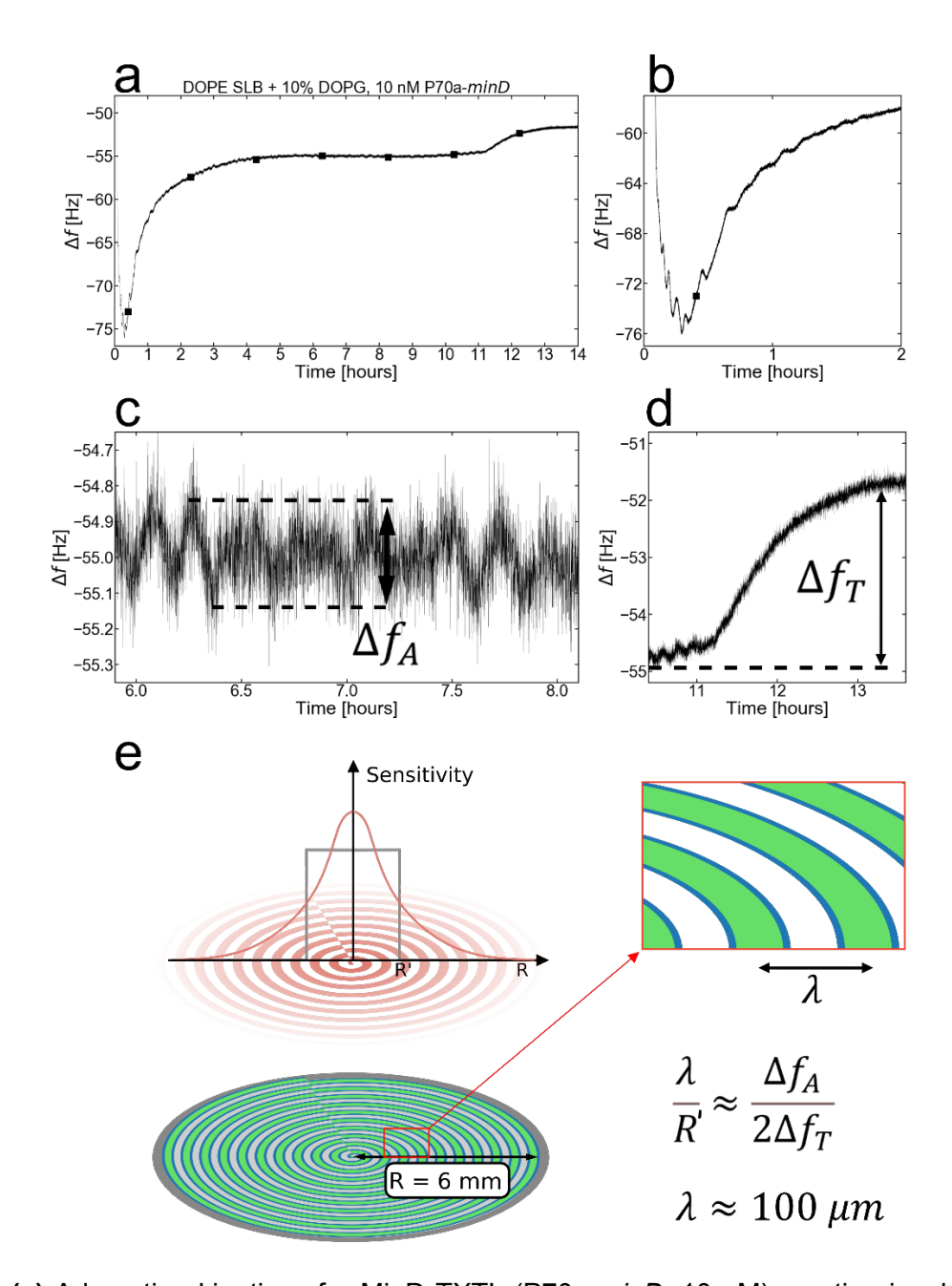


Fig. S20. (a) Adsorption kinetics of a MinD TXTL (P70a-*minD*, 10 nM) reaction incubated onto DOPE + 10% DOPG SLB. (b) Large amplitude oscillations during the first 2 hours of incubation. (c) Small-amplitude oscillations during the middle of the incubation. The amplitude of a single oscillation is labeled as Δf_A . (d) The increase in frequency at the end of the reaction due to ATP depletion is labeled as Δf_T . (e) Assuming that the Min patterns are radially symmetric fronts moving from the center of the sensor-SLB system to the edge, then Δf_A is proportional to the mass of the outermost ring escaping the boundaries of the most sensitive area of the sensor (grey box, $r < R' \approx R/3$) , while Δf_T is proportional to the mass of all rings combined within the most sensitive area of the sensor. Since the escaping ring is twice the mass of the average ring within the box, then we can approximate the wavelength as in the equation in the panel. This approximation yields a wavelength of approximately 100 μm from the parameters obtained in (c) and (d).

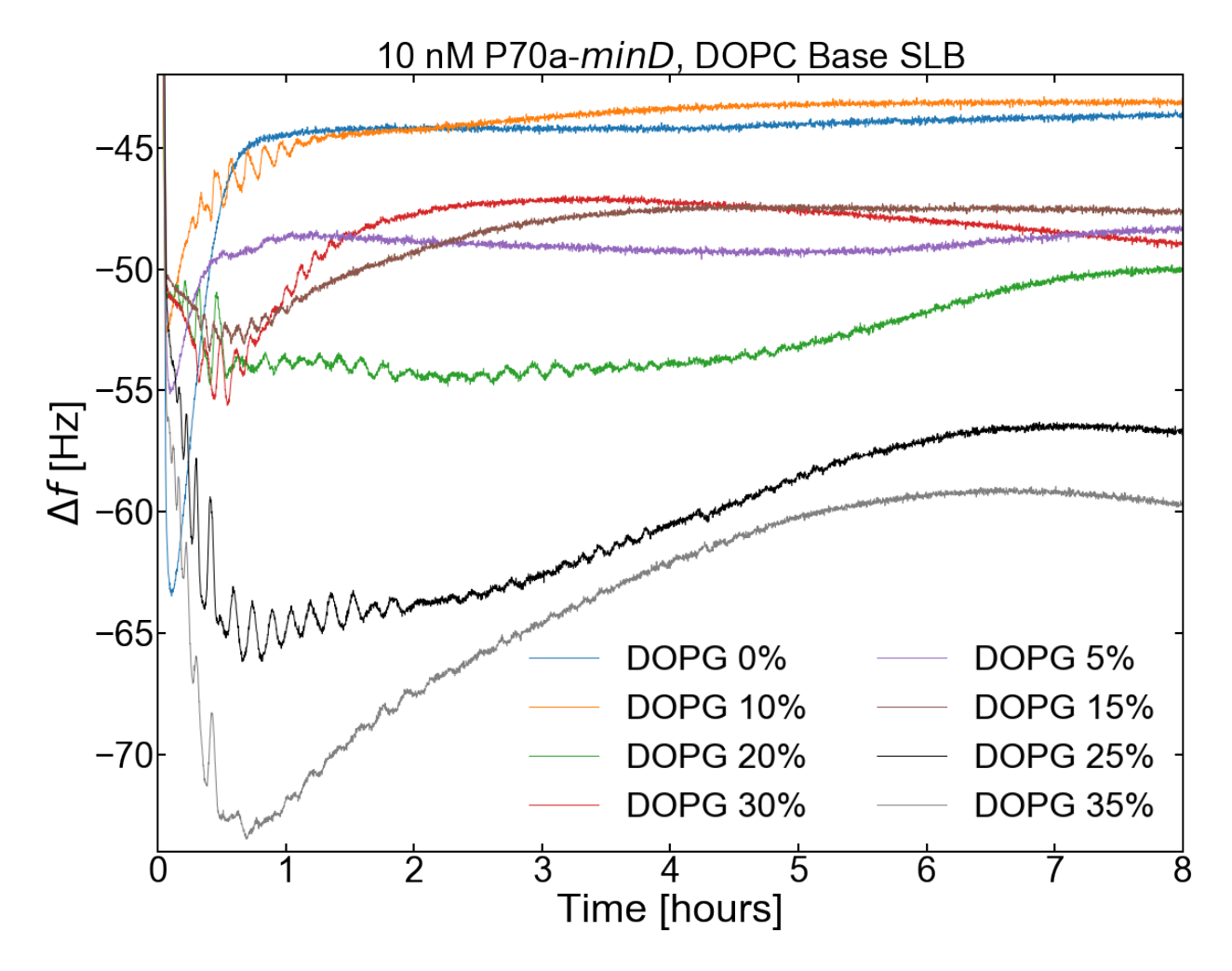


Figure S21. Adsorption kinetics of a MinD TXTL (P70a-*minD*, 10 nM) reaction for a range of different DOPG/DOPC composed SLBs.

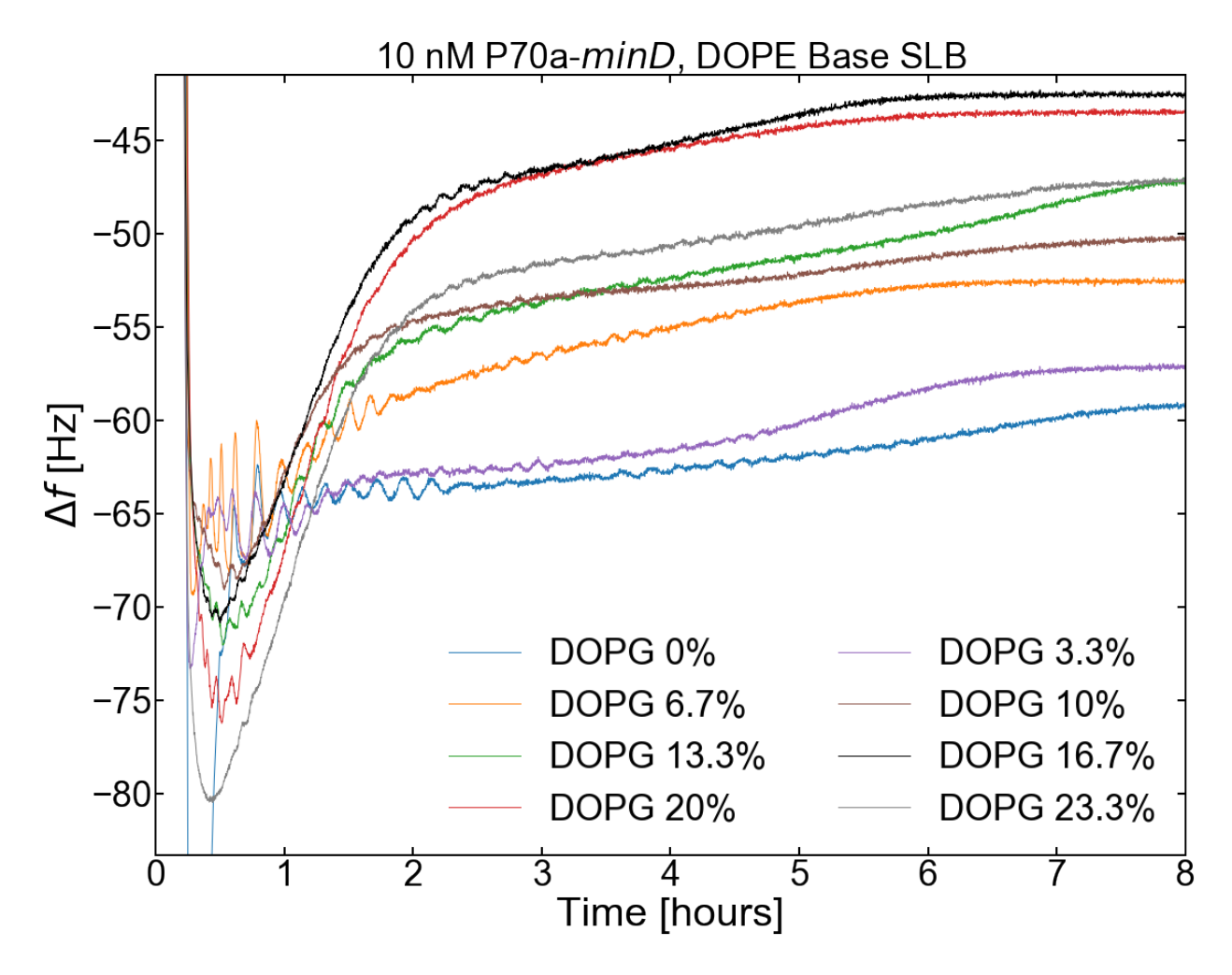


Figure S22. (a) Adsorption kinetics of a MinD TXTL (P70a-*minD*, 10 nM) reaction for a range of different DOPG/DOPE composed SLBs.

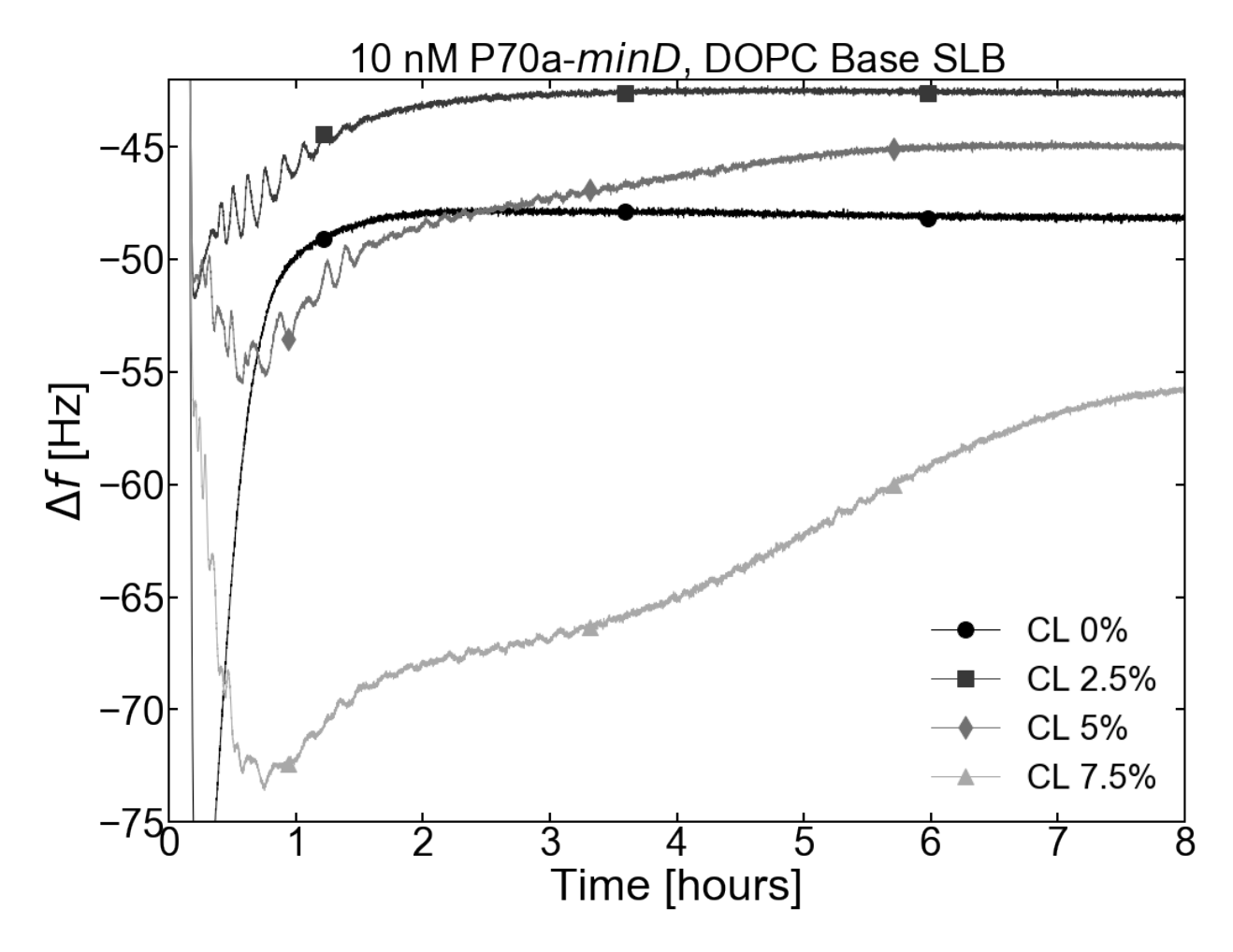


Figure S23. Adsorption kinetics of a MinD TXTL (P70a-*minD*, 10 nM) reaction for a range of different CL/DOPC composed SLBs.

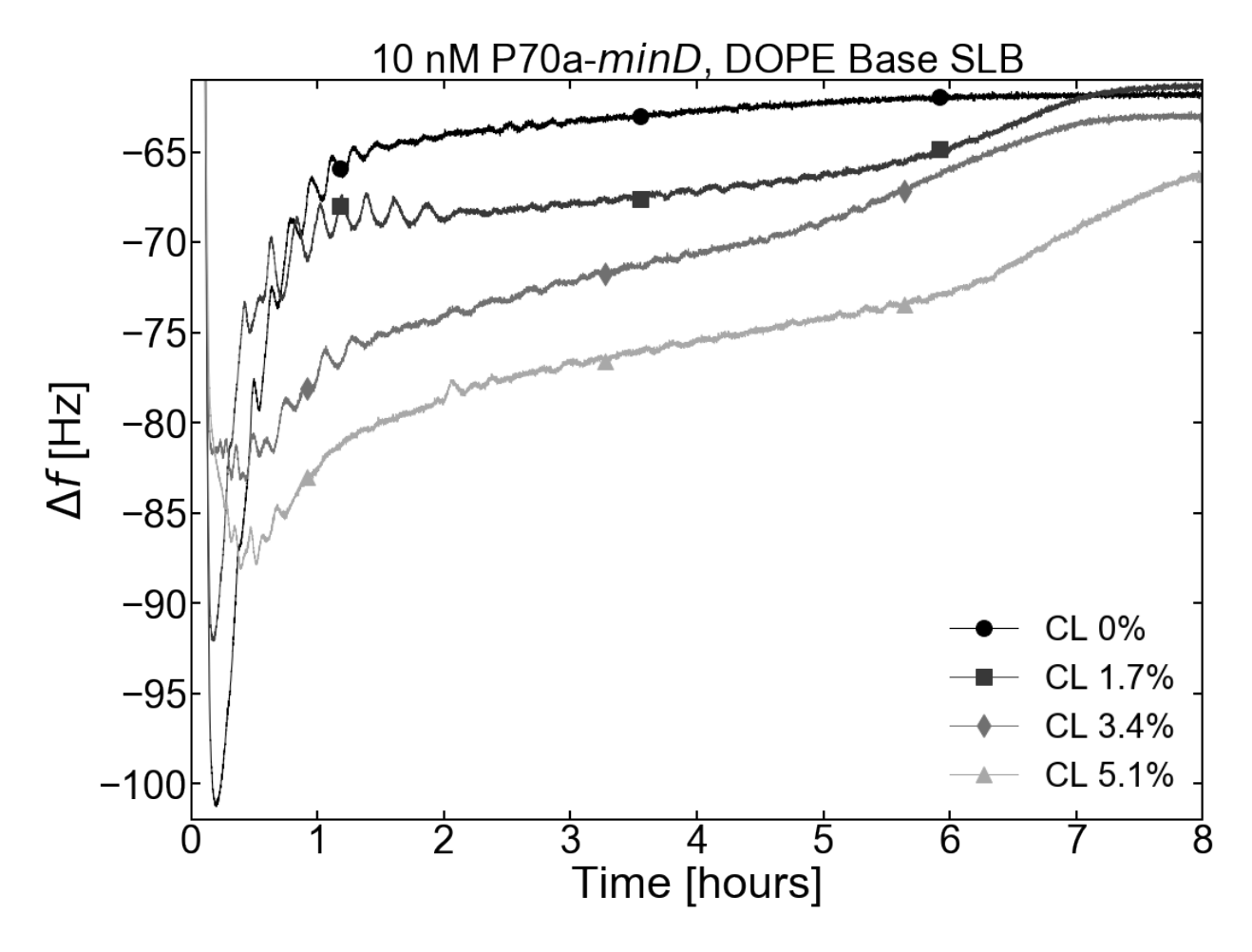


Figure S24. Adsorption kinetics of a MinD TXTL reaction (P70a-*minD*, 10 nM) for a range of different CL/DOPE composed SLBs.

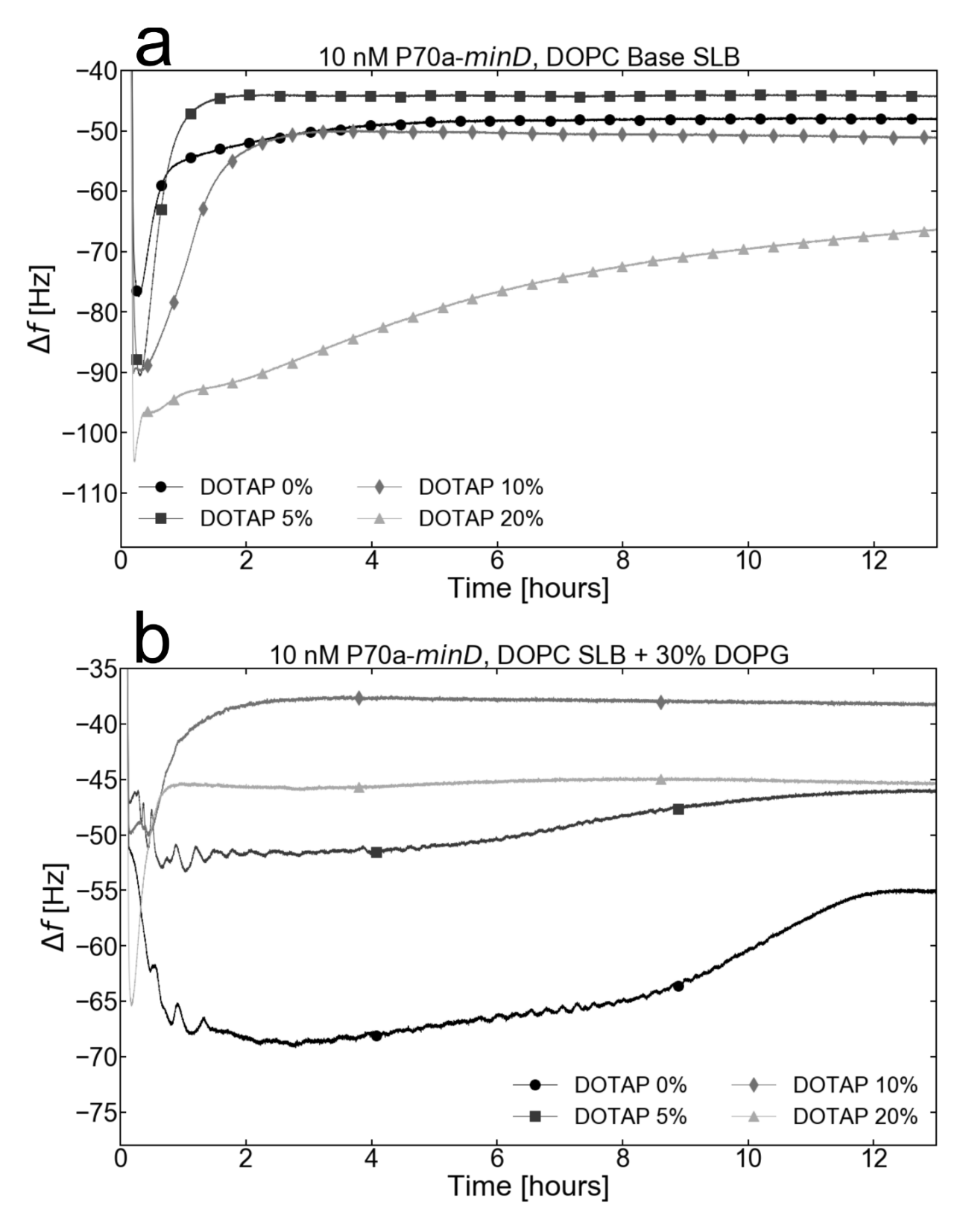


Figure S25. (a) and (b) Adsorption kinetics of a MinD TXTL (P70a-*minD*, 10 nM) reaction for a range of different DOTAP SALB concentrations for a pure DOPC SLB and a DOPG/DOPC SLB respectively.

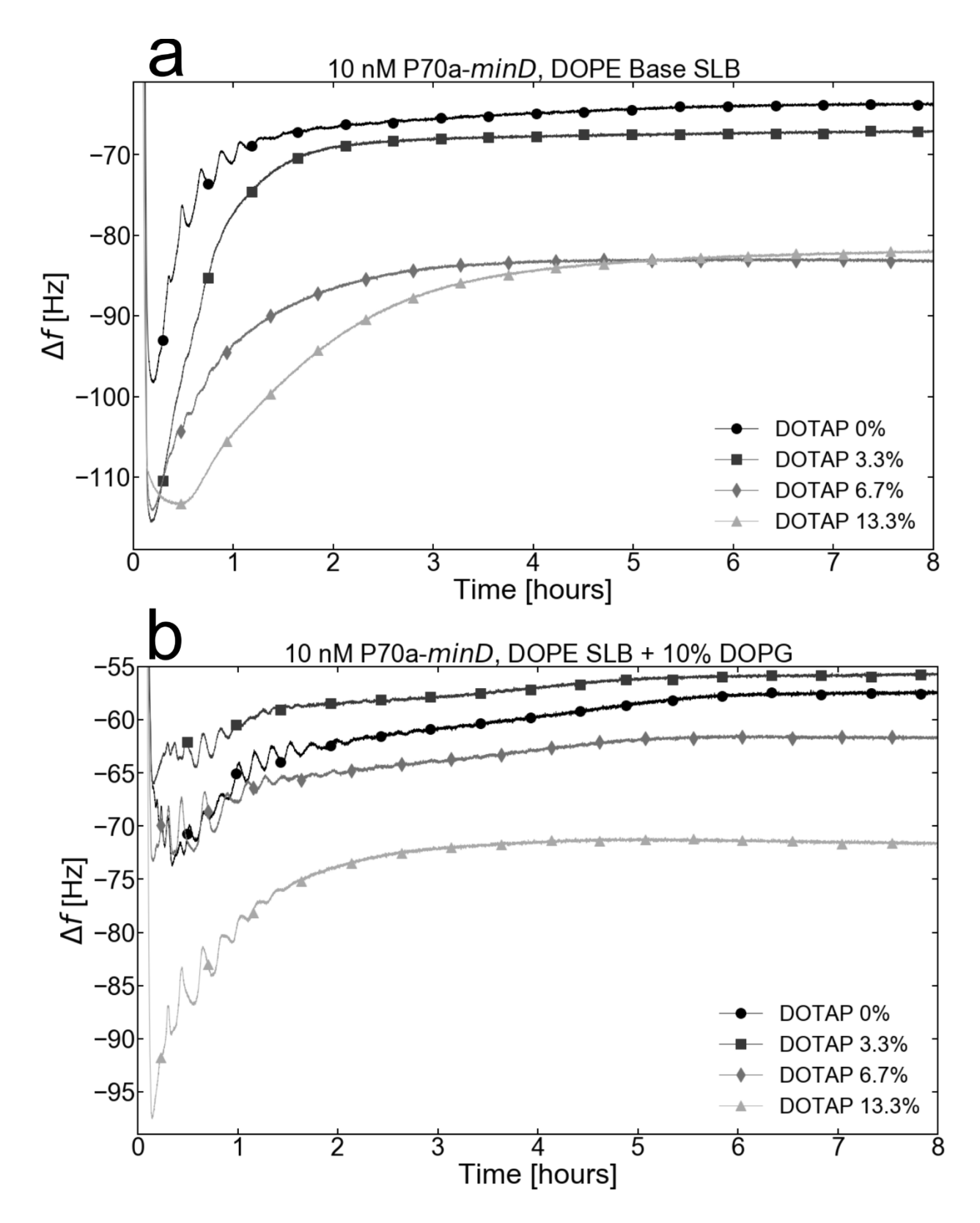


Figure S26. (a) and (b) Adsorption kinetics of a MinD TXTL (P70a-*minD*, 10 nM) reaction for a range of different DOTAP SALB concentrations for a pure DOPE SLB and a DOPG/DOPE SLB respectively.

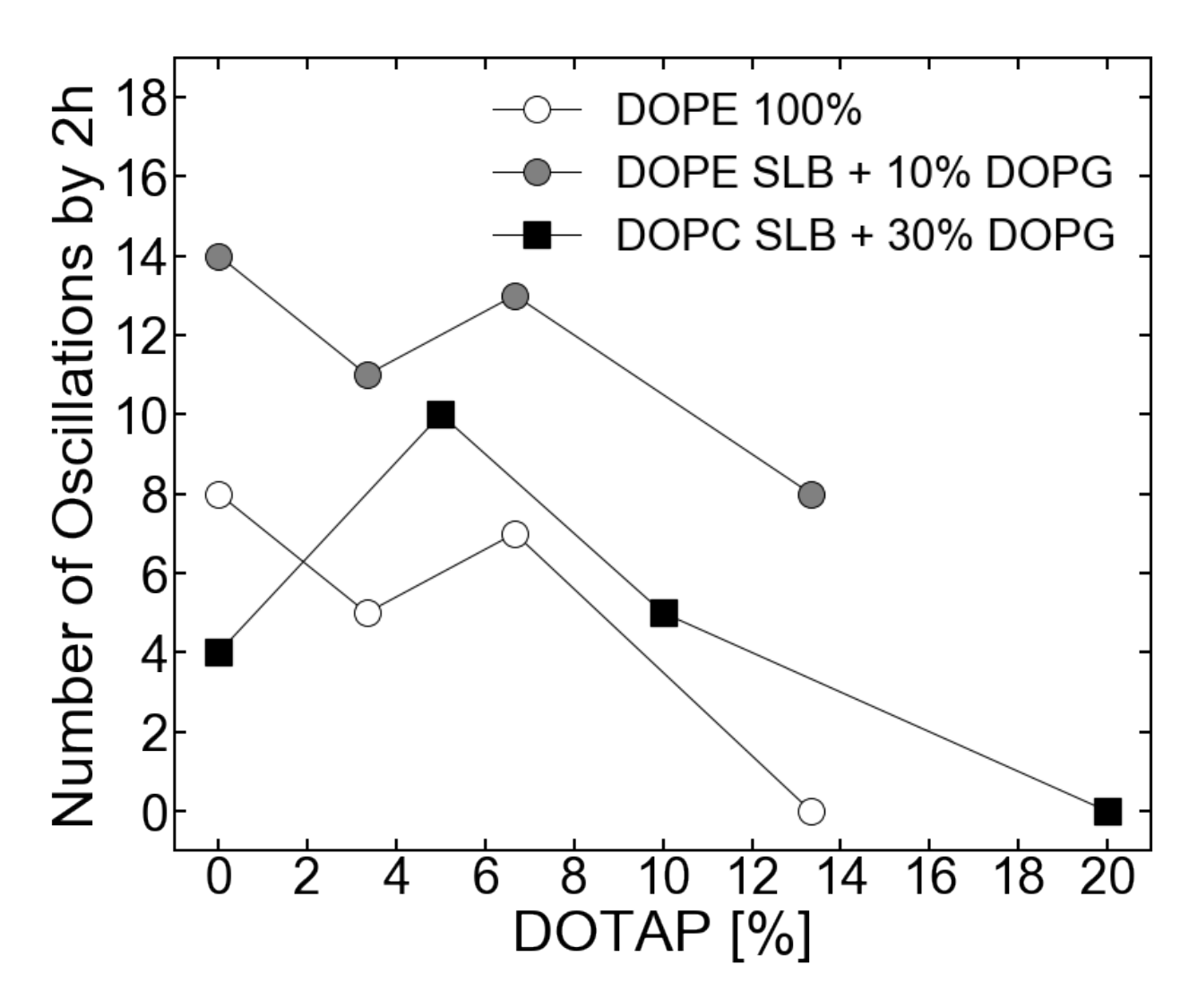


Figure S27. The number of oscillation peaks within the first 2 hours as a function of the relative DOTAP concentration during SALB for either a DOPE SLB, a DOPG/DOPE SLB, or a DOPG/DOPC SLB (P70a-*minD*, 10 nM).

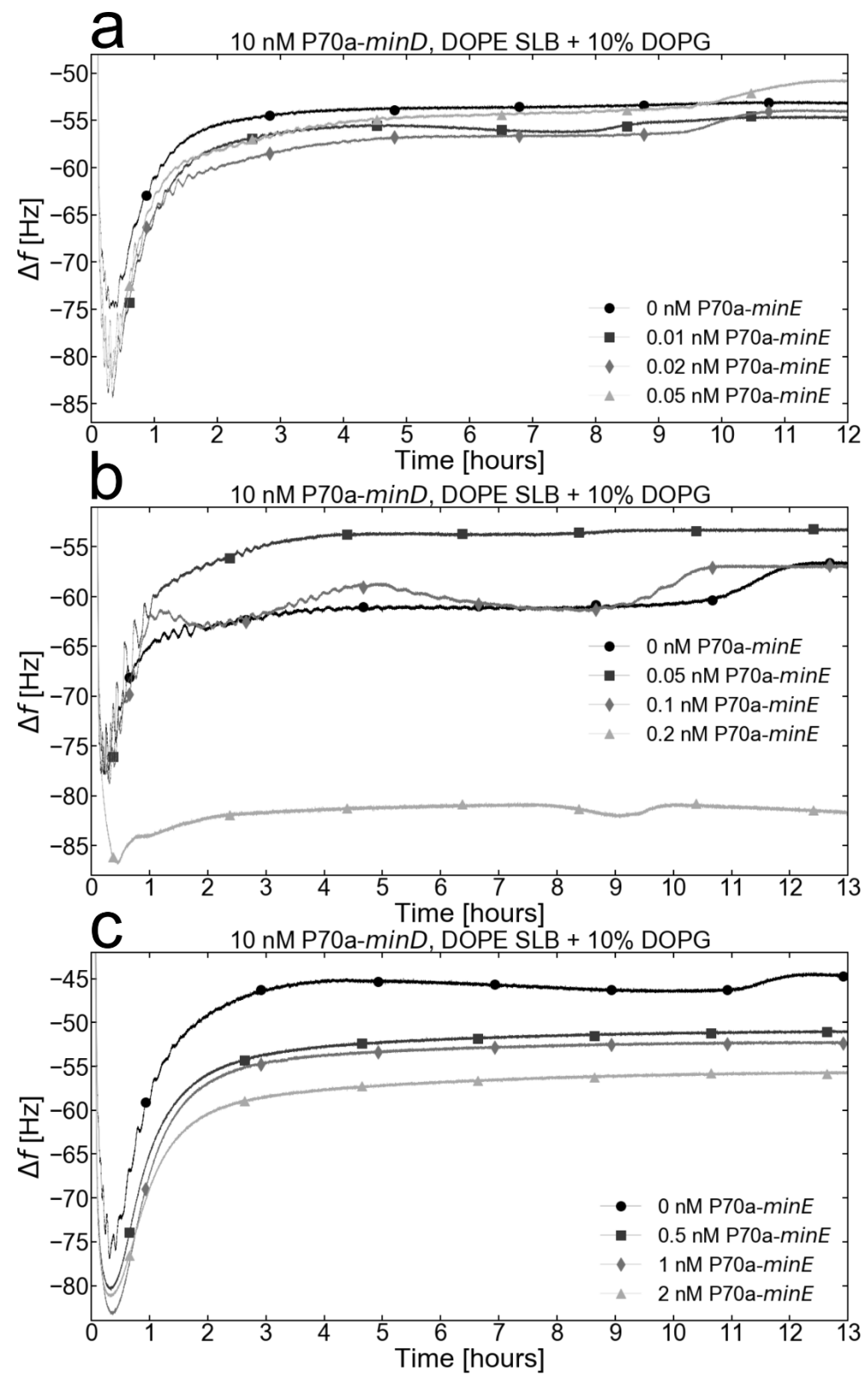


Figure S28. (a), (b), and (c) Adsorption kinetics of a MinDE TXTL (P70a-*minD*, 10 nM, P70a-*minE*, varied) reaction for different P70a-*minE* concentrations into a DOPG/DOPE 10% mol. Ratio SLB.

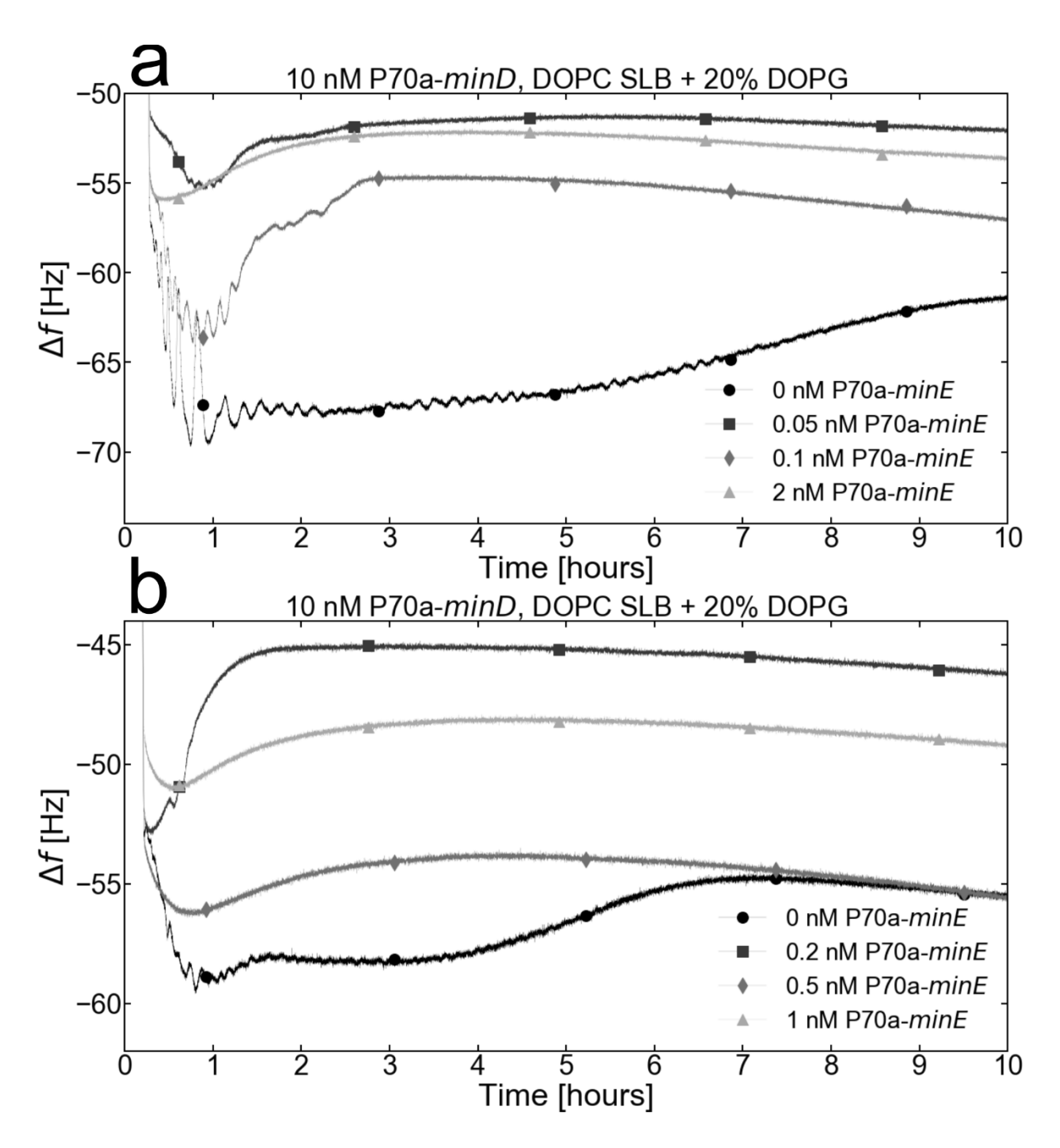


Figure S29. (a) and (b) Adsorption kinetics of a MinDE TXTL (P70a-minD, 10 nM, P70a-minE, varied) reaction for different P70a-minE concentrations into a DOPC + 20% DOPG SLB.

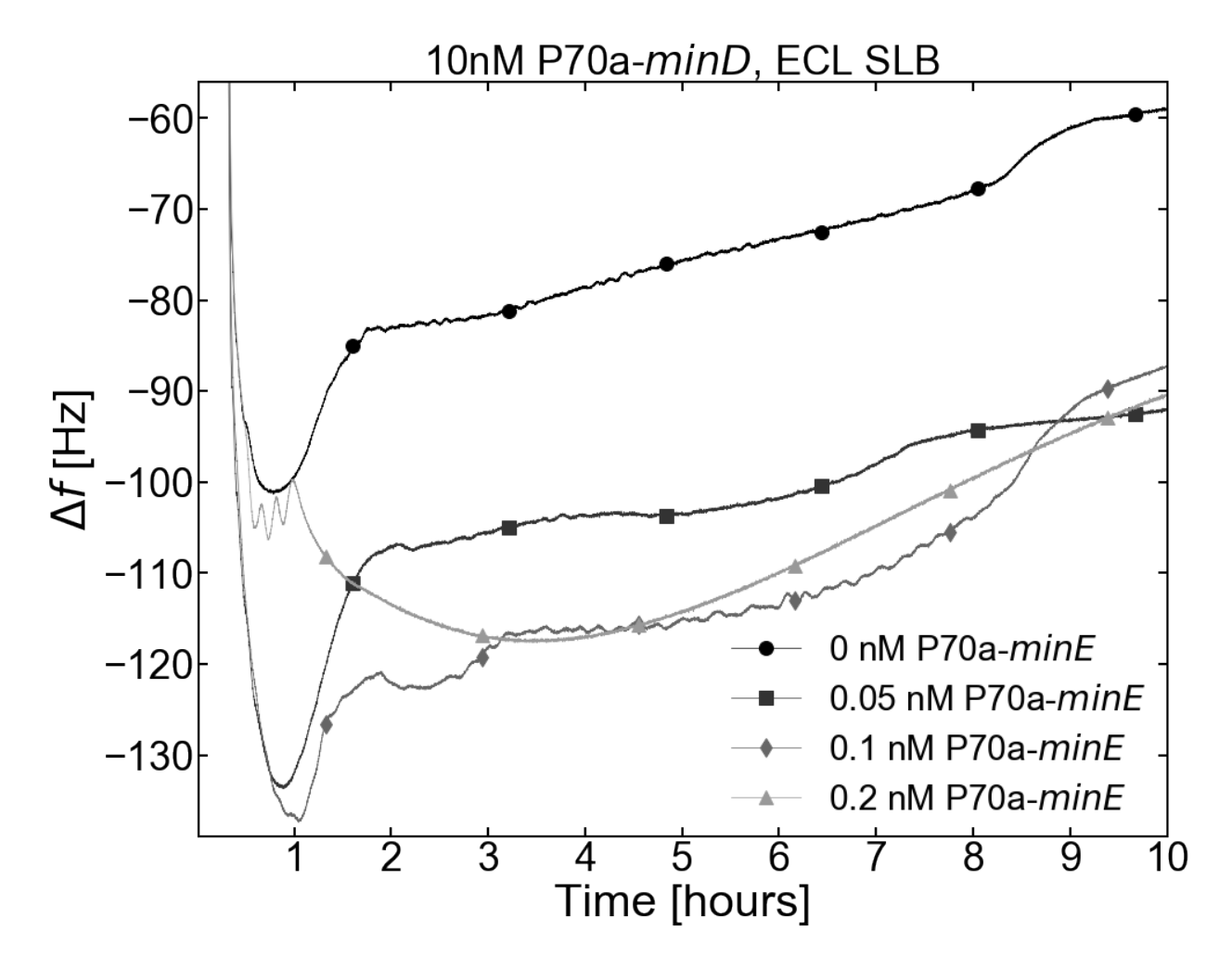


Figure S30. Adsorption kinetics of a MinDE TXTL (P70a-*minD*, 10 nM, P70a-*minE*, varied) reaction for different P70a-*minE* concentrations into a ECL SLB.

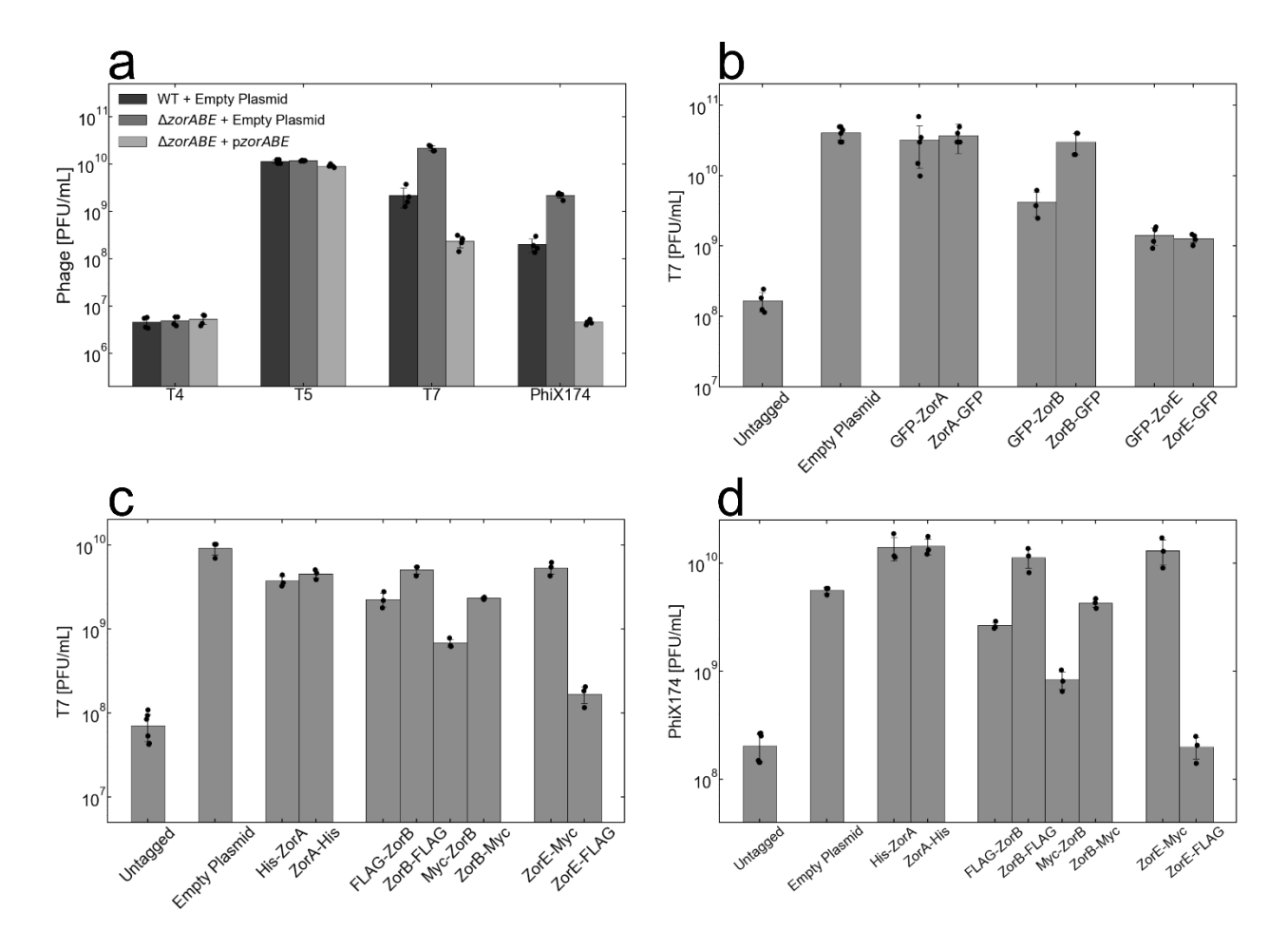


Figure S31. Tagging of Zorya proteins disrupts defense against phages. (a) Reduction in plaque forming units in the presence of Zorya. (b) Reduction in T7 phage plaque forming units in the $\Delta zorABE$ knockout mutant. Zorya was supplemented on plasmids containing different combinations of the GFP tag at the termini of the respective proteins. (c) Reduction in the T7 plaque forming units in the $\Delta zorABE$ knockout mutant. Zorya was supplemented on plasmids containing different combinations of His, Myc, and FLAG tags at the termini of the respective proteins. (d) Reduction in the phiX174 plaque forming units in the $\Delta zorABE$ knockout mutant. Zorya was supplemented on plasmids containing different combinations of His, Myc, and FLAG tags at the termini of the respective proteins. The value and the uncertainty of the bars are the mean and standard deviation of at at least 3 replicates.

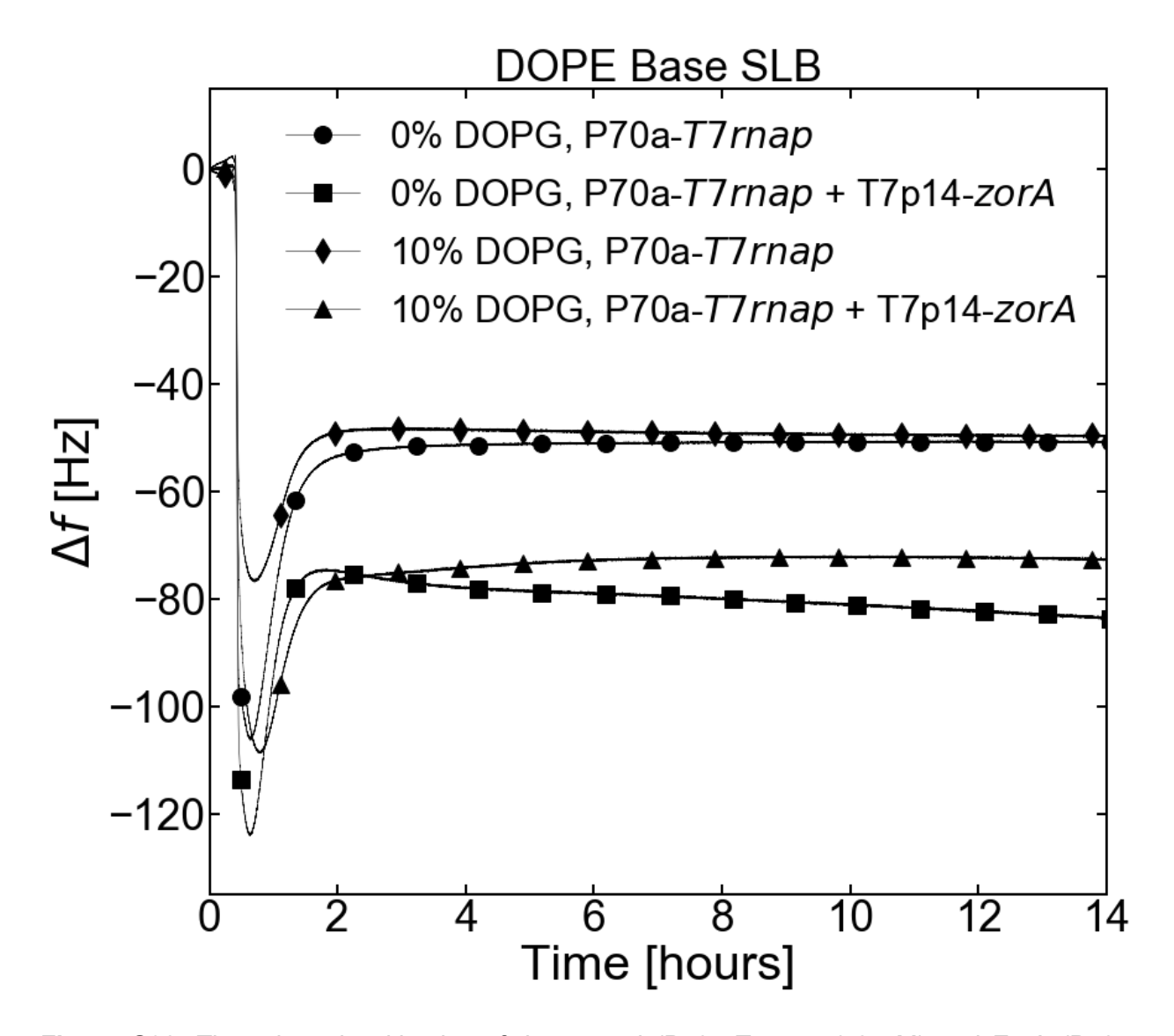


Figure S32. The adsorption kinetics of the control (P70a-*T7rnap*, 0.2 nM) and ZorA (P70a-*T7rnap*, 0.2 nM, T7p14-*zorA*, 10 nM) conditions with either a pure DOPE or DOPE + 10% DOPG SLBs.

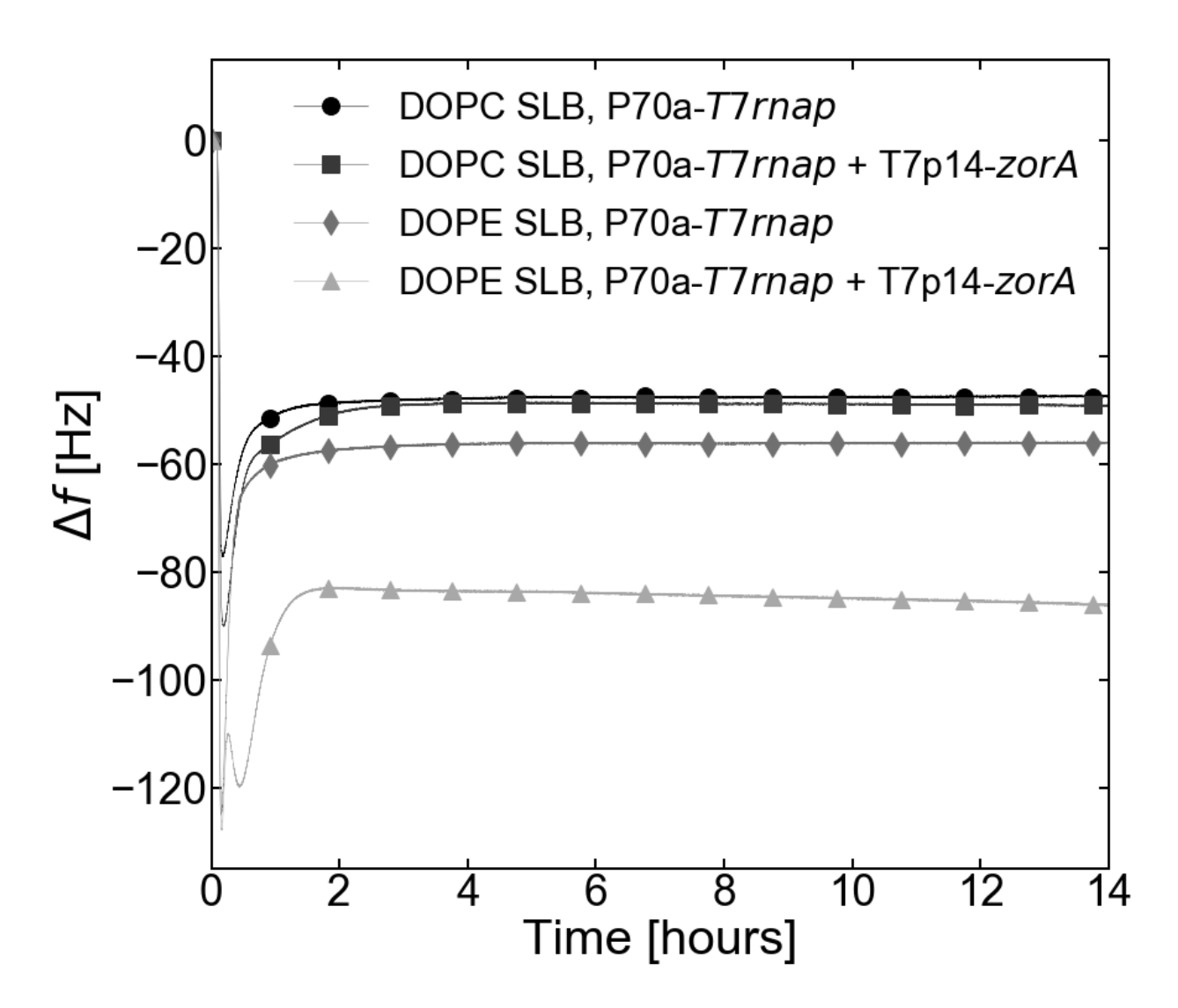


Figure S33. The adsorption kinetics of the control (P70a-*T7rnap*, 0.2 nM) and ZorA (P70a-*T7rnap*, 0.2 nM, T7p14-*zorA*, 10 nM) conditions with either a pure DOPC or pure DOPE SLBs.

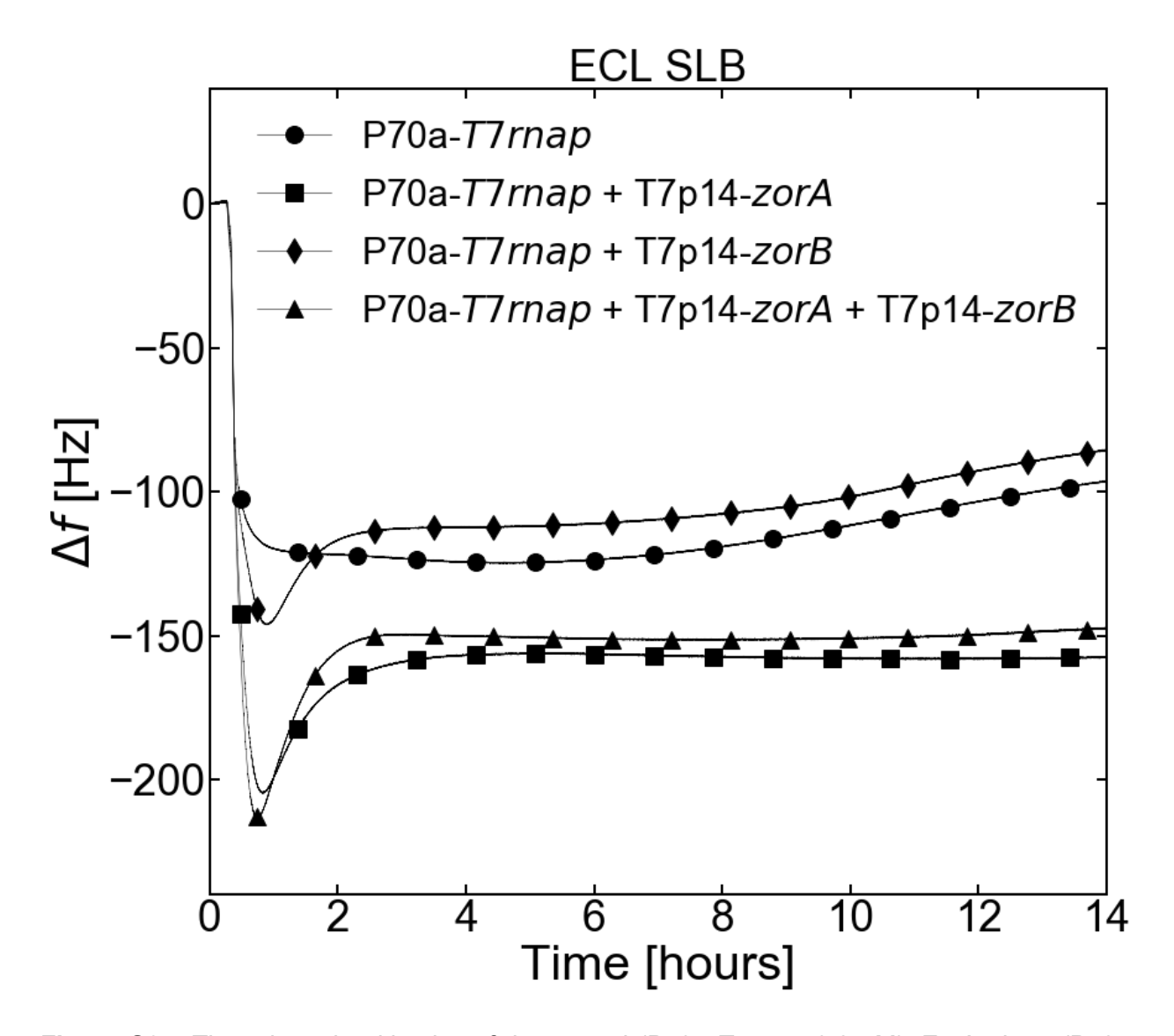


Figure S34. The adsorption kinetics of the control (P70a-*T7rnap*, 0.2 nM), ZorA alone (P70a-*T7rnap*, 0.2 nM, T7p14-*zorA*, 10 nM), ZorB alone (P70a-*T7rnap*, 0.2 nM, T7p14-*zorB*, 10 nM), and ZorA and ZorB together (P70a-*T7rnap*, 0.2 nM, T7p14-*zorA*, 10 nM, and T7p14-*zorB*, 10 nM) with an ECL SLB.

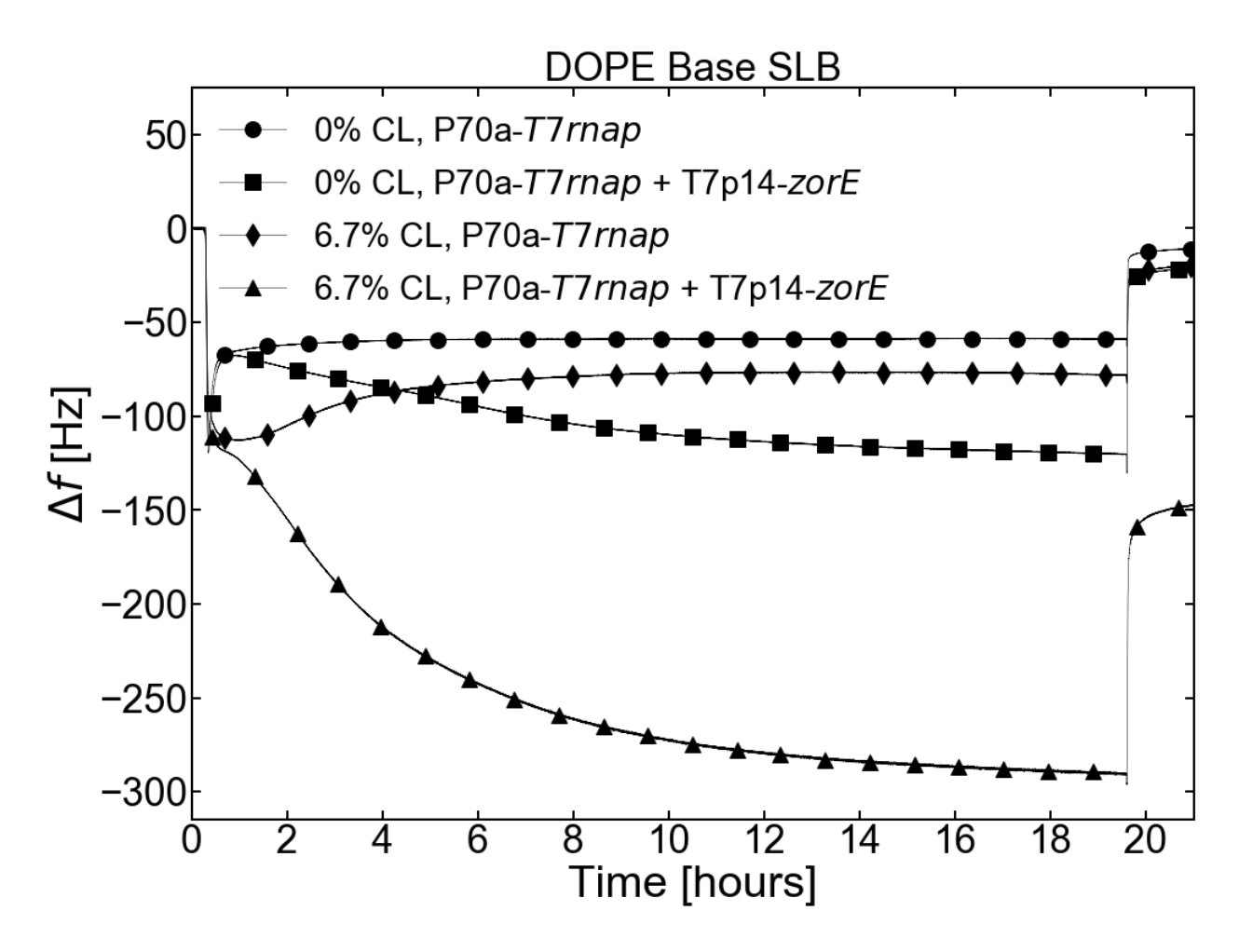


Figure S35. Same as in **Fig. 6f** but with the measurement extended to t = 21 h after TXTL incubation start. The 1-h Tris NaCl flush starts at t = 19.6 h.

SLB composition	concentration (mM)	mass density (mg/mL)
DOPC	1.3 mM	1 mg/mL
EggPC	1.3 mM	1 mg/mL
DOPE	1.95 mM	1.5 mg/mL
E. coli lipids (ECL)	3 mM (approximated)	3 mg/mL

Supplementary Table S1. Concentrations of phospholipids in IPA during SALB formation to obtain full coverage of the QCMD sensor and no nonspecific TXTL adsorption. Note that ECL are a mix of several phospholipids of different molecular weights, the average molecular weight of which is not communicated by the manufacturer but roughly estimated from its approximate composition.

References

- 1. Hamill, O. P. & Martinac, B. Molecular Basis of Mechanotransduction in Living Cells. *Physiological Reviews* **81**, 685–740 (2001).
- 2. Hillier, A. C. & Ward, M. D. Scanning electrochemical mass sensitivity mapping of the quartz crystal microbalance in liquid media. *Anal. Chem.* **64**, 2539–2554 (1992).

List of plasmids and linear DNA used in this study

DNA Name	Plasmid or Linear	ID	Benchling Link
			https://benchling.com/s/seq-
		No	1gNUXg0A3IBVf556eAXw?m=slm-
P70a-deGFP (Plasmid)	Plasmid	ID	nMLpZCFR9Gaw7jLqSTsF
			https://benchling.com/s/seq-
		No	rAhPBqYvIG7zTaUGC2iF?m=slm-
P70a-T7RNAp (Plasmid)	Plasmid	ID	ilQuca6mgC1l85vv3D8A
			https://benchling.com/s/seq-
		No	JhiUQwAQhJCodnSWSo4A?m=slm-
T7p14-deGFP (Plasmid)	Plasmid	ID	Y8hrFrHrg12N4PLGE2qk
			https://benchling.com/s/seq-
		No	Q1of0ufkrvJfn1kLdYB2?m=slm-
T7p14-MscL (Plasmid)	Plasmid	ID	NcNrlxmDvjehtllYv2LC
			https://benchling.com/s/seq-
T7p14-aHL-eGFP		No	ReWms9Pv6eWuCcDW9WtT?m=slm-
(Plasmid)	Plasmid	ID	1hAwFn7qVoLruklk6YYT
			https://benchling.com/s/seq-
P70a-eGFP-LactC2		No	5wgQIAMPP7oiaOfZr6qk?m=slm-
(Plasmid)	Plasmid	ID	JMV9zcV5njYsKTYI982A
			https://benchling.com/s/seq-
		No	P9tMTfEpKqf6zn7YympR?m=slm-
P70a-MinD	Linear	ID	O5uV66h40py0DxHZ5F8U
			https://benchling.com/s/seq-
		No	Bz5QSKvYUqgU26dei5k3?m=slm-
P70a-MinE	Linear	ID	WdxE1xtsglR211boklX2
			https://benchling.com/s/seq-
		No	kdLu9i9uStCEJ265sE4u?m=slm-
P70a-MinC	Linear	ID	b973qHb6Xp7AJiFCEAPR
Zorya (zorABE from			https://benchling.com/s/seq-
DSM-1576 in pSG		CBS-	GCoULHjWslwgEWmsCDBe?m=slm-
(ATCC 8739)	Plasmid	5891	jxQrbhly8EdBAKv3Vh67
pKD13 Lambda Red			https://benchling.com/s/seq-
recombineering		CBS-	zm5YCVYWj72qS0IVCTQn?m=slm-
plasmid	Plasmid	217	ahBh68usU5X1Vbljo8sf
pCP20 Lambda Red			https://benchling.com/s/seq-
recombineering		CBS-	6w98X5CyYnlhT6z34kFA?m=slm-
plasmid	Plasmid	218	krmpkl1Tla5BXvhg1XoH
pKD46 Lambda Red			https://benchling.com/s/seq-
recombineering		CBS-	T9kbgiwOTDCA9HAicsqy?m=slm-
plasmid	Plasmid	219	WdI0GZoV0zLoFYnGXUv5
			https://benchling.com/s/seq-
Zorya DSM-157 ZorA		OD-	bURXCcWOY4liay1iwjRd?m=slm-
N-GFP (Plasmid	Plasmid	686	jAHBw3IPJR5oJFQKH8uI

			https://benchling.com/s/seq-
7 00144577 4		0.5	kKwQHzJUnTVb5Z8EwrS2?m=slm-
Zorya DSM-157 ZorA C-GFP	Plasmid	OD- 687	fcsBBrlSu5JitFLe6F0L
C-GFF	Flasilliu	007	https://benchling.com/s/seq-
7 5014 457 7 5		0.5	v0e5fwPsgA8dt0LTL562?m=slm-
Zorya DSM-157 ZorB N-GFP	Plasmid	OD- 688	fU7VZv5f6n6mxmstV8fn
N-GFF	riasiiiu	000	https://benchling.com/s/seq-
7 5014 457 7 5		0.0	SDZ5c7BitFo0kMom510F?m=slm-
Zorya DSM-157 ZorB C-GFP	Plasmid	OD- 689	u7qNneSHfs57WyMczC6B
C-G1 F	Hasiiia	009	https://benchling.com/s/seq-
70m/0 DCM 457 70mF		00	jLAHw9noBGbwGmykbplo?m=slm-
Zorya DSM-157 ZorE N-GFP	Plasmid	OD- 690	opaXyzohUfoESu2kyO3J
N-GI F	i iasiiia	030	https://benchling.com/s/seq-
7 DOM 457 7		0.0	gyw4KShLp2LVTvbLpnWs?m=slm-
Zorya DSM-157 ZorE C-GFP	Plasmid	OD- 691	UEcOStbQVtpLHwJrCNHX
0-01 T	i idamiid	031	https://benchling.com/s/seq-
70m/0 DCM 1576 70rA		OD-	IbkQmDq30FKQanEpfQMA?m=slm-
Zorya DSM-1576 ZorA N-His	Plasmid	953	Bq3VDPsaDj4r61J8IUII
141110		000	https://benchling.com/s/seq-
Zorya DSM-1576 ZorB		OD-	dW2baJobidD79Pl9CNC5?m=slm-
N-FLAG	Plasmid	954	yNx0obSuMvLQBql3iMix
			https://benchling.com/s/seq-
Zorya DSM-1576 ZorB		OD-	vMoGy3mKXItlcSeWkpVU?m=slm-
C-Myc	Plasmid	955	nHrWaXgWf9zTixfknwh9
, -			https://benchling.com/s/seq-
Zorya DSM-1576 ZorE-		OD-	m6Nl8R35Dfww62Y4AqP9?m=slm-
C3xFLAG	Plasmid	956	DOuCOFIm4z7SmchLul9J
			https://benchling.com/s/seq-
Zorya DSM-1576 ZorB		OD-	GiZzWdpQN8j55YhFmtSS?m=slm-
N-Myc	Plasmid	957	UfQGUbJwobMIU95mlu6A
•			https://benchling.com/s/seq-
Zorya DSM-1576 ZorA		OD-	g593EN35xSTcMCrvPjCm?m=slm-
C-His	Plasmid	958	3ru0xBxzH4hbUyLe8eKs
			https://benchling.com/s/seq-
Zorya DSM-1576 ZorE		OD-	mCuifTZkK9dei82Ql6tj?m=slm-
C-Myc	Plasmid	959	Mj5RUkQ24G866gD1x4ft
			https://benchling.com/s/seq-
Zorya DSM-1576 ZorB		OD-	BqdggFDaNLTu3Dn0U4FH?m=slm-
C-FLAG	Plasmid	960	8bIN0PgiY7OmiYPz7J8V
			https://benchling.com/s/seq-
		No	kucNipM65t3OUAgZZ4Tg?m=slm-
T7p14-ZorA	Linear	ID	b5YPUZ3pilxPcOle5AoO
			https://benchling.com/s/seq-
		No	Fi8GIsp5XOyezW6tdU0s?m=slm-
T7p14-ZorB	Linear	ID	o87Mrr7ausTbZpkMeGEq
			https://benchling.com/s/seq-
		No	oxj65rw6pujF98N2QqSj?m=slm-
T7p14-ZorE	Linear	ID	mLMh0to7dfCn90v5tMB1

List of strains and phages used in this work.

ID	Strain	Descritption	Source
CBS-			
521	Escherichia coli DSM1576 (ATCC 8739)		DSMZ
OD-675	Escherichia coli DSM1576 (ATCC 8739)	ΔzorABE (4,265,744 -> 4,269,528)	This work
	Enterobacteria phage T4	DSM No.: 4505	DSMZ
	Enterobacteria phage T5	DSM No.: 16353	DSMZ
	Enterobacteria phage T7	DSM No.: 4623	DSMZ
	Enterobacteria phage phiX174	DSM No.: 4497	DSMZ